

# **Modelling the Movement and Concentration of Discharge for the Proposed Guthalungra Prawn Farm**

prepared for

**Pacific Reef Fisheries (Bowen) Pty Ltd**

**Luciano Mason and Tom Hardy**

*Marine Modelling Unit*  
**School of Engineering**  
**James Cook University**

*CRC Reef*

Marine Modelling Unit  
School of Engineering  
James Cook University  
Townsville, Q. 4814

Phone. (07) 4781 4476  
Fax. (07) 4775 1184  
Email. [Thomas.Hardy@jcu.edu.au](mailto:Thomas.Hardy@jcu.edu.au)  
Web. <http://mmu.jcu.edu.au>

## Scope

This study models the movement and concentration of the discharge from the proposed pawn farm at Guthalungra in North Queensland (Figure 1). The following items define the scope of the project:

1. Simulations were conducted for the outfall location shown in Figure 1.
2. The discharge was continuously discharged at the rate of 200 ML per day during the period of farming operations. The farm is assumed to operate for the first half of each year. The discharge will be discharged along the last 100 m of the pipeline by a diffuser. The discharge is assumed to be thoroughly mixed throughout the water column in the vicinity of the diffuser.
3. Simulations were conducted using a three-dimensional (3D) model with a horizontal resolution of approximately 70 m and five evenly spaced sigma layers in the vertical.
4. Two six month simulations were conducted (i) 1 Jan 1990 to 30 June 1990 and (ii) 1 Jan 1998 to 30 June 1998.
5. The discharge was modelled as a cloud of neutrally buoyant particles that are released at each model timestep and tracked during the six-month period. The effects of settling and biological activity on discharge concentrations were not modelled.
6. Model forcing was astronomical tides, wind and East Australian Current (EAC). The hydrodynamic effects of density differences were not modelled. Wave induced currents were not considered.
7. Results of the modelling are presented as plots of concentration of total nitrogen, phosphorus, and chlorophyll-a. Movies were produced that show the evolving changes with time in concentration for selected scenarios.

## Model Description

In this section a brief description of the numerical model, *MMUHYDRO*, is given. The equations of motion, details of the computational grid and open boundary conditions are included. Also described briefly are the numerical procedures for solution of the finite difference equations.

### Equations of Motion

The equations of motion are the three-dimensional (3D) long wave equations, describing conservation of momentum and mass for a homogeneous fluid. In the present work, these equations are formulated in a terrain following  $\sigma$ -coordinate system, based on the following transformation of standard spherical polar coordinates  $(\lambda, \theta, z)$ , used in models over significant portions of the earth's surface:

$$\lambda^* = \lambda, \quad \theta^* = \theta, \quad \sigma = \frac{z - \eta}{\eta - h}, \quad t^* = t. \quad (1)$$

Here,  $\lambda$  is east longitude,  $\theta$  is north latitude,  $z$  measures elevation above a Mean Sea Level (MSL) datum,  $\eta$  is the surface elevation,  $h$  is the bottom elevation and  $t$  is time. Thus,  $\sigma$  ranges from  $\sigma = 0$  at the free surface ( $z = 0$ ), to  $\sigma = -1$  at the sea floor ( $z = h$ ). By the use of the hydrostatic approximation, the equations become (on deleting the asterisks that denote the transformed coordinate system):

$$\begin{aligned} \frac{\partial U}{\partial t} + \frac{1}{a \cos \theta} \left[ \frac{\partial}{\partial \lambda} \left( \frac{U^2}{D} \right) + \frac{\partial}{\partial \theta} \left( \frac{UV \cos \theta}{D} \right) \right] + \frac{1}{D} \frac{\partial UW}{\partial \sigma} - \frac{UV}{aD} \tan \theta - fV \\ = -\frac{gD}{a \cos \theta} \frac{\partial \eta}{\partial \lambda} - \frac{1}{D} \frac{\partial}{\partial \sigma} \frac{K_m}{D} \frac{\partial U}{\partial \sigma} + A_m \nabla_h^2 U, \end{aligned} \quad (2)$$

$$\begin{aligned} \frac{\partial V}{\partial t} + \frac{1}{a \cos \theta} \left[ \frac{\partial}{\partial \lambda} \left( \frac{UV}{D} \right) + \frac{\partial}{\partial \theta} \left( \frac{V^2 \cos \theta}{D} \right) \right] + \frac{1}{D} \frac{\partial VW}{\partial \sigma} - \frac{U^2}{aD} \tan \theta + fU \\ = -\frac{gD}{a} \frac{\partial \eta}{\partial \theta} - \frac{1}{D} \frac{\partial}{\partial \sigma} \frac{K_m}{D} \frac{\partial V}{\partial \sigma} + A_m \nabla_h^2 V, \end{aligned} \quad (3)$$

$$\frac{\partial \eta}{\partial t} + \frac{1}{a \cos \theta} \left[ \frac{\partial U}{\partial \lambda} + \frac{\partial (V \cos \theta)}{\partial \theta} \right] + \frac{1}{D} \frac{\partial W}{\partial \sigma} = 0. \quad (4)$$

In Eqns. (2) and (3), contributions from atmospheric pressure are omitted. Additional notation is as follows:  $f$  is the Coriolis parameter (equal to  $2\Omega \sin \theta$ , where  $\Omega = 7.292 \times 10^{-5} \text{ s}^{-1}$  is the earth's angular velocity);  $D = \eta - h$  is total water depth;  $a$  is the earth's radius;  $K_m$  is the vertical eddy viscosity;  $A_m$  is the horizontal eddy viscosity; and  $\nabla_h^2$

denotes the horizontal Laplacian operator. The components of transport ( $U$ ,  $V$  and  $W$ ) are, defined by  $(U, V, W) = D(u, v, w)$ , where  $(u, v, w)$  are the components of fluid velocity.

### Vertical shear stress

The physical process whereby horizontal momentum is transferred vertically by shear stresses is parameterised by eddy diffusion. This is represented by the vertical diffusion terms in the momentum equations, (2) and (3). The vertical eddy viscosity ( $K_m$ ) in these terms varies spatially, and is largely determined by the vertical velocity shear. The turbulence closure model of Mellor and Yamada (1982) is used to calculate  $K_m$ . This is a sub-model of the hydrodynamic model and calculates the production, dissipation and advection of turbulent kinetic energy and turbulence length scales that are then used to calculate vertical eddy viscosity.

At the water surface, boundary conditions for the vertical diffusion terms are determined by the imposed wind stress ( $\tau_s$ ). Wind stress, when required, is modelled conventionally through the quadratic drag law,

$$\vec{\tau}_s = C_{10} \rho_a \left| \vec{W}_{10} \right| \vec{W}_{10}, \quad (5)$$

where  $\vec{W}_{10}$  is the wind at a standard anemometer height of 10 m,  $\rho_a$  is the density of air and  $C_{10}$  is the surface drag coefficient. The (dimensionless) drag coefficient is a function of the magnitude of the wind speed. The formula used in the present study is that of Wu (1982):

$$C_{10} = (0.8 + 0.065 \left| \vec{W}_{10} \right|) \times 10^{-3}, \quad (6)$$

where the magnitude of  $\vec{W}_{10}$  is given in  $\text{ms}^{-1}$ .

At the sea bed, the bottom shear stress  $\vec{\tau}_b$  is expressed in terms of the total near bottom transport  $Q_b = (U_b^2 + V_b^2)^{1/2}$  (the transport taken from the lowest  $\sigma$ -level) and total water depth  $D$ , by the quadratic friction law:

$$\vec{\tau}_b = (\tau_{bx}, \tau_{by}) = \frac{\rho C_b |Q_b|}{D^2} (U_b, V_b), \quad (7)$$

where  $\rho$  is the density of seawater and  $C_b$  is a drag coefficient. For fully developed turbulent flow, the near bottom currents are very closely approximated by a logarithmic profile. From this relationship, it can be shown that the drag coefficient can then be expressed as:

$$C_b = \left[ \frac{\kappa}{\ln(z_b / z_0)} \right]^2 \quad (8)$$

where  $\kappa = 0.4$  is the well known von Karman constant,  $z_b$  is the elevation of the lowest horizontal transports ( $U_b, V_b$ ), and  $z_0$  is the bottom roughness length.

### **Initial conditions and lateral boundaries**

Eqs. (2), (3) and (4) are integrated through time by a numerical marching procedure starting from a specified initial state. Unless data or the results of a previous simulation (*hot start*) are available, it is usual to start computations from the condition of initial quiescence:  $U = V = 0$  at all  $\sigma$ -levels, and  $\eta = 0$ .

Disturbances that are partially or completely generated outside the computational grid can be introduced into the computational domain only by supplying appropriate water heights or velocities at the grid boundaries. This is the case when modelling tides as most of the tidal momentum of a continental scale model enters the model domain through the open boundaries. In the case of wind driven flows, momentum is added directly to the water column through surface stresses. For a sufficiently large domain, a majority of the wind-induced momentum will be directly introduced into the computational domain. This means that water levels from wind forcing are not needed at the open boundaries provided the region of interest is sufficiently far from the open boundaries (nested grids, below).

### **Numerical Procedures**

In the horizontal, the variables  $U, V$  and are specified on a spatially staggered finite difference grid (the Arakawa  $C$  scheme). Through the vertical, the variable  $W$  is staggered about the levels on which ( $U, V$ ) values are defined. The 3D Eqs. (2) to (4) are solved by a fully implicit splitting procedure, based originally on work by Wilders *et al.* (1988), which was developed originally for 2D models. The procedure has been extended here to three dimensions, by a further splitting of horizontal and vertical difference operators. Changes from the original 2D scheme of Wilders *et al.* are described in more detail in Bode & Mason (1994) and include the use of transport rather than velocity components as prognostic variables, implicit bottom friction, and an implicit method for treating the Coriolis terms on a staggered grid. Changes have also been made to the treatment of advective terms. In the 3D model, the vertical diffusive part of the calculations is solved implicitly through the inversion of a tridiagonal matrix system. A pre-conditioned version of the conjugate gradient squared method is used to invert the sparse matrices generated by the difference scheme. Further modifications to the difference scheme have been implemented to accommodate the reef parameterisation algorithms.

### **Reef modelling**

The coral reefs of the Great Barrier Reef (GBR) can have a considerable effect on the propagation of the tidal wave and on wind driven flow. The high spatial complexity of the reefs is difficult to explicitly model at an acceptable spatial resolution with available computer resources. The approach adopted here is to use a sub-grid-scale reef

parameterisation scheme, Bode *et al.* (1997), which incorporates hydrodynamic effects of the effective porosity of the reef matrix by introducing four additional parameters at each grid point. The additional parameters are generated automatically in a dynamically consistent manner from digitised reef outlines.

## Model grids and model forcing

This section describes the grid layout used in this project and the forcing mechanism important in driving currents at the study site. This study used four successively finer resolution grids. Forcing mechanisms considered most likely to effect the dispersal of discharge in the study area are the astronomical tide, wind and East Australian Current (EAC).

The hydrodynamic effects of density differences associated with both, larger scale salinity and temperature gradients within Abbot Bay and smaller scale density differences between discharge and seawater were not modelled. Wave-induced currents generated by wave breaking near shore were also not considered.

### Description of model grids

The main rationale behind the use of nested grids is the need to overcome open boundary condition problems, which are commonly encountered in limited area fine-scale modelling. By means of nesting, the finest-scale grid, which surrounds the area of interest, is linked to the dynamics of the continental shelf, so that open boundary problems are largely transferred further afield, where: (i) The extensive range of tidal data from the shelf region can be utilised for boundary conditions. (ii) Any inaccuracies in the specification of boundary conditions will have negligible influence on the evolution of model solutions in the region of interest. (iii) The essentially unknown boundary conditions associated with wind forcing are assumed to be zero.

Four nested grids are used for computational efficiency so that accurate oceanic, wind driven and tidal boundary conditions can be supplied to the finest grid. A 5:1 increase in resolution between successive grids was used to obtain an approximately 70m resolution in the study area. The outer grid (*A*-grid, Figure 2) has a 5' resolution, and extends over most of the western Coral Sea from Papua New Guinea in the north to south of Fraser Island and half way to new Caledonia to the east. This grid is necessary to produce a representation of the oceanic currents, particularly the East Australian Current. The *B*-grid (Figure 3) has resolution of 1' covering the continental shelf along the tropical Queensland coast from just North of the Whitsunday Islands to Cape Cleveland near Townsville. The *C*-grid increases the resolution to about 370 m for the region well to the north and south of Abbot Bay as shown in Figure 3. The final, high resolution *D*-grid (Figure 4) covers the waters adjacent to the outfall location. It's grid spacing is 0.04' or approximately 74 m. The varying oblique orientations of the grids are achieved by using transformed spherical coordinate systems. The *D*-grid is run in full 3D mode, with five equally spaced layers in the vertical. The three coarser models, used to supply boundary to the *D*-grid, were run in 2D mode.

### Model bathymetry

The primary sources of information for the model bathymetry were navigational charts and the national bathymetric series maps. This was supplemented by bathymetric survey

supplied by the client for the immediate vicinity of the discharge point. Figure 4 shows the location of survey transects.

### **Tidally induced currents**

Tidal currents are largely cyclic in nature, and therefore, will tend to bring water back to the point of origin. The primary effect of the tides on the dispersal of a continuously discharged discharge is to increase the effective volume into which the discharge is being introduced. This effective volume is determined by the tidal current speed, and changes through a spring/neap cycle. Through non-linear hydrodynamics (e.g. caused by bottom friction and irregular topography) tidal currents can also produce weak residual currents that can cause further dispersion of the discharge.

Tidal forcing is introduced in the model by supplying tidal water levels at each open boundary point of the model grid. For all the modelled scenarios, water levels calculated from the amplitude and phase of over 22 selected tidal constituents, are imposed along the open boundaries of the *B*-grid. The amplitude and phase result from tidal modelling (not presented here) on a separate model grid, which covers the Queensland coast out past the continental shelf at a 1' resolution. The modelled tide was further calibrated, at the resolution of the *B*-grid, to produce model results that match with measurements at the Bowen, Abbott Point and Cape Ferguson tide gauges (see Figure 6).

Figure 5 shows the comparison between *modelled* and *predicted* tidal levels at the Abbott Point tide gauge. Figure 5a shows the comparison for approximately a month long period at the time of the first water level and current measuring deployment. Figure 5b shows a smaller segment of this time bounded by the vertical lines in Figure 5a. The tidal calibration results shown in Figure 5 indicate that the tidal modelling is a good estimate of the predicted tides.

The currents produced by a single tidal constituent can be represented by plotting the tip of the current vector for one cycle. This forms of an ellipse. It is often sufficient to plot just major and minor axes of the ellipse, where the length indicates current speed and the orientation the current direction. The tidal ellipses for the  $M_2$  tidal constituent are shown in Figure 6. The  $M_2$  has the largest amplitude of all the constituents and often gives a good indication of total tidal currents. Note at the study site (indicated by the small box in Figure 6) that the currents are along-shore. The flood tide goes to the south and the ebb tide to the north for the study area; therefore, the ellipses in the study region approach straight lines.

### **Wind forcing**

At the study location winds will be the forcing mechanism that causes effective dispersal of the discharge plume. The bulk of the wind driven currents are forced to move either north or south following the shoreline depending on the direction of the along shore wind component and will move discharge away from the discharge site. If



the wind has a strong shoreward component, as produced by the sea breeze, overturning of the water will occur with the surface water moving towards shore and bottom water moving away. This will shear the discharge plume in the vertical and disperse the discharge. During periods of weak or variable wind, discharge may pond near the discharge site.

Wind speed and direction data were obtained from the Australian Institute of Marine Science automatic weather stations at Cape Bowling Green, Davies Reef and Hardy Reef. The wind station locations are shown in Figures 1 and 2. The 16 years of data available at Cape Bowling Green were low pass filtered (500 h) to remove high frequency variability and show trends in wind speed (Figure 7a) and direction (Figure 7b). Figure 7b suggests that winds are predominantly from the east, coming from the south-east in winter and north-east in summer. This means that the wind driven component of flow should most often be toward the north.

The three arrows in Figure 7a indicate periods of weak or variable wind during which the environmental effects of discharge might be more critical. After analysis of these data, two six-month simulation periods were chosen to investigate effect of wind on the dispersal of the discharged discharge. The first period from 1 Jan to 30 June 1990 (Figure 8) has a prolonged period of weak and variable winds during the period of farm operation. The 1 Jan to 30 June 1998 period (Figure 9) has more persistent winds although there are 4 to 5 day periods with weak winds.

Winds measured at the three stations have similar trends. However the winds at Hardy and Davies reefs tend to be stronger than those at Cape Bowling Green which is nearer the coast. The Cape Bowling Green station has a stronger sea-breeze signal. For all the modelling results that follow, winds used to force the *A* and *B*-grid simulations were taken from Hardy Reef while winds from Cape Bowling Green were used for the *C* and *D* grids.

### **East Australian Current (EAC)**

A dynamically simple and economical model of the oceanic currents is used to represent the effect of the EAC on the continental shelf. This model, developed on the *A*-grid (Figure 2), simplifies the upper ocean dynamics by setting a false bottom at 300 m depth in conjunction with a very low friction coefficient in deep water. This simulates the effects of stratification which tends to isolate the surface circulation from the deeper currents. Water height boundary conditions applied to the *A*-grid were set as follows: (i) spatially, by reference to known oceanic current patterns, including the results of global oceanic models; (ii) temporally, from the mean seasonal signals extracted from various long term tidal records from the western Coral Sea.

Figure 10 give a snap shot of the currents produced when both the wind and EAC are applied to the *A*-grid model. It shows oceanic waters approaching the Queensland coast and splitting into two arms moving north and south along the continental shelf break. The current moving south is called the EAC. Near the study site it persist towards the south throughout the year. On the continental shelf the effects of the EAC weaken

toward the coast and currents are dominated by the winds. However the persistence of the EAC may play an important role in discharge dispersal during periods of weaker winds. Note also that the southerly set of the EAC is opposite to currents produced by the commonly occurring south-easterly winds.

## Model Calibration and Verification

A current and tide measuring instrument was deployed for two time periods during 2002 (28 May to 3 July and 1 Aug to 5 Sept). This measurement program was not conducted by MMU staff and results were provided under a separate contract. The location of the two deployments is shown in Figure 4. Currents are only available for the second deployment and were recorded 1.5 m above the seabed in water depth of approximately 5 m.

Model results using tidal and wind forcing [Hardy Reef (*A* and *B* grids) and from Cape Bowling Green (*C* and *D* grids)] are compared with measurements of water level (Figure 11 and 12). For Figures 11a and 12a show the water heights over the whole measurement time and 11b and 12b show a shorter time indicated by the black lines in (a). The measured and modelled water levels match well. Differences as seen in Figure 12b can be explained as, long period, water level changes caused by oceanic processes that were not modelled. Figure 13 shows the difference between measured and modelled water levels for both deployments. The higher frequency noise with amplitude of about 0.15 m is largely caused by errors in the modelled tide. The much longer period trends will raise and lower the mean water surface (as in Figure 12b) with little effect on the currents.

At this near-shore shallow site, wave-induced bottom stress can have an important contribution to current speed and direction. Since wave modelling was not coupled with current modelling in this project the effect of wave-induced bottom stress was included by calibrating the value of  $z_0$  (Grant and Madsen, 1979). A multiplication factor of 30 was used, on the *D*-grid, over that which we usually use for deeper water modelling.

Comparison between measured and modelled currents (only available for deployment 2) is shown in Figure 14. Three time history plots are included in this figure. Figure 14a shows the current in the principal component direction. The principal component direction is defined as the direction along which the current variation is greatest. Its orientation is indicated by the red line in Figure 14d (thicker part show the positive direction) and is calculated from the modelled currents. Figures 14b and 14c have the comparisons for the *x* and *y* components of the current. Figure 14d is a Hodograph giving a 2-dimensional representation of the current by representing each current vector in the time history by a dot plotted at the tip of the vector.

We believe that the differences between model and measurements are mainly caused by the inadequate representation of the wind at the study site. The shore normal component of the wind pushes surface water towards the coast and causes a return flow near the bottom. The current meter recordings, shown in Figure 14, were taken 1.5 m above the bottom, in the lower part of the water column. In Figure 14b, the large pulses of offshore directed current therefore suggest that the shore normal wind component at the site is stronger in the immediate study area than at the Cape Bowling Green wind gauge. Overall, the results of model comparisons with field measurements indicate that the model is capable of producing realistic current speeds and direction of the study area.

## Dispersal Modelling

Two simulations (i) 1 Jan 1990 to 30 June 1990) and (ii) 1 Jan 1998 to 30 June 1998 were conducted. The model time steps were 10800, 600, 300 and 300 s and for the  $A$ ,  $B$ ,  $C$  and  $D$  grids, respectively. A bottom roughness length,  $z_0$ , equal to 0.030 m is used. Imposition of horizontal momentum diffusion was not necessary in the present case, as the grid resolution is very fine with most of the eddy activity being explicitly modelled. Therefore, a horizontal eddy viscosity equal to zero ( $A_m = 0$ ) was used in Eqns. (2) and (3).

In order to reduce the effects of initial transients on the solutions, model forcing was increased from zero over time via a cosine factor. In the case of tidal modelling, an 18 hour buildup period was found to be sufficient for the semi-diurnal dominated tides of the study region. For wind forcing, an 18 hour buildup was also used.

As with the comparison of model results and field measurements, the wind forcing for the model simulations used wind data from Hardy Reef for  $A$  and  $B$  grids and from Cape Bowling Green for  $C$  and  $D$  grids.

## Particle Tracking and Concentration Calculations

The major objective of the study is to determine the movement of dissolved nutrients, which have been released into the water column. For this study the dissolved nutrients were modelled as groups of neutrally buoyant particles that are advected by the currents calculated by the 3D hydrodynamic model. The effects of sub-grid scale shear dispersion and turbulent diffusion on the positions of the particles were not included. It is expected that these effects will play only a minor role in the movement. A 3D (5  $\sigma$ -levels) model with high horizontal resolution (74 m) was used, which will explicitly account for most of the shearing of the particle plume. The high grid resolution means that most eddies generated in the study area will be explicitly modelled and affect particle movement directly. A large proportion of horizontal shearing of the particle plume will be associated with the vertical position of particles in the water column. The horizontal velocity varies with vertical position because of the effects of boundary layers at both the surface and the bottom. The exclusion of both particle settling and turbulent dispersion will tend to *overestimate* the discharge concentrations; therefore, these omissions create a conservative result.

The time series of instantaneous particle positions were obtained by numerical integration of the three components of the following vector, ordinary differential equation:

$$\frac{d\mathbf{x}_k}{dt} = \left( \frac{dx_k}{dt}, \frac{dy_k}{dt}, \frac{dz_k}{dt} \right) = \mathbf{v}_k(\mathbf{x}_k, t) = (\bar{u}_k, \bar{v}_k, \bar{w}_k) = \frac{1}{D}(U_k, V_k, W_k), \quad (9)$$

where  $\mathbf{v}_k(\mathbf{x}_k, t)$  is the vector velocity at time  $t$  of particle  $k$ , with instantaneous vector position,  $\mathbf{x}_k$ . The equations are integrated by a second order Runge-Kutta scheme (modified Euler). The value of  $\mathbf{v}_k(\mathbf{x}_k, t)$  is obtained by linear interpolation of the velocity

fields (or actually from the transport, as indicated in the equations above) provided at each time step by the hydrodynamic component of the model. Higher order integration and interpolation schemes could be used to calculate particle positions. However numerical experimentation indicated that these more expensive alternatives were not warranted in the present case. If improved accuracy is desired the most effective way is to decrease the particle tracking time step. In the present application, three particle time steps were used for every hydrodynamic model time step, which meant that the position of a particle was determined every 100 s.

Each time step, 50 particles were released in a box that models the diffuser at the end of the outfall pipe. The size of this receiving box had horizontal dimensions of  $100 \times 8$  m and a height equal to depth of the water column. The diffuser was given as 100 m long. The 8 m width accounted for the horizontal velocity of the discharge as it exits the diffuser. This width was determined from separate work commissioned by the client. The release position of each individual particle was on a grid in horizontal, with the 50 particles evenly spaced along the outside of the box, and at randomly chosen vertical positions. The outfall location is shown in Figure 15.

Given discharge rate and concentration of the discharge and the number of particles released in each time step, the concentration of discharge in any computational cell is given as

$$c = \frac{N_p M_p}{V} \quad (10)$$

where  $N_p$  is the number of particles in any computational grid cell, and  $V$  is the volume of the computational cell and  $M_p$  is the mass of discharge associated with a single particle given as

$$M_p = \frac{c_e Q_e \Delta t}{N_e} \quad (11)$$

In which  $c_e$  is the concentration of the discharge,  $Q_e$  is the discharge rate of the discharge,  $\Delta t$  is the time step and  $N_e$  is the number of particles released each time step.

## Results

The discharge will contain nitrogen, phosphorus and chlorophyll-a that have the potential to have adverse effects on the local aquatic environment. Although the water will already contain background levels of these substances, adverse effects may occur if concentrations persist above threshold levels. The threshold levels used here will be those for seagrass. Table 1 lists the assumed discharge, background and threshold levels that were given by the client for this modelling exercise.

**Table 1** Values of given concentrations for discharge, background and threshold of damage.

Substance	Discharge mg/l	Background mg/l	Threshold mg/l
Nitrogen	2.0	0.1	0.15
Phosphorus	0.15	0.015	0.025
Chlorophyll-a	0.03	0.001	0.003

Note that for all the dispersal simulations, a constant discharge rate is assumed even though the actual rate will vary throughout the prawn farming season. The discharge rate used here is 200 Ml/d. and corresponds to the *maximum* expected rate that occurs during February of each year. This means that except for February the results shown below are conservative.

The results of the modelling will be presented in the following formats: (i) time histories of absolute concentrations at a point; (ii) spatial contours average concentrations; (iii) spatial contour plots of the percent time that threshold levels were exceeded; (iv) movies which show the change with time of concentration. Only the first three can be shown in this report. The movies are in an accompanying CD.

Figure 15 shows a segment of the *D* grid. Concentric circles centred on the outfall locations with radii of 500, 1000 and 2000 m are shown (and will be shown in some the following figures) for reference. Two points, 500 m north and south of the outfall at which time series are presented below, are shown as dots. The colour in this figure indicates the water depth with darker blue indicating deeper water and light red indicating shallower water.

### Concentration time series

Concentration time series are shown at the four points marked in Figure 15 for nitrogen in order to illustrate typical temporal variability in concentration at a point in space as wind and tide advect and disperse the discharge throughout the area. Figure 16 (1990) and Figure 17 (1998) have three plots. Time series (a) is the concentration of nitrogen at the point 500 m north of the outfall and (b) is the same for a point 500 m to the south.

Time series (c) is of a much shorter time period for both north and south locations indicated by the vertical lines through (a) and (b). Figures 18 and 19 are a repeat of figures 16 and 17 except that the time history locations are 1000 m to the north and south of the outfall.

Recall that the two simulation time periods were chosen to represent periods of weaker winds (1990) and average winds (1998). Notice that Figures 16 to 19 all show concentrations that are always above 0.1 mg/l since that is the assumed background level for nitrogen.

All of these time series are punctuated by sharp changes in concentration. These high frequency changes are caused by the ebb (to the north), and flood (to the south) of the tide. For example the north point receives a pulse of discharge during ebb tide, but concentrations will drop sharply during flood tide. Of course the opposite occurs for the south point. The clusters of higher concentrations (example near the end of Mar 1998, Figure 17) are caused during periods of weaker winds in which the discharge is not as rapidly advected from the study area. During stronger winds the concentration levels approach background levels. The expanded time series in Figures 16c and 17c show that what appears as concentrations that are persistently at high levels in (a) and (b) are actually closely group spikes of concentration separated by reduced levels.

For Figures 18a and 19a (location 1000 m north) the overall concentrations time histories are significantly reduced compared to the closer 500 m location. However, for Figures 18b and 19b (location 1000 m south) the peak concentration levels tend to be similar to the 500 m distant counterpart. This difference can be attributed to the wind conditions. When the plume moves to the south wind tend to be weak and variable creating less diffusion and dispersion than the stronger south-easterly winds which push the plume to the north, see below.

The results in Figures 16 to 19 are for single points and it is impractical to produce such plots for all points, and indeed it would be very difficult for one to analyse this information if it were available. The threshold levels used here are estimates of the long term concentration levels required to damage seagrasses and therefore require an integrated measure of concentration levels to establish where damage may occur.

### **Concentration maps**

In the following, average concentration contour plots give an integrated representation of the discharge impact on the area surrounding the outfall. Also present are plots indicating the amount of time that concentrations are above threshold levels. Parts (a), (b), and (c) of the following figures contain results for nitrogen, phosphorus, and chlorophyll-a respectively.

#### *Six-month*

In Figures 20 (1990) and 21 (1998) colour contour of average concentrations, for the six-month simulation, indicate where high concentration of discharge borne substances

persist. Also plotted on these figures are contours for the *background plus 10%* and the *threshold* levels. In some plots the *threshold* contour may not be visible as it is tightly bound around the outfall location. One common feature of these plots is the along-shore elongation of the contours. This is caused by the predominately along-shore nature of both the tidal and wind driven currents. Also notable is the northward offset of the contours relative to the outfall. This indicates that the south-easterly winds have a large influence on the discharge dispersal. Even though the simulation years of 1990 and 1998 were chosen for their different wind patterns (weak and average) the concentration pattern at higher levels are very similar. In Figures 20a and 21a the *threshold* contour for nitrogen extents from approximately 250 m south to 700 m north of the outfall and is 200 m at its widest. For 1998 (Figure 21a) the *background plus 10%* concentration contour is pushed further north than in 1990 (Figure 20a). It is at this and lower concentration levels that the different yearly winds have greatest influence on the concentration patterns. In Figure 20a a long tongue at low average concentrations extends south from the outfall. This was generated during the period of low winds identified in February 1990.

The average six-month concentrations for phosphorus and chlorophyll-a are calculated from the same particle cloud that generated results for nitrogen. However, different discharge, background and threshold concentration levels for each substance means that the extent of the ‘background plus 10%’ and the threshold contours can be significantly different. For these substances the *threshold* contours are not visible since levels above the threshold occur only in a very small region at the outfall.

An alternative way of exploring the data is by looking at the percentage of time during a specified period that the concentration levels exceed the threshold level for each substance. We will refer to this quantity as *% exceeding threshold*. Figures 22 and 23 are colour contour plots of the *% exceeding threshold* for the six-month periods in 1990 and 1998.

These plots suggest that concentrations above the threshold level can occur over a relatively large area near the coast. However, these higher concentrations are not often long lived and occur when a patch of discharge rich water is advected past a site. These events are similar to the concentration peaks, seen in the time series plots above, where concentrations can jump to a higher level for a number of hours. At low *% exceeding threshold* levels, the contour patterns are significantly different for 1990 and 1998 as determined by the wind patterns for that year. The contour line indicates the 10% *exceeding threshold* limit. For locations outside this line, concentrations were above the threshold less than 10% of the six-month simulation time. The extent and pattern of the 10% *exceeding threshold* contours are similar for both simulation years for each substance.

### *February*

Figures 24 to 27 correspond to Figures 20 to 23 except that they represent results for the month of February 1990 and 1998. During February the discharge rate from the farm will peak and be approximately 200 MI/d. This is also a time of year when winds can be



more variable in direction and tend have a more north-easterly direction (Figures 7, 8 and 9).

For February, in both 1990 and 1998 (Figures 24 and 25), the extent of the *background plus 10%* and the *threshold* contours for average concentration are significantly larger than those calculated for the six-month analysis. The extent of the *threshold* contour for nitrogen (Figures 24a and 25a) increased by a factor of approximately 6 for 1990 and 1.7 for 1998 over the six-month values. However for phosphorus and chlorophyll-a (Figures 24b, 24c, 25b and 25c) *threshold* contours still remain tightly bound around the outfall site. Note also that the contour pattern is offset to the south in 1990 and slightly north in 1998. This again suggests that the common south-easterly winds are less dominant during this part of the year.

In Figures 26 and 27, representing the % *exceeding threshold* for February, the 10% *exceeding threshold* contour have similar the patterns in the average concentrations and are also larger in extent than those for the six-month analysis. Note, however, that the 10% *exceeding threshold* now represents a total time of 2.8 days compared with total time of 18 days for the six-month period.

## Movies

The results of the 1990 and 1998 simulations for nitrogen can be viewed in a series of movies that show the temporal and spatial evolution of nitrogen concentrations (Table 2). These movies are contained on the CD accompanying this report and can be viewed by double clicking the hyperlinked movie titles in Table 2. The movies show a segment of the *D*-grid with the same extent as Figures 20 to 27. The outfall location is shown as a line. Also drawn are concentric circles centred on the outfall at 500, 1000 and 2000 m. The movies contain 1 frame for each hour of the six-month simulations.

**Table 2: Movies**

Total Nitrogen
2 Jan to 30 June 1990
2 Jan to 30 June 1998

Some features to note in these movies are: (i) the predominately northward movement of the discharge plume caused by wind from the south-easterly quadrant; (ii) the along shore oscillatory nature of the tidal currents; (iii) the shore normal vertical shearing of the plume; (iv) the ponding of discharge during weak winds; (v) the way patches of discharge higher concentration pulse, with the tide, past a fixed location (as identified in the time series plots).

## Conclusion

This project uses a 3D hydrodynamic model and a particle tracking model to investigate the dispersal of prawn farm discharge discharged into Abbot Bay. Two six-month simulation were undertaken using a constant discharge of 200 Ml/d and constant concentrations of total nitrogen, phosphorus and chlorophyll-a in both the discharge and as a background in the seawater. Each simulation used the hydrodynamic forcing produced by the wind and tide and EAC.

Conclusions that arise from this modelling are:

1. The tidal and wind driven currents are mainly along-shore.
2. Wind at the site is mostly likely stronger than that recorded at Cape Bowling Green.
3. Hydrodynamic model does a good job at reproducing water heights and currents.
4. Discharge is most often dispersed in northerly direction.
5. Plume is dispersed quickly when the wind is strong. This occurs most often when the wind is in the south-easterly quarter.
6. The discharge ponds when winds are weak and variable and have with some component from the north.
7. In both the 1990 and 1998 simulation years, February has the most extensive periods of weak winds.
8. The area impacted by higher than threshold average concentrations for nitrogen is about 200 m by 900 m. For Phosphorus and Chlorophyll-a above threshold average concentrations only occur in the immediate vicinity of the outfall. The impact area for nitrogen is larger in February, but is still largely confined to the immediate vicinity of the outfall for Phosphorus and Chlorophyll-a.
9. Concentrations tend to pulse as patches of water with higher discharge concentration are moved by the tide past a location.
10. Pulses in concentration higher than threshold can occur over a much larger area than the impact areas for average concentration.

## References

- Bode, L. and Mason, L.B. (1994) Application of an implicit hydrodynamic model over a range of spatial scales. *Computational Techniques and Applications*: CTAC93, D. Stewart *et al.*, Eds., World Scientific Press, 362-370.
- Bode, L., Mason, L.B. and Middleton, J.H. (1997) Reef parameterisation schemes with applications to tidal modelling. *Prog. Oceanog.*, Vol. 40, 285-324.
- Grant, W.D. and Madsen, O.S. (1979). Combined wave and current interaction with a rough bottom, *J. Geophysical Research*, Vol 84, No. C4, pp. 1797-1808.
- Mellor, G.L. and Yamada, T. (1982) Development of a turbulence closure model for geophysical fluid problems. *Reviews of Geophysics and Space Physics*, 20(4), 851-875.
- Wilders, P., van Stijn, Th.L., Stelling, G.S. and Fokkema, G.A. (1988) A fully implicit splitting method for accurate tidal computations. *International Journal for Numerical Methods in Engineering*, 26, 2707-2721.
- Wu, J. (1980) Wind-stress coefficients over sea surface near neutral conditions: a revisit. *Journal of Physical Oceanography*, 10, 727-740.

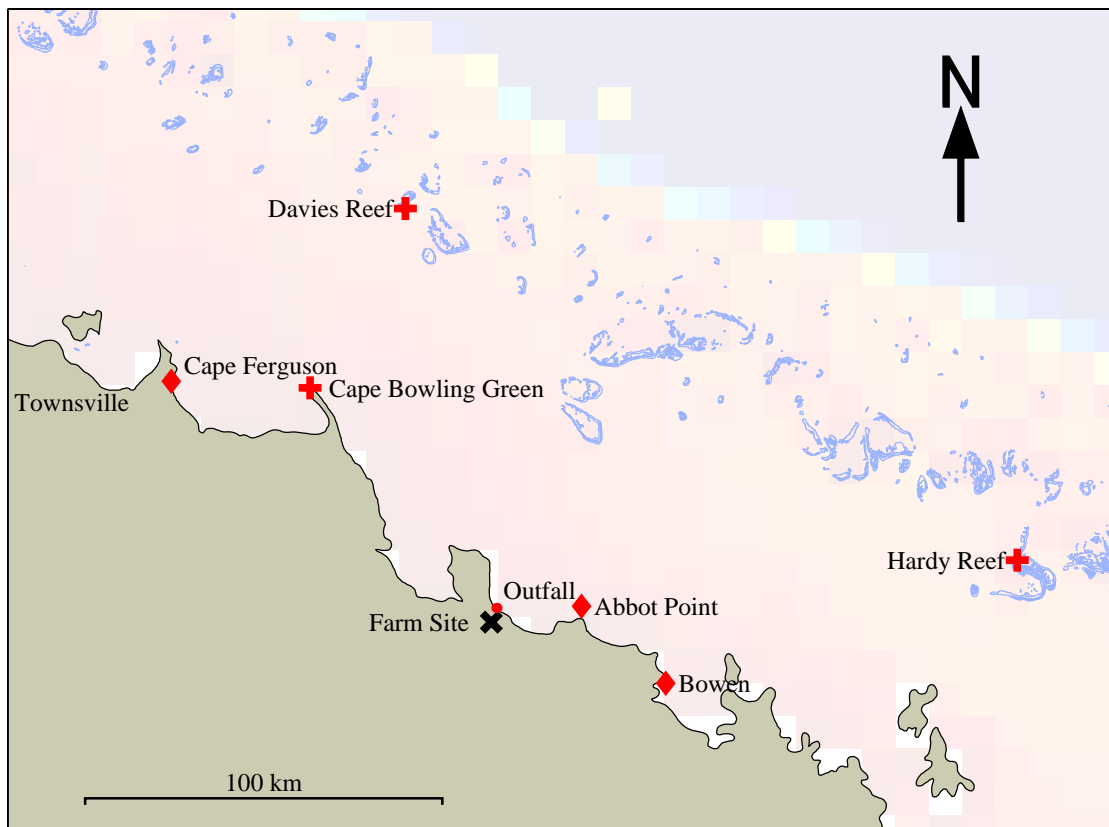


**Figure 1.** Study Location: ● indicates the outfall site, + indicates wind stations, ◆ indicates tidal stations.



**Figure 2.** *A*-Grid – the outermost and coarsest resolution of 5' (9266 m). Also shown is the extent of *B* and *C* grids. + indicates wind stations.

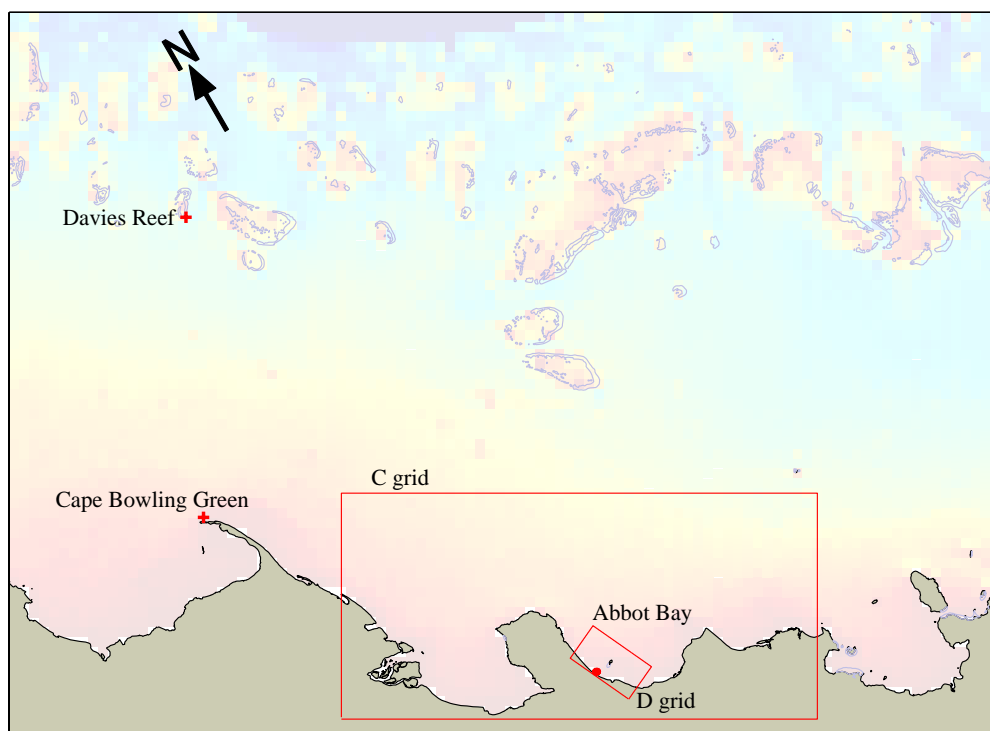


**Figure 3.** *B*-Grid – the middle grid with resolution of 1' (1853 m). Also shown is the extent *C* and *D* grids, ● indicates the outfall sites. + indicates wind stations.

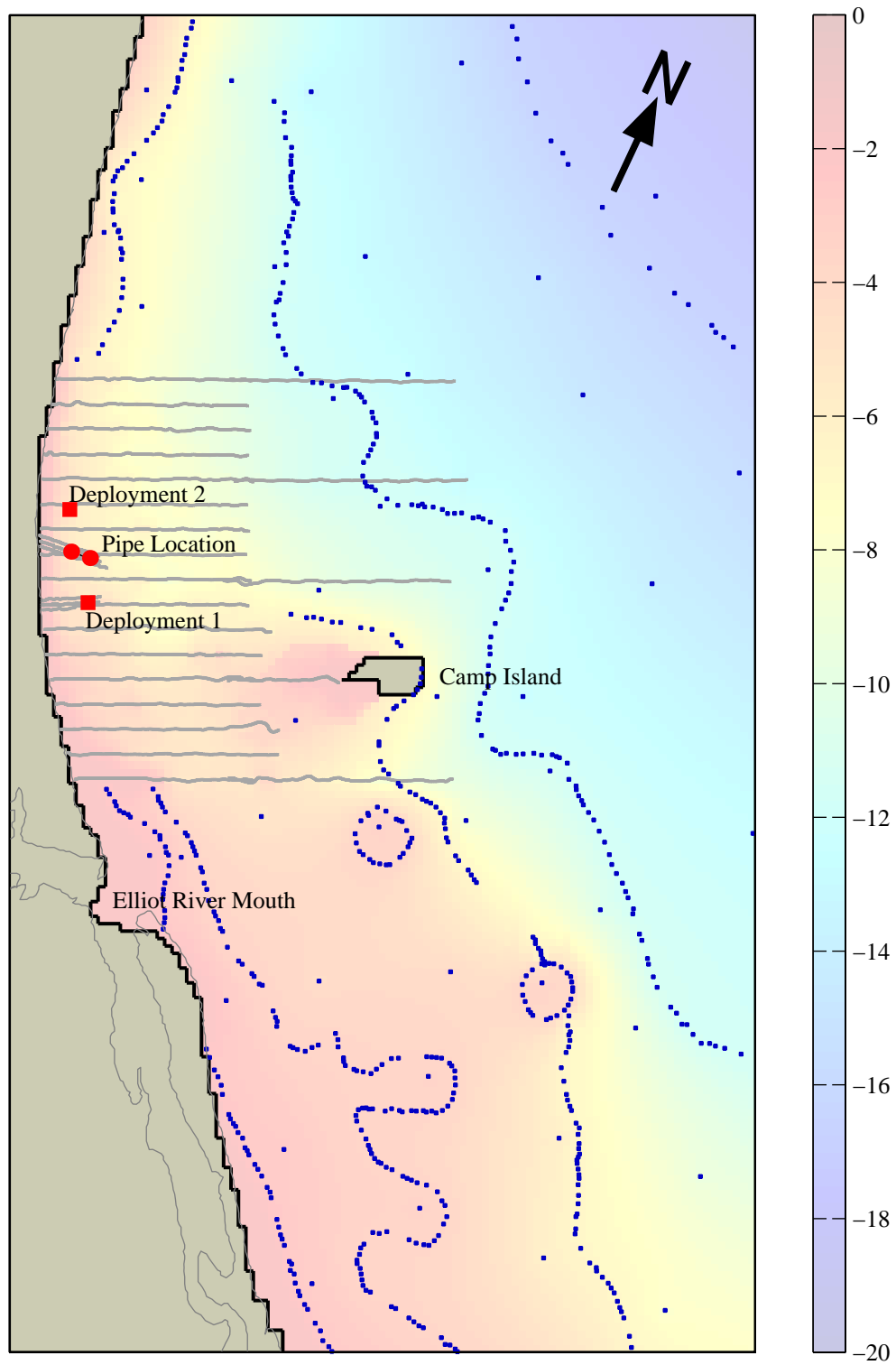


**Figure 4.** *D*-Grid - resolution of 0.04' (74 m). ● indicates the ends of the inlet and outlet pipes. ■ indicate the current meter deployment locations. Blue dots are the location of depths from navigational charts. Grey dots indicate the location of the supplementary depth survey.

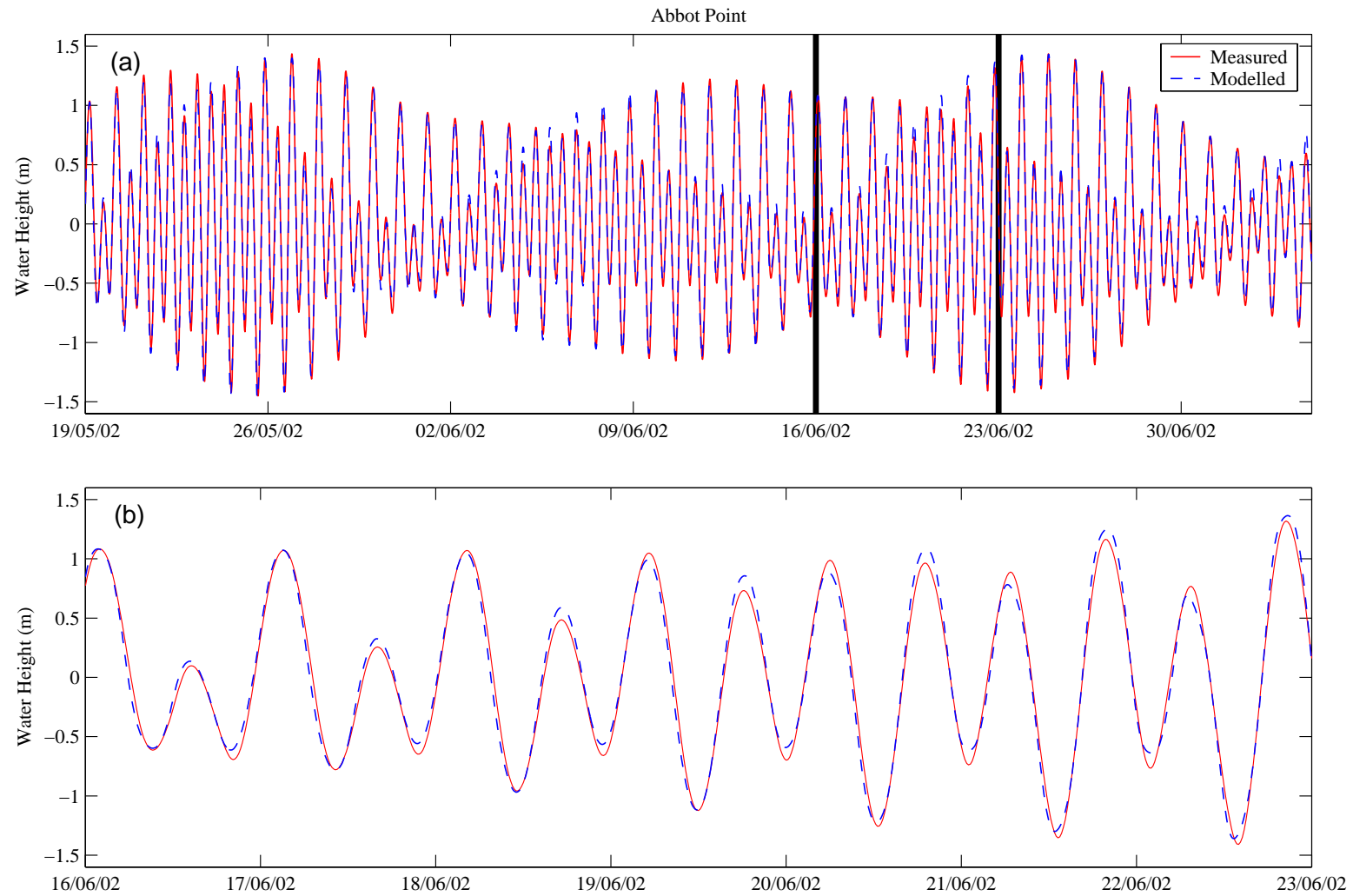


**Figure 5.** Abbot Point, time histories of predicted and modelled tide heights: (a) for a number of spring neap cycles; (b) for a 1 week segment bounded by the black lines in (a).



## $M_2$ Amplitude and Tidal Ellipses

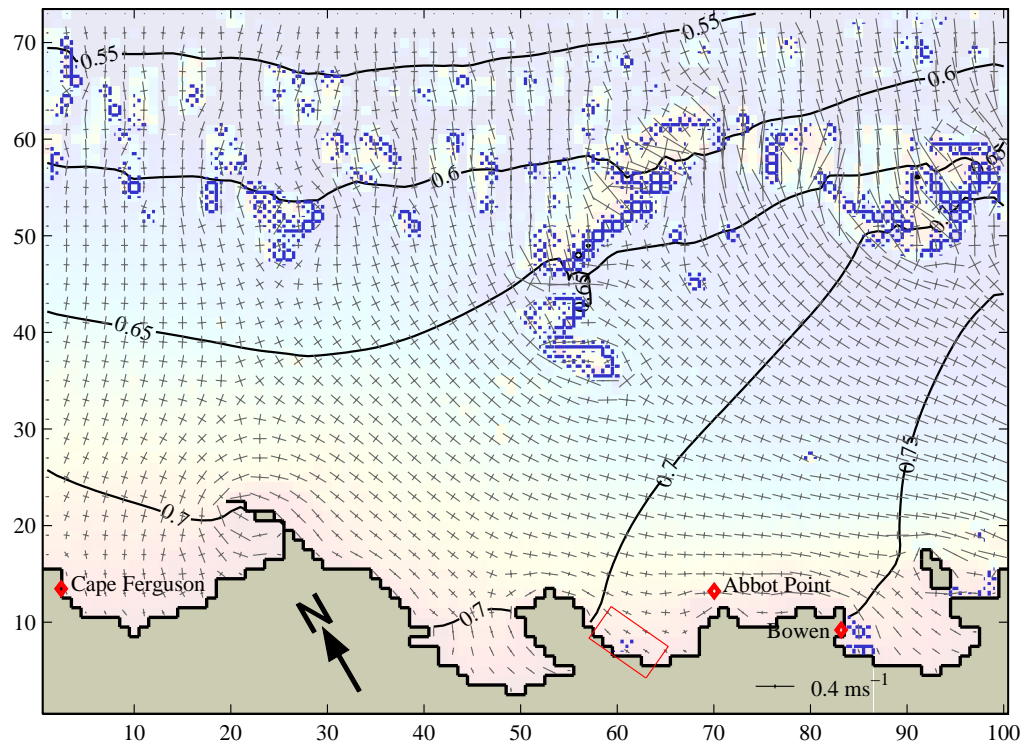


**Figure 6.** Computed  $M_2$  tidal amplitude (contours) and ellipses (crosses). ♦ indicates tidal stations.

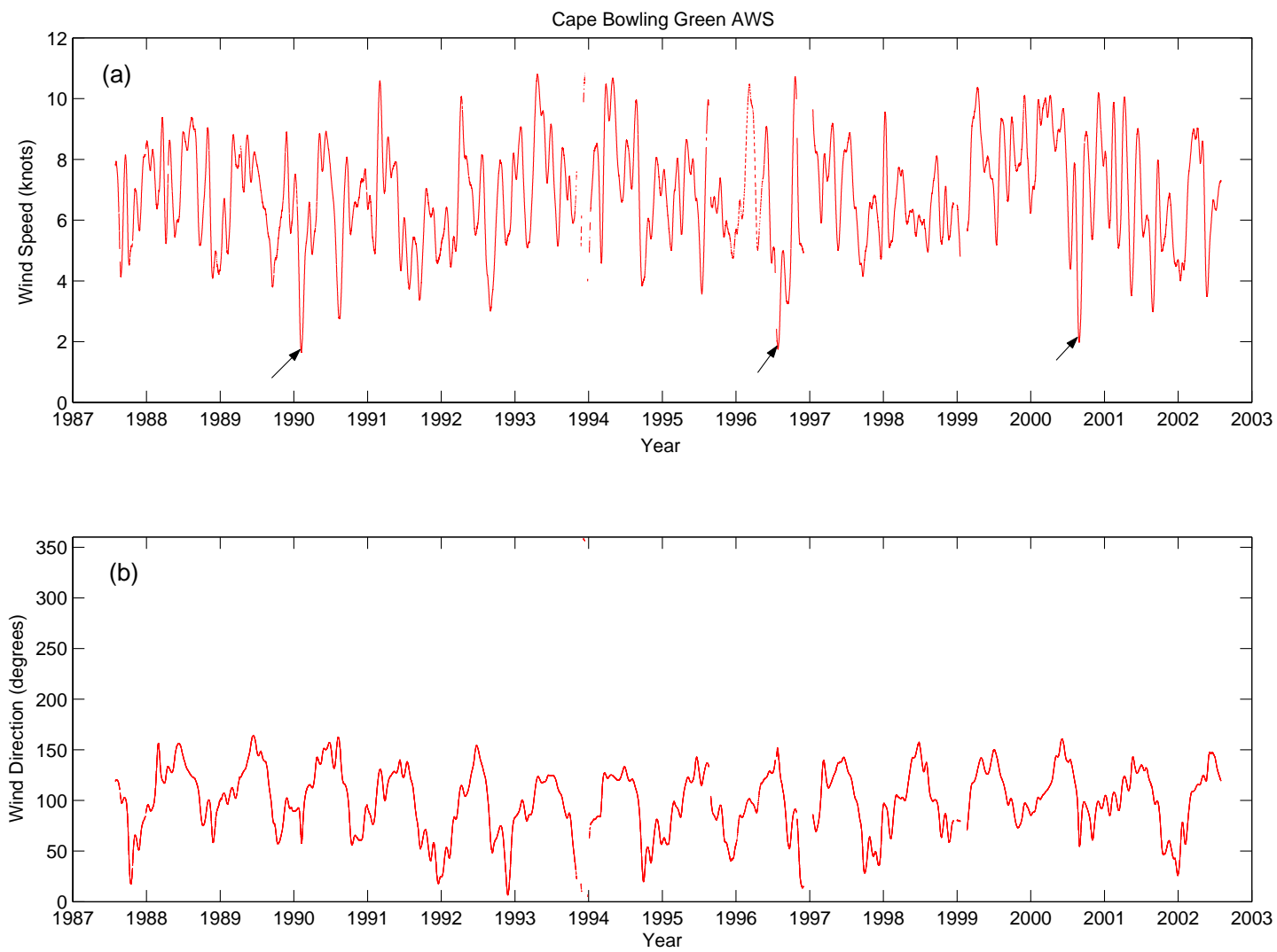


**Figure 7.** Low pass filtered (500 h) at the Cape Bowling Green wind station: (a) speed; (b) direction.

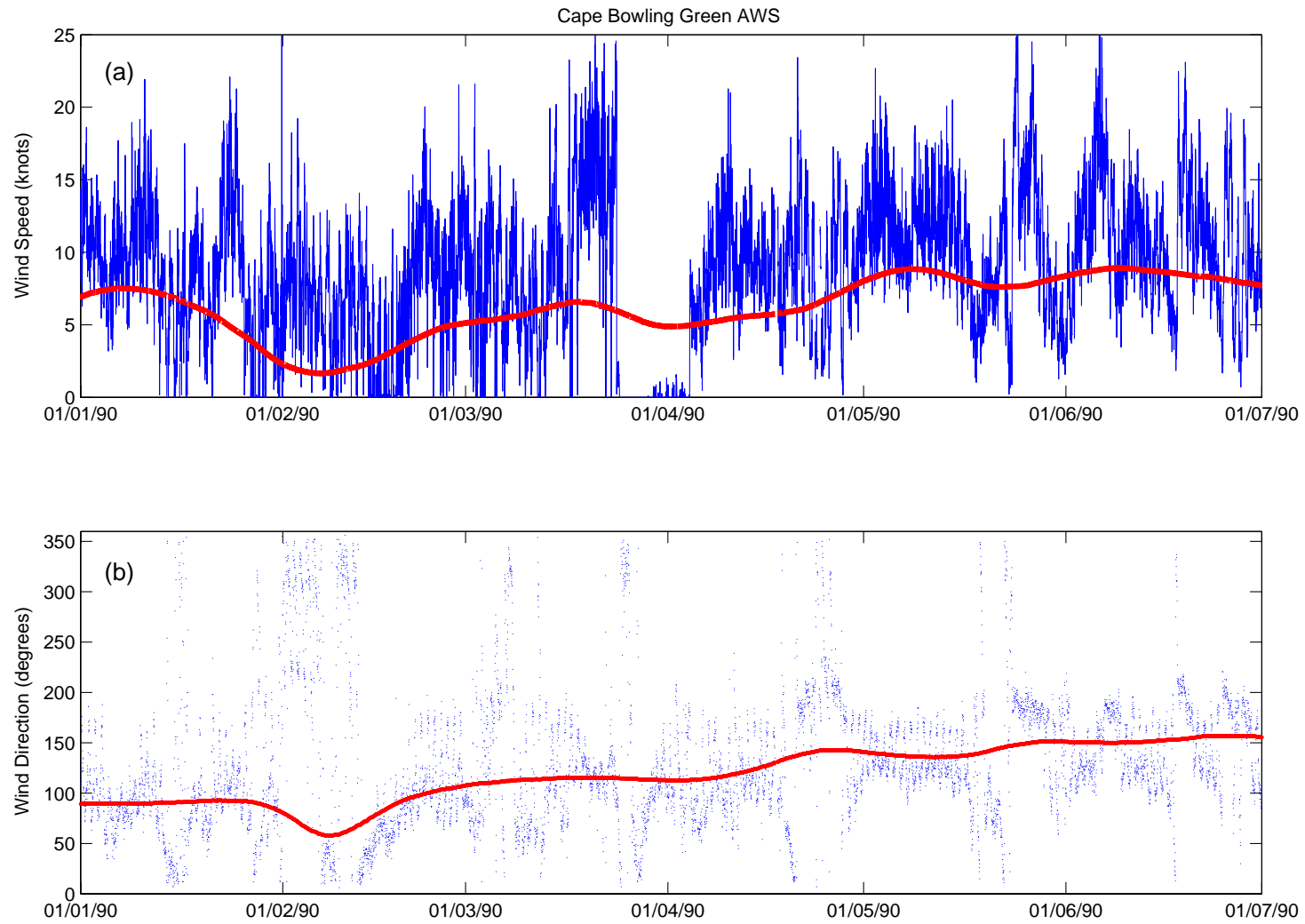


**Figure 8.** Cape Bowling Green winds for the 1 Jan to 30 June 1990 period: (a) wind speed (blue – raw winds, red – low pass filtered); (b) wind direction (blue – raw winds, red – low pass filtered).

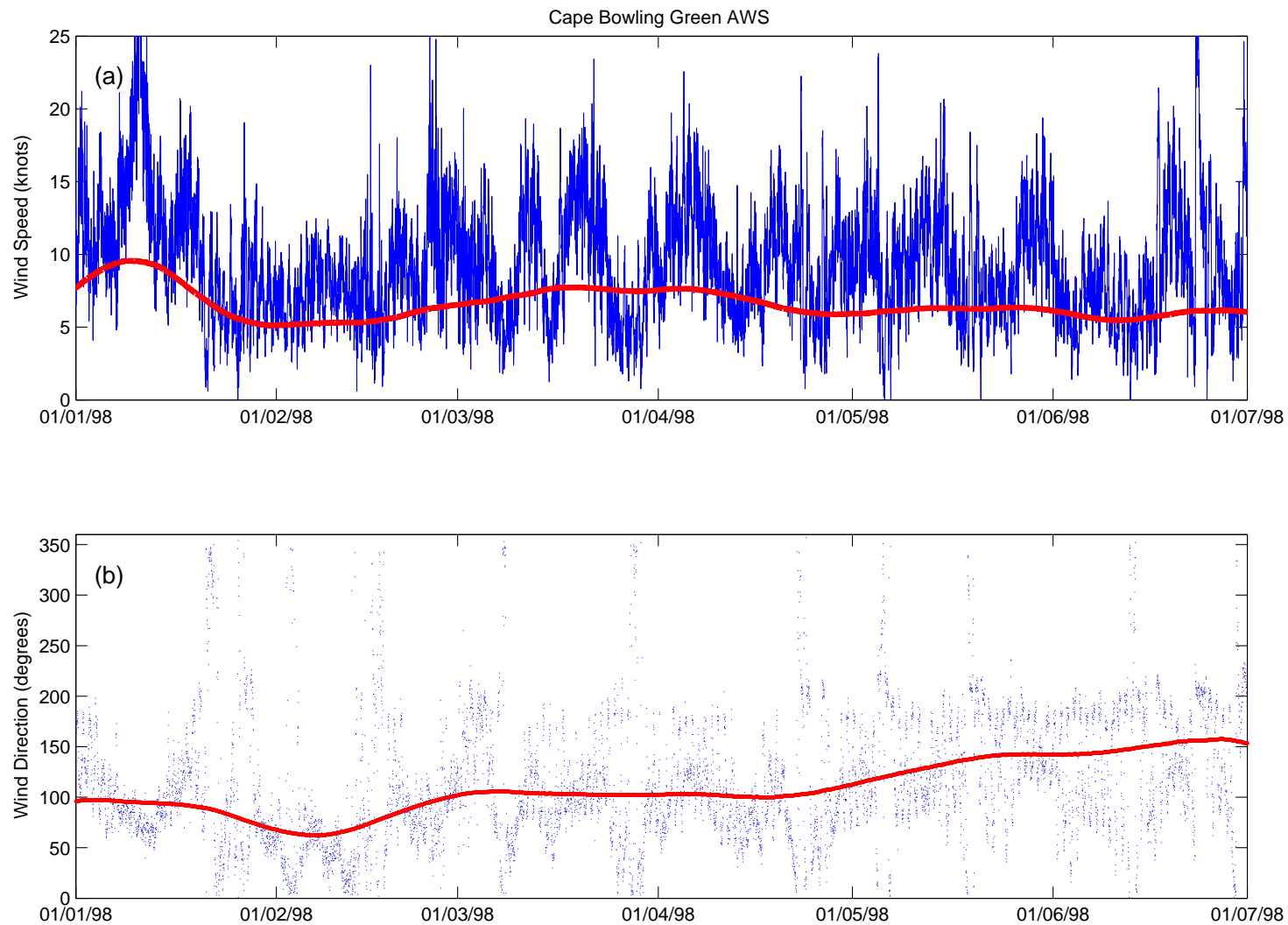


**Figure 9.** Cape Bowling Green winds for the 1 Jan to 30 June 1998 period: (a) wind speed (blue – raw winds, red – low pass filtered); (b) wind direction (blue – raw winds, red – low pass filtered).

### Synthetic EAC and Cape Bowling Green Winds

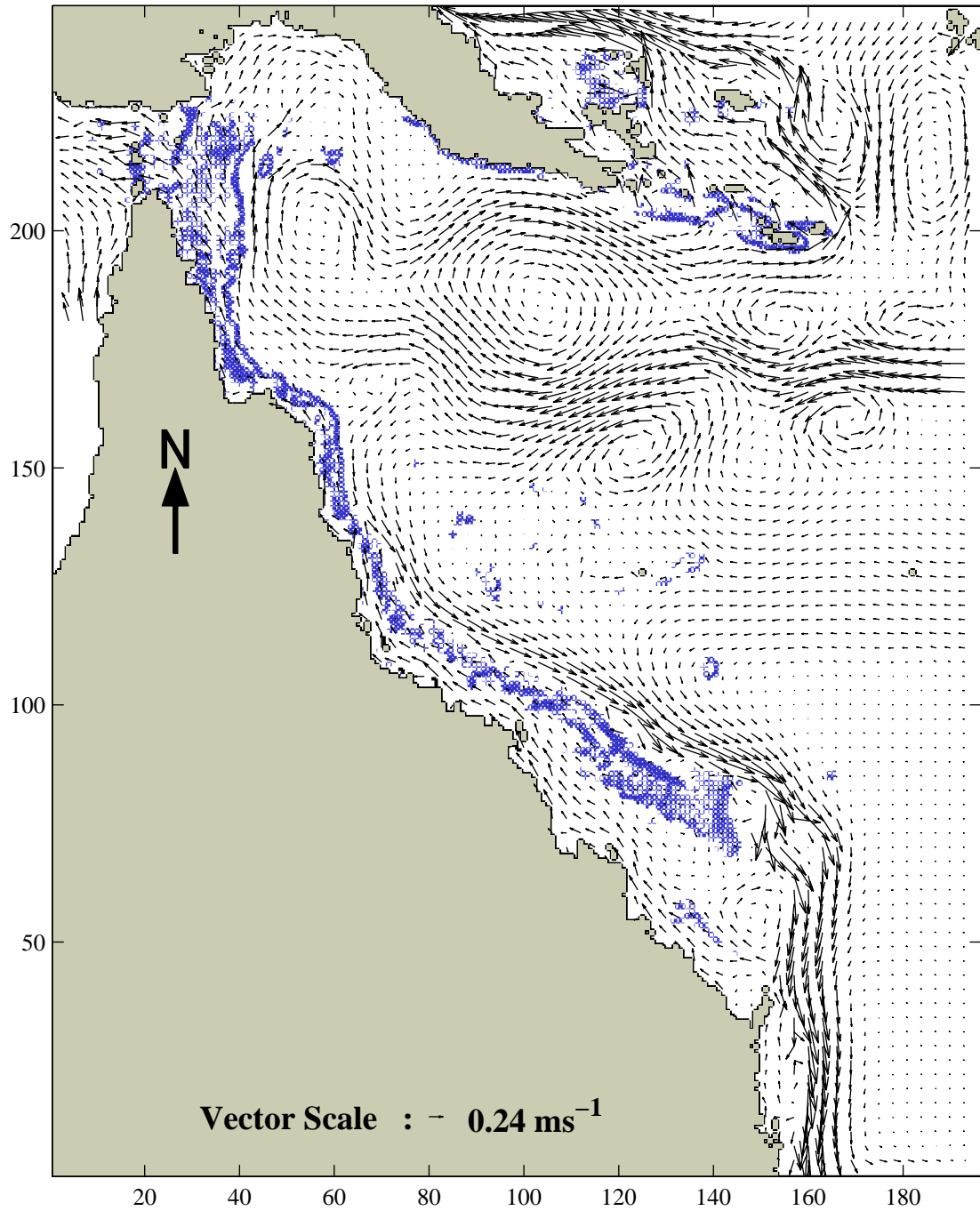


**Figure 10.** A snap shot of a computed East Australian Current with wind forcing. An *A*-grid simulation with vectors plotted every third grid point.

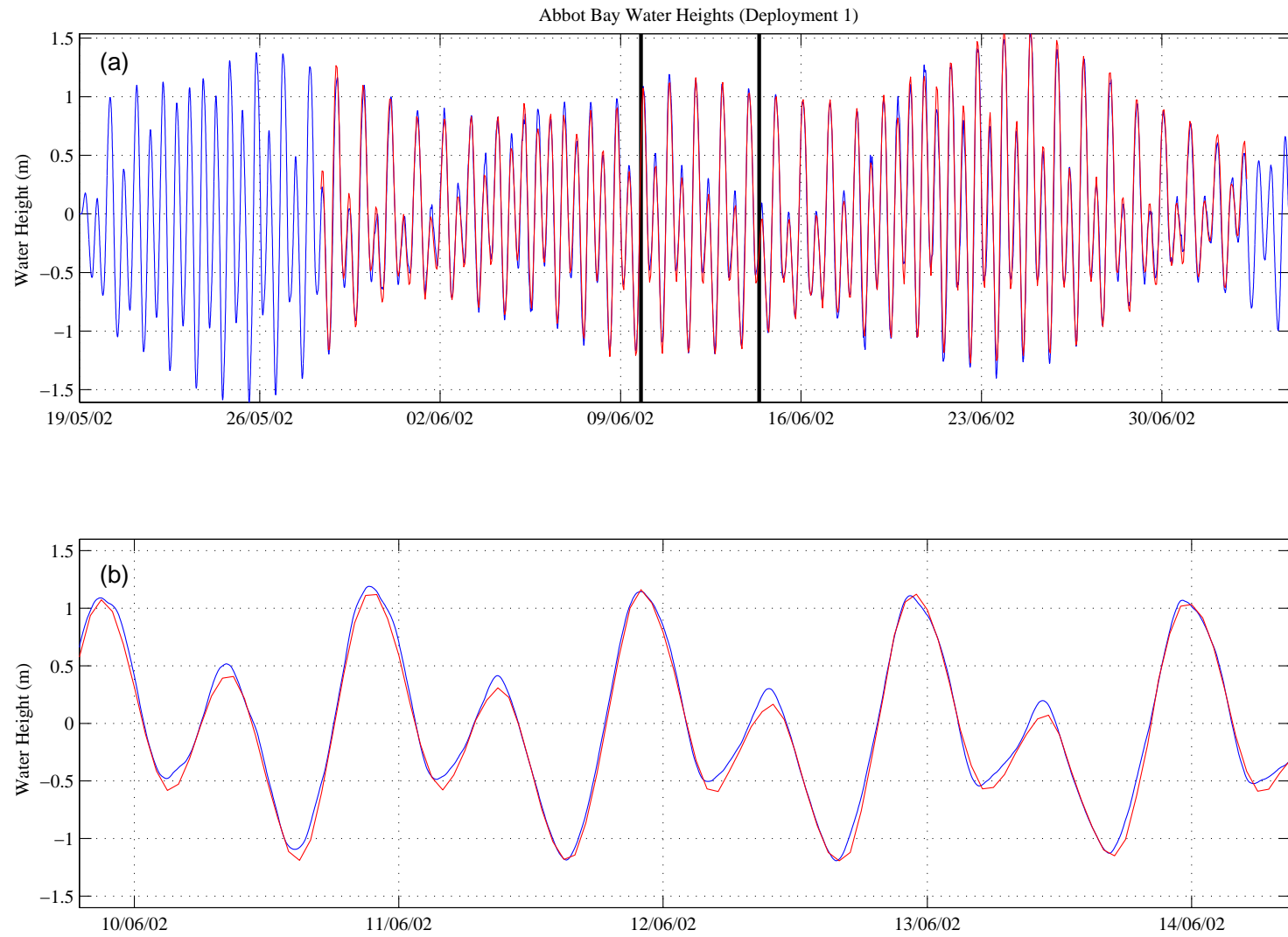


**Figure 11.** Comparison of modelled and measured water height time histories during deployment 1 (28 May to 3 July): (a) shows the complete time histories; (b) for a shorter time segment bounded by the black lines in (a).

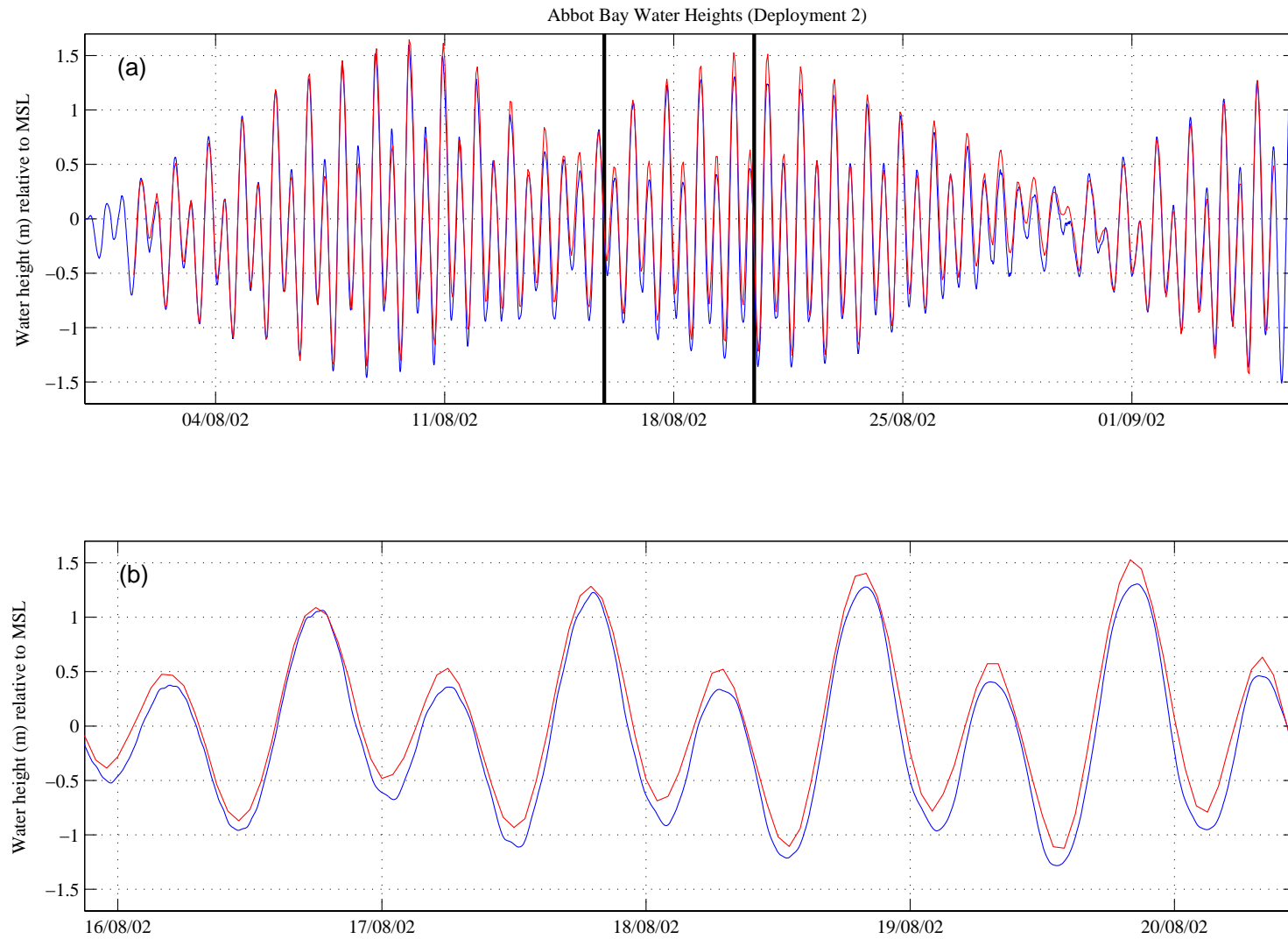


**Figure 12.** Comparison of modelled and measured water height time histories during deployment 2 (1 Aug to 5 Sept): (a) shows the complete time histories; (b) for a shorter time segment bounded by the black lines in (a).

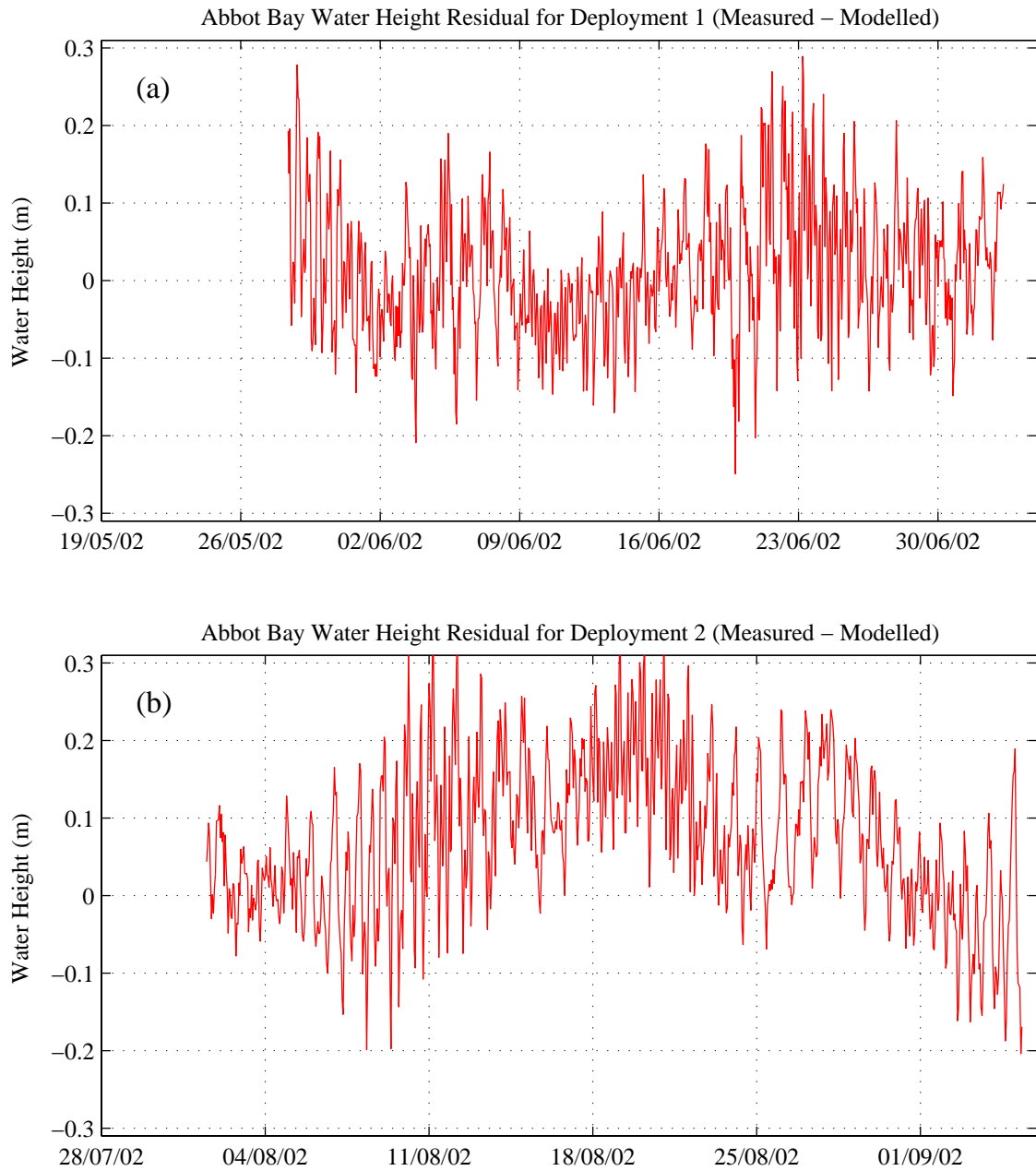


**Figure 13.** Water height residuals calculated as measured minus modelled: (a) deployment 1; (b) deployment 2.



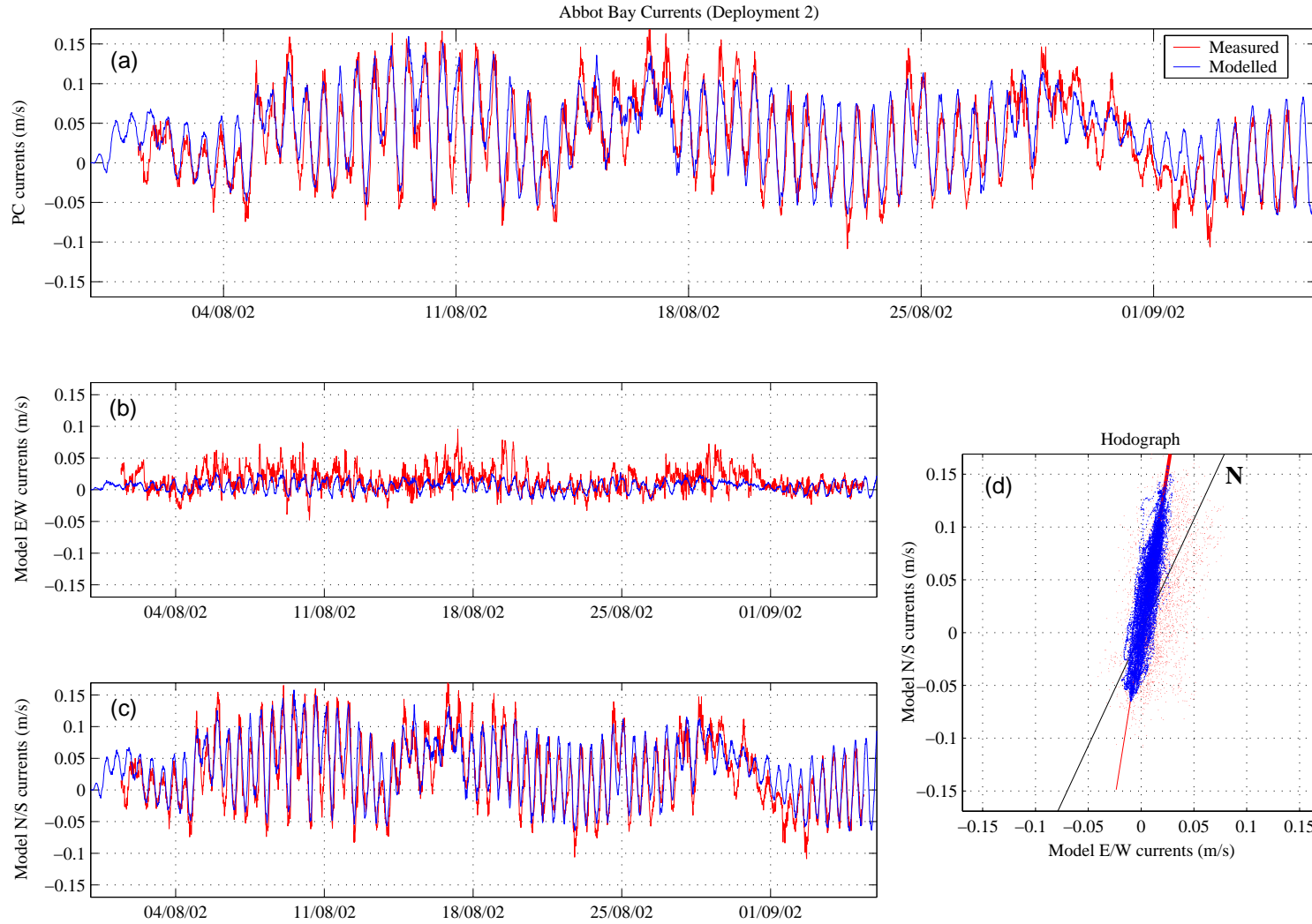


**Figure 14.** Comparison of modelled and measured current time histories during deployment 2: (a) Principal component current; (b) X directed current component; (c) Y directed current component; (d) Hodograph, black line is drawn north-south, red show principal component orientation with the thicker part indicating the positive direction.

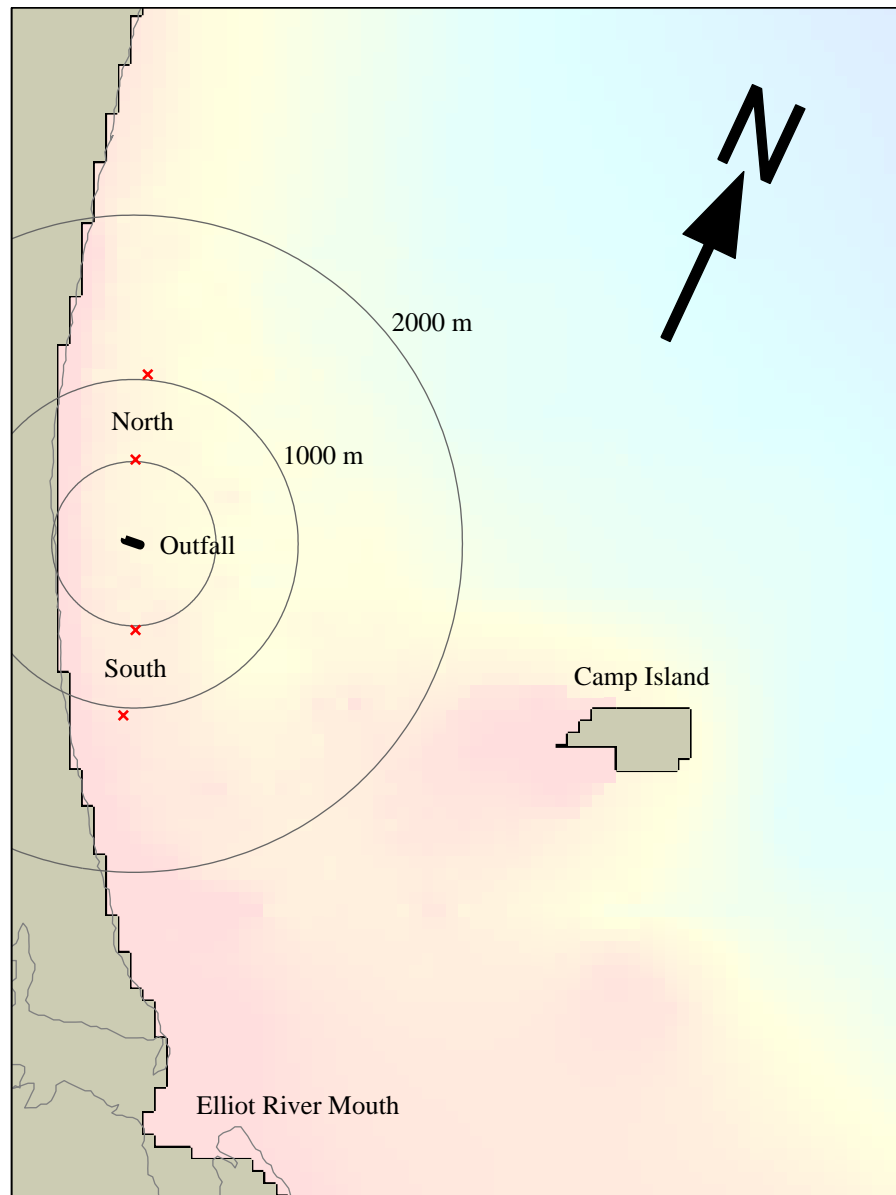


**Figure 15.** Outfall site. The concentric circles centred on the outfall locations have radii of 500, 1000 and 2000 m. × indicate location where concentration time history are output.

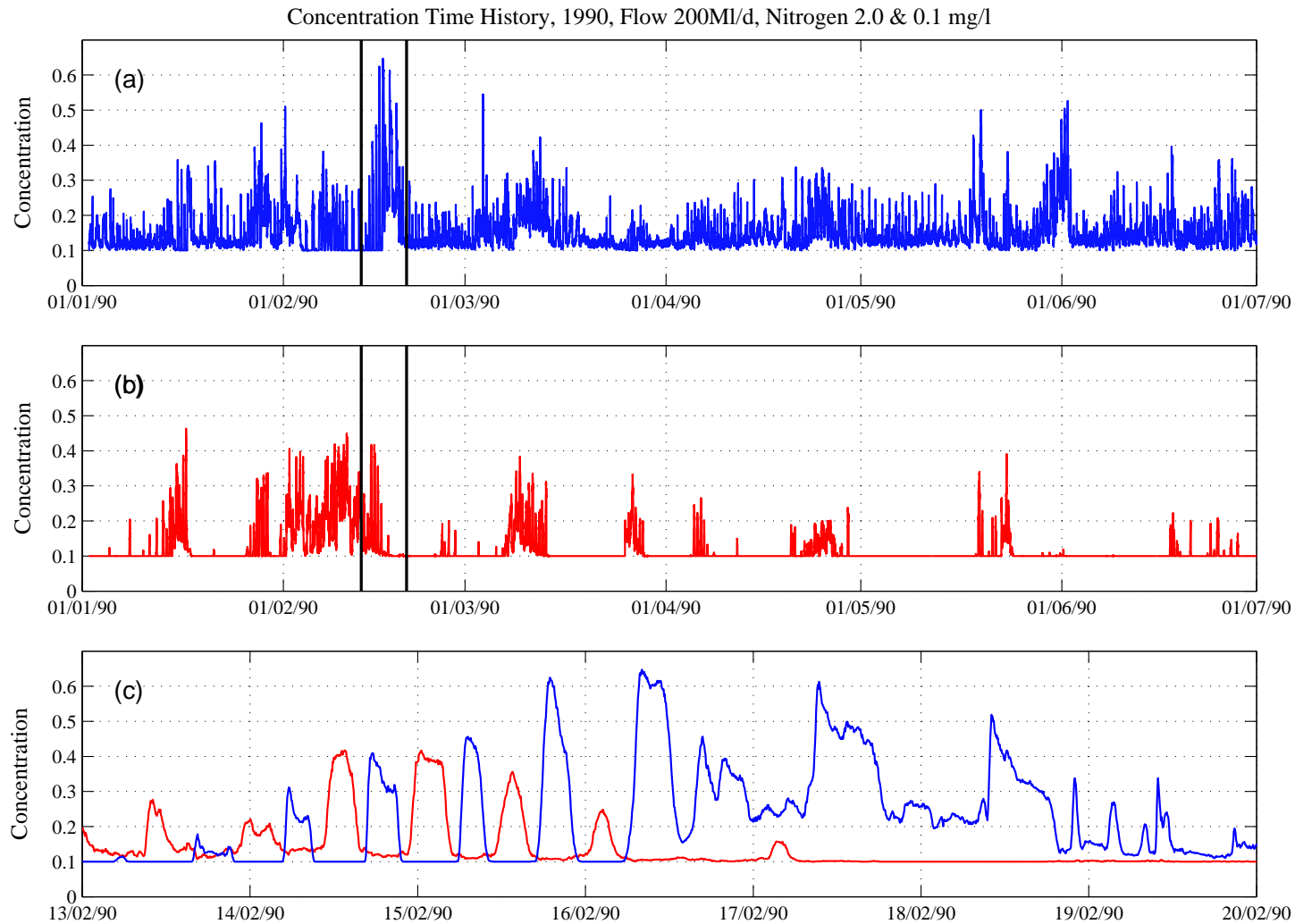


**Figure 16.** Concentration time history for Nitrogen during year 1990; (a) blue, point 500 m north of outfall; (b) red, point 500 m south of outfall; (c) shorter time window indicated by vertical lines in (a) and (b). Assumes a discharge of 200 Ml/d, Discharge concentration 2.0 mg/l, Background concentration 0.1 mg/l. Concentric circles at 500, 1000 and 2000 m radii.

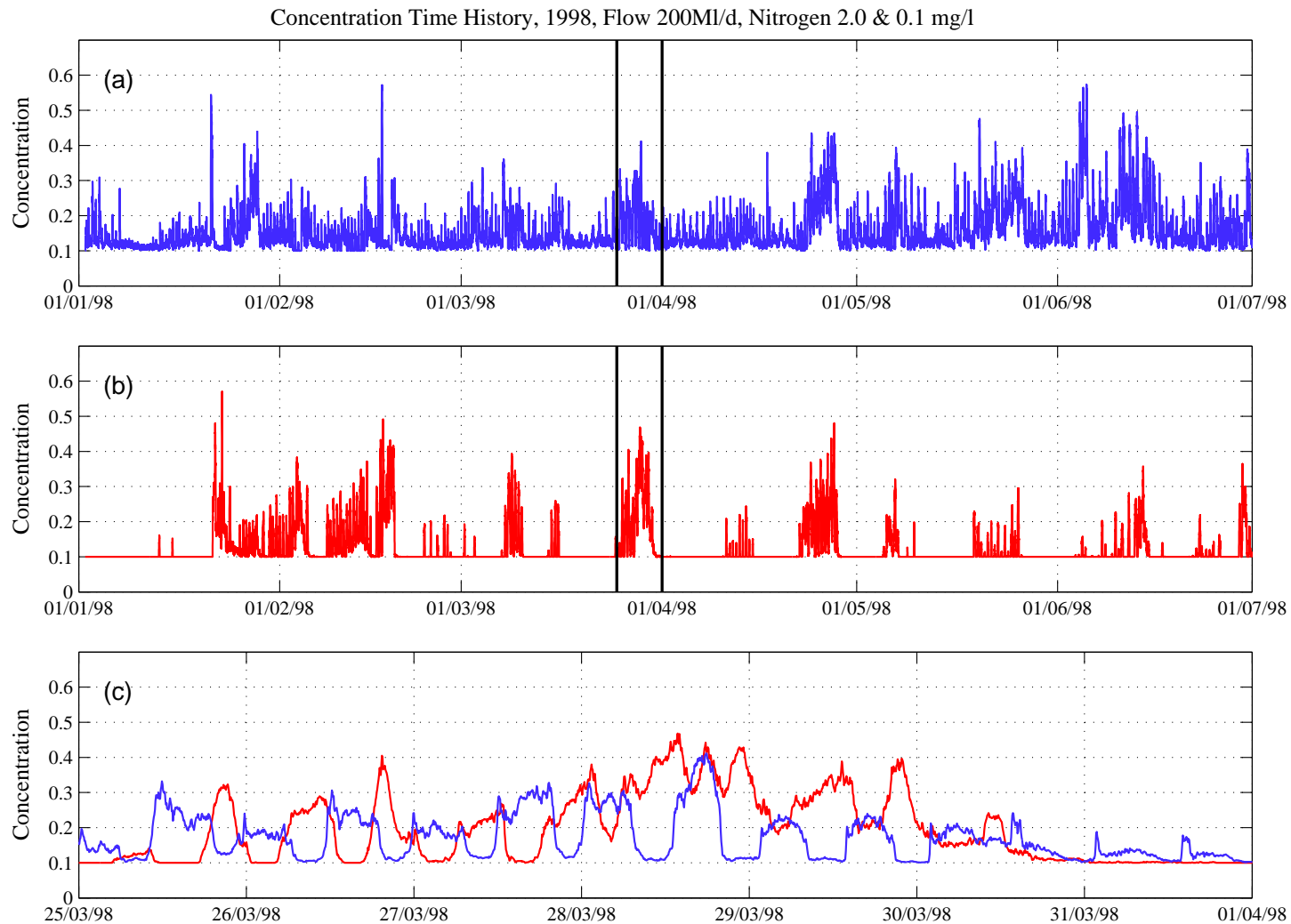


**Figure 17.** Concentration time history for Nitrogen during year 1998; (a) blue, point 500 m north of outfall; (b) red, point 500 m south of outfall; (c) shorter time window indicated by vertical lines in (a) and (b). Assumes a discharge of 200 Ml/d, Discharge concentration 2.0 mg/l, Background concentration 0.1 mg/l. Concentric circles at 500, 1000 and 2000 m radii.

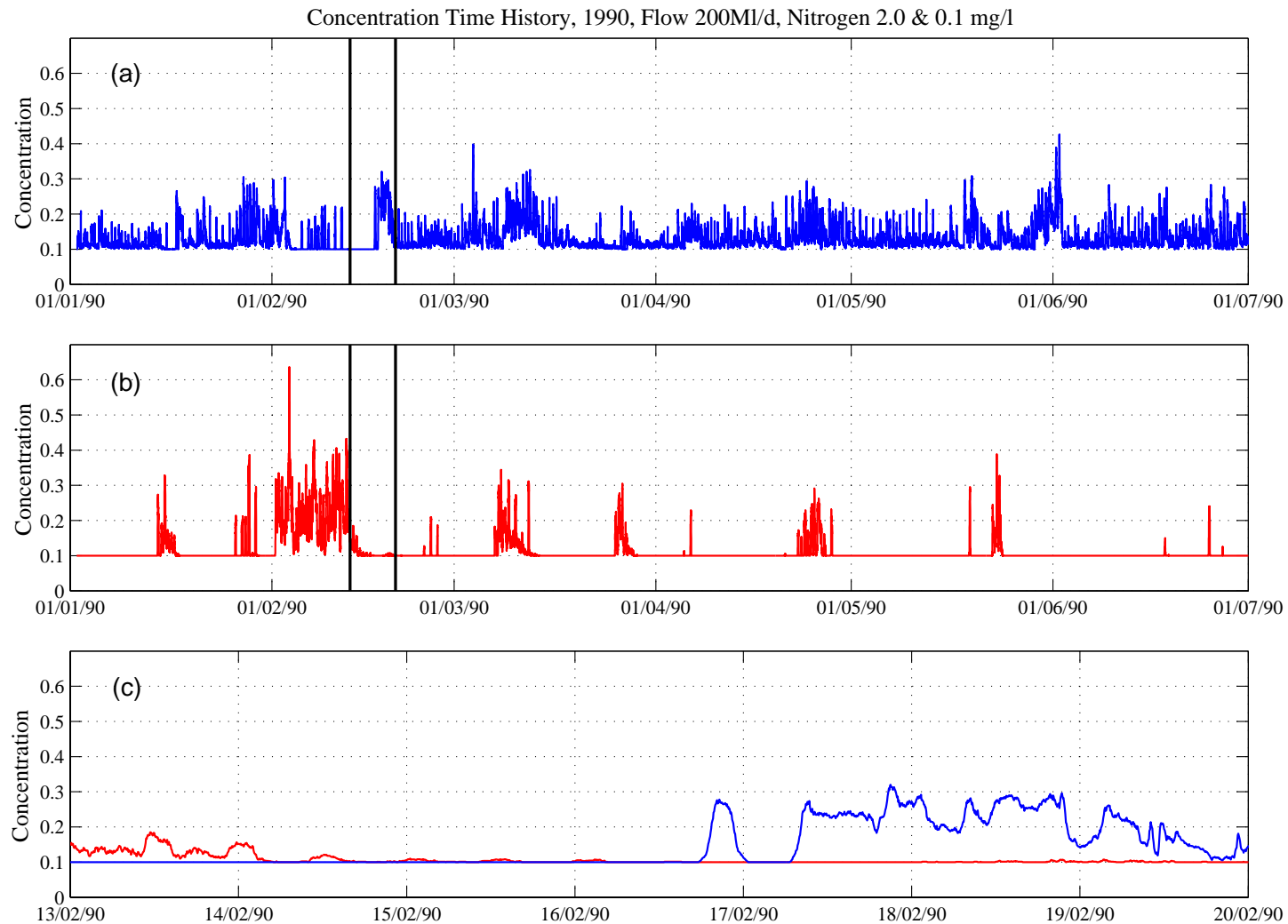


**Figure 18.** Concentration time history for Nitrogen during year 1990; (a) blue, point 1000 m north of outfall; (b) red, point 1000 m south of outfall; (c) shorter time window indicated by vertical lines in (a) and (b). Assumes a discharge of 200 Ml/d, Discharge concentration 2.0 mg/l, Background concentration 0.1 mg/l. Concentric circles at 500, 1000 and 2000 m radii.

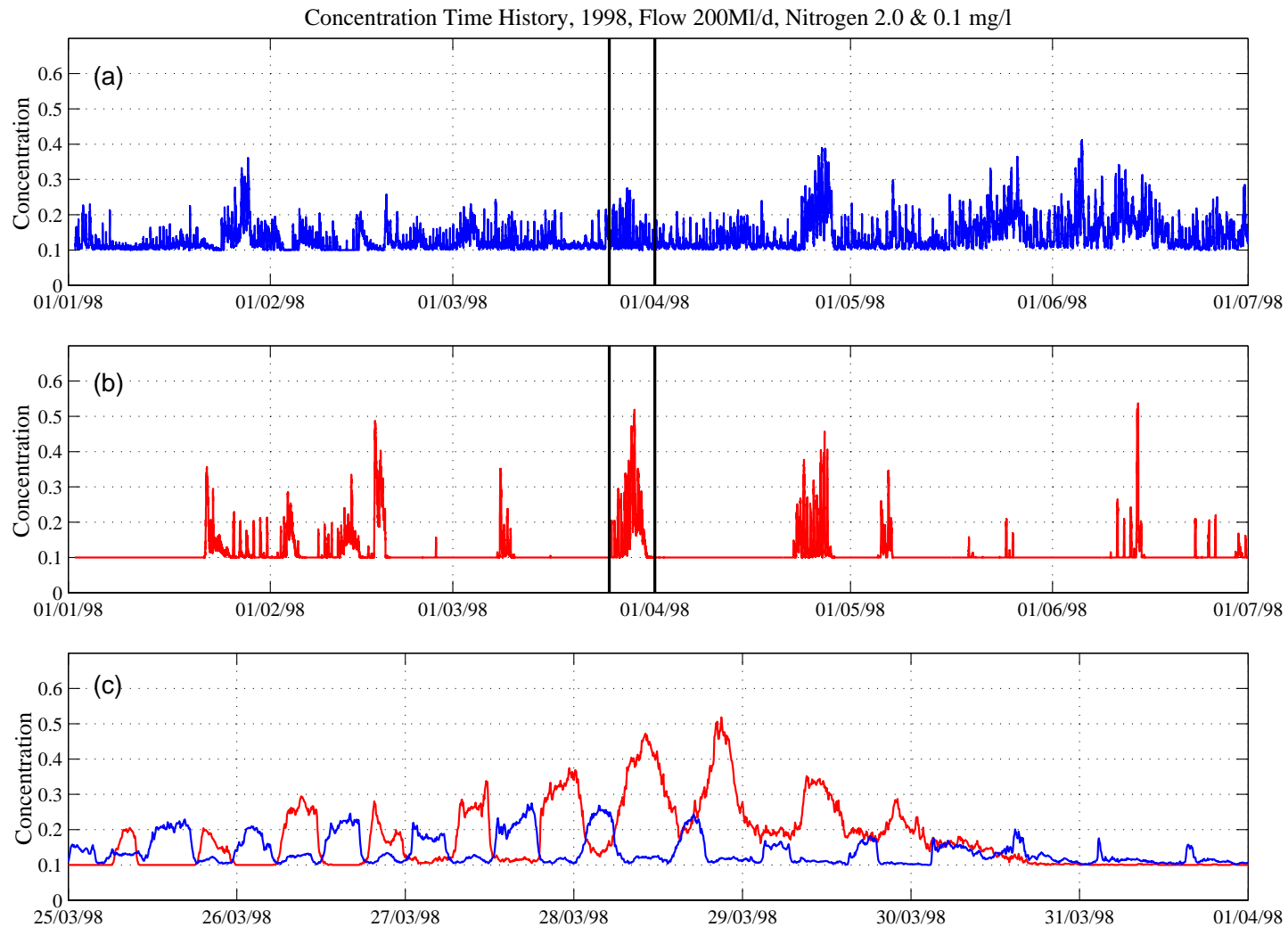


**Figure 19.** Concentration time history for Nitrogen during year 1998; (a) blue, point 1000 m north of outfall; (b) red, point 1000 m south of outfall; (c) shorter time window indicated by vertical lines in (a) and (b). Assumes a discharge of 200 MI/d, Discharge concentration 2.0 mg/l, Background concentration 0.1 mg/l. Concentric circles at 500, 1000 and 2000 m radii.

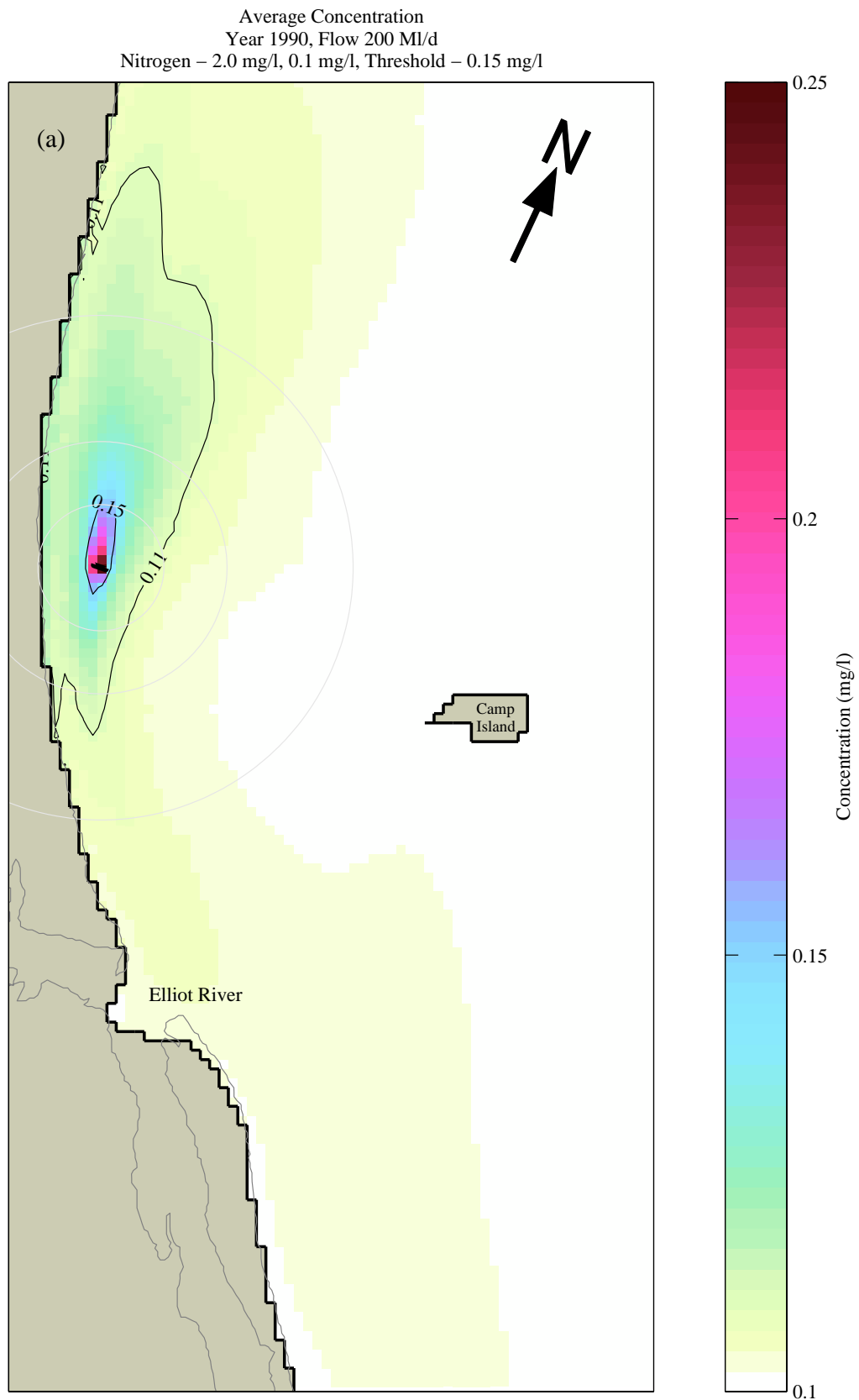


**Figure 20a.** Average Concentration (*Nitrogen*) for the six-month discharge period of 1990 (200MI/d). Contours indicate the background plus 10% (0.11 mg/l) and the threshold (0.15 mg/l) levels. Concentric circles at 500, 1000 and 2000 m radii.

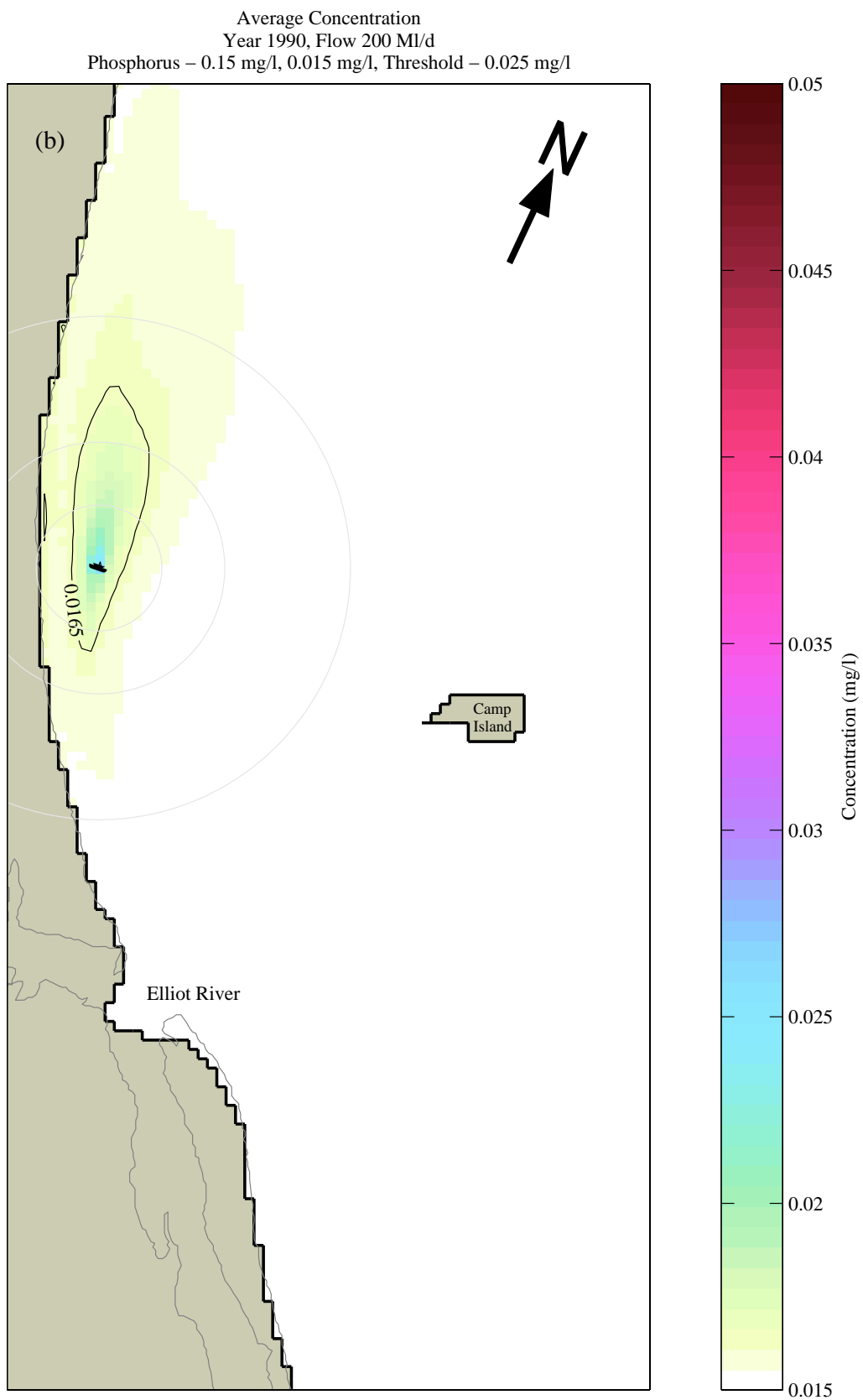


**Figure 20b.** Average Concentration (*Phosphorus*) for the six-month discharge period of 1990 (200Ml/d). Contours indicate the background plus 10% (0.0165 mg/l) and the threshold (0.025 mg/l) levels. Concentric circles at 500, 1000 and 2000 m radii.



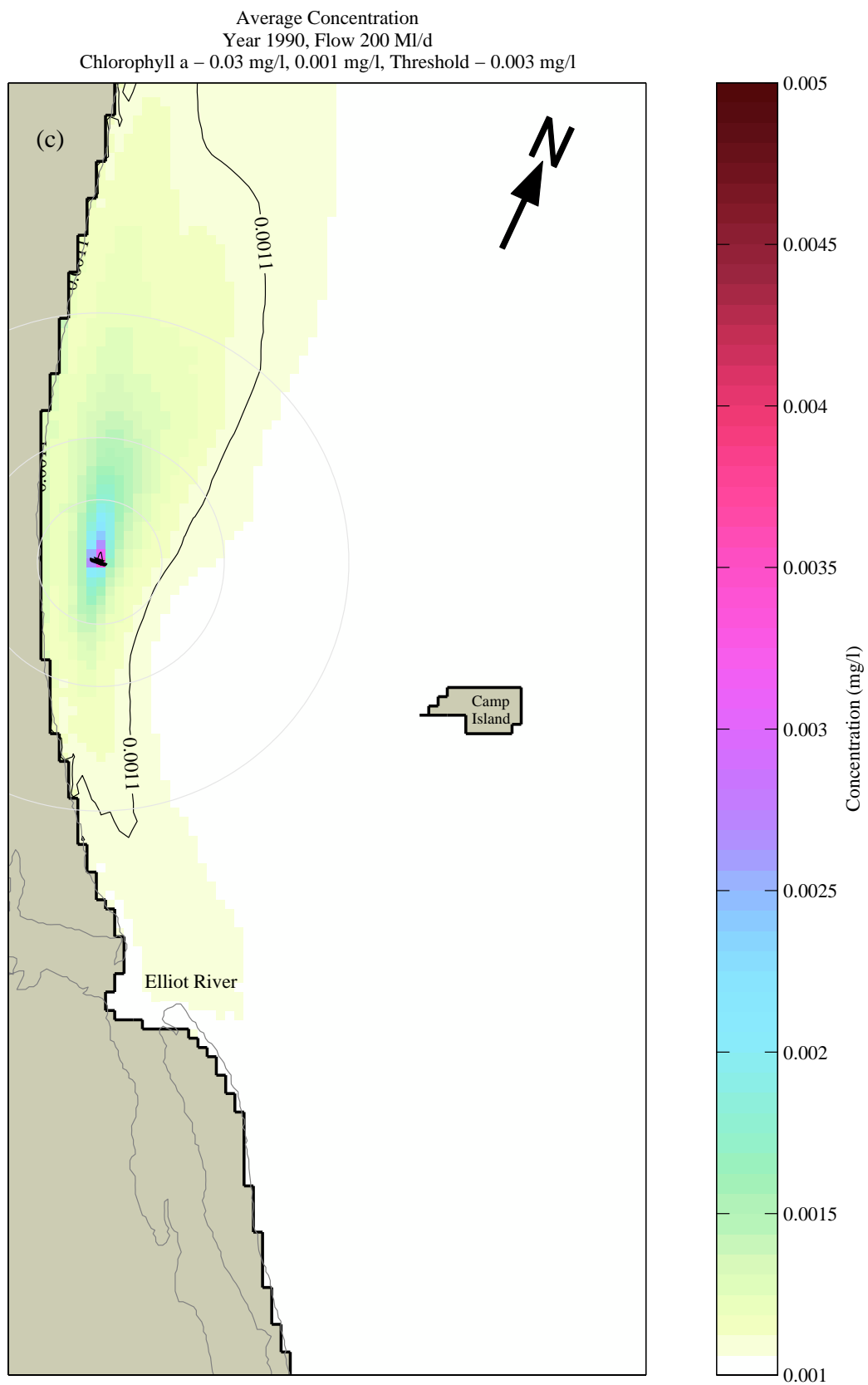


**Figure 20c.** Average Concentration (*Chlorophyll-a*) for the six-month discharge period of 1990 (200MI/d). Contours indicate the background plus 10% (0.0011 mg/l) and the threshold (0.003 mg/l) levels. Concentric circles at 500, 1000 and 2000 m radii.

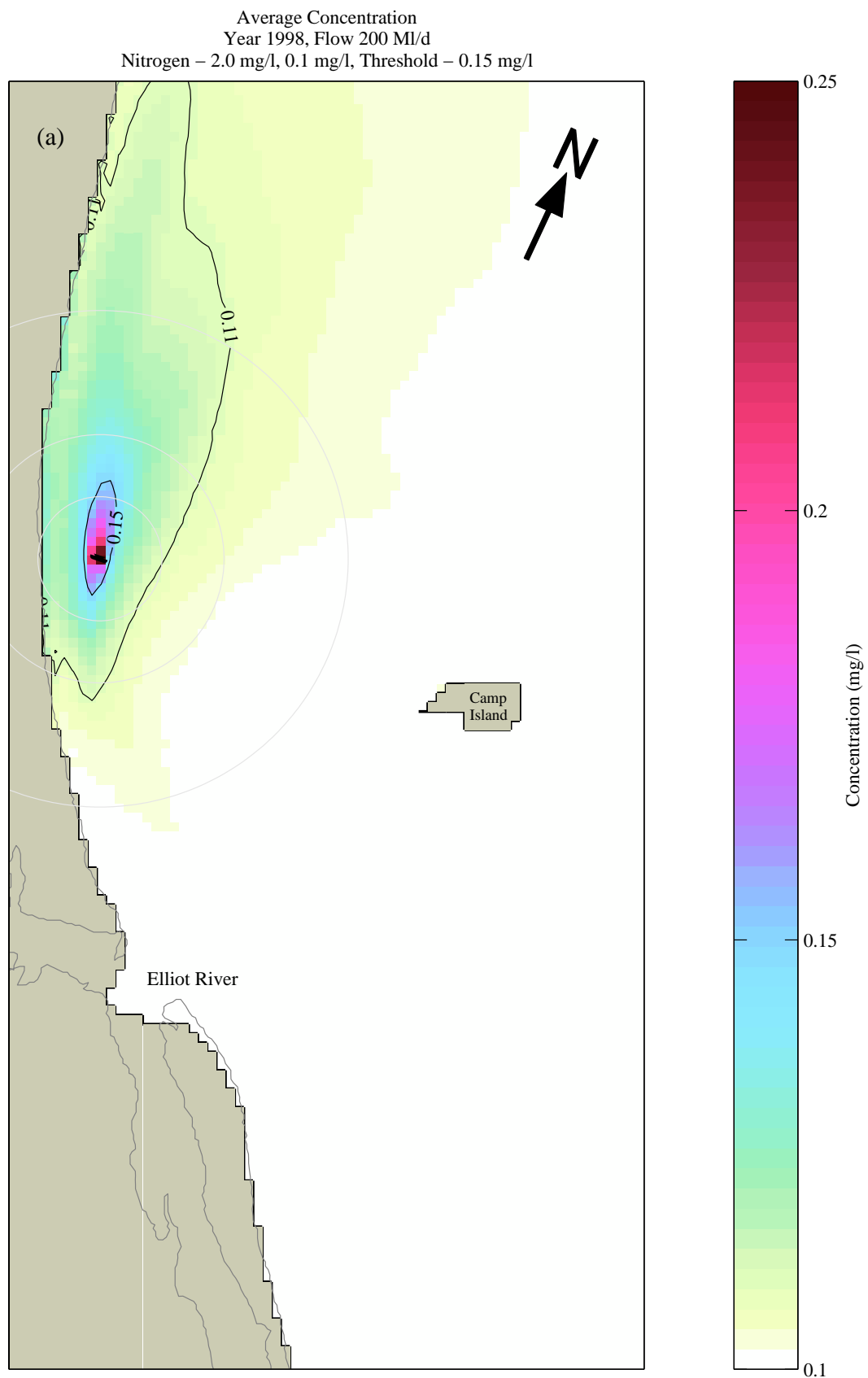


**Figure 21a.** Average Concentration (*Nitrogen*) for the six-month discharge period of 1998 (200Ml/d). Contours indicate the background plus 10% (0.11 mg/l) and the threshold (0.15 mg/l) levels. Concentric circles at 500, 1000 and 2000 m radii.

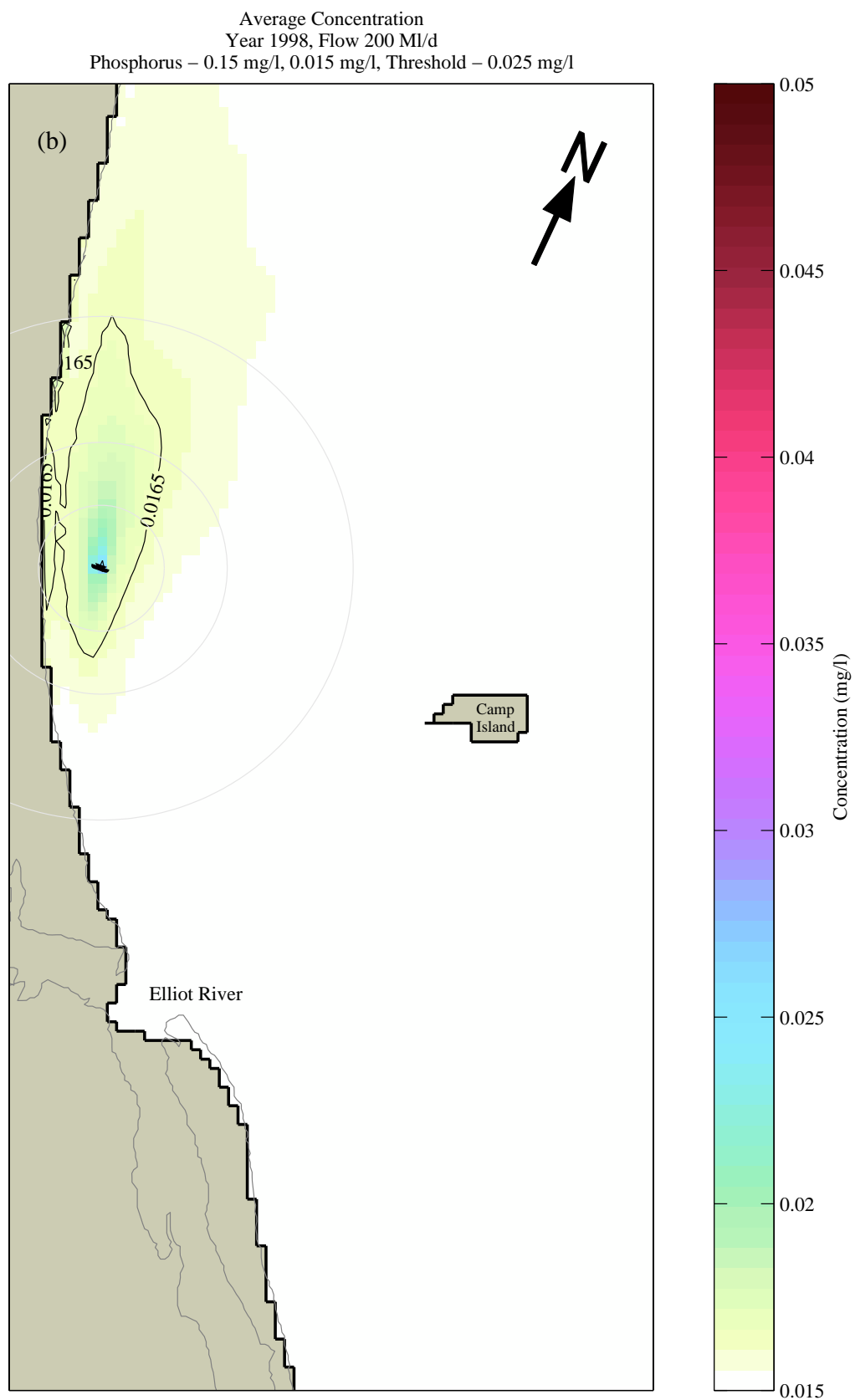


**Figure 21b.** Average Concentration (*Phosphorus*) for the six-month discharge period of 1998 (200ML/d). Contours indicate the background plus 10% (0.0165 mg/l) and the threshold (0.025 mg/l) levels. Concentric circles at 500, 1000 and 2000 m radii.

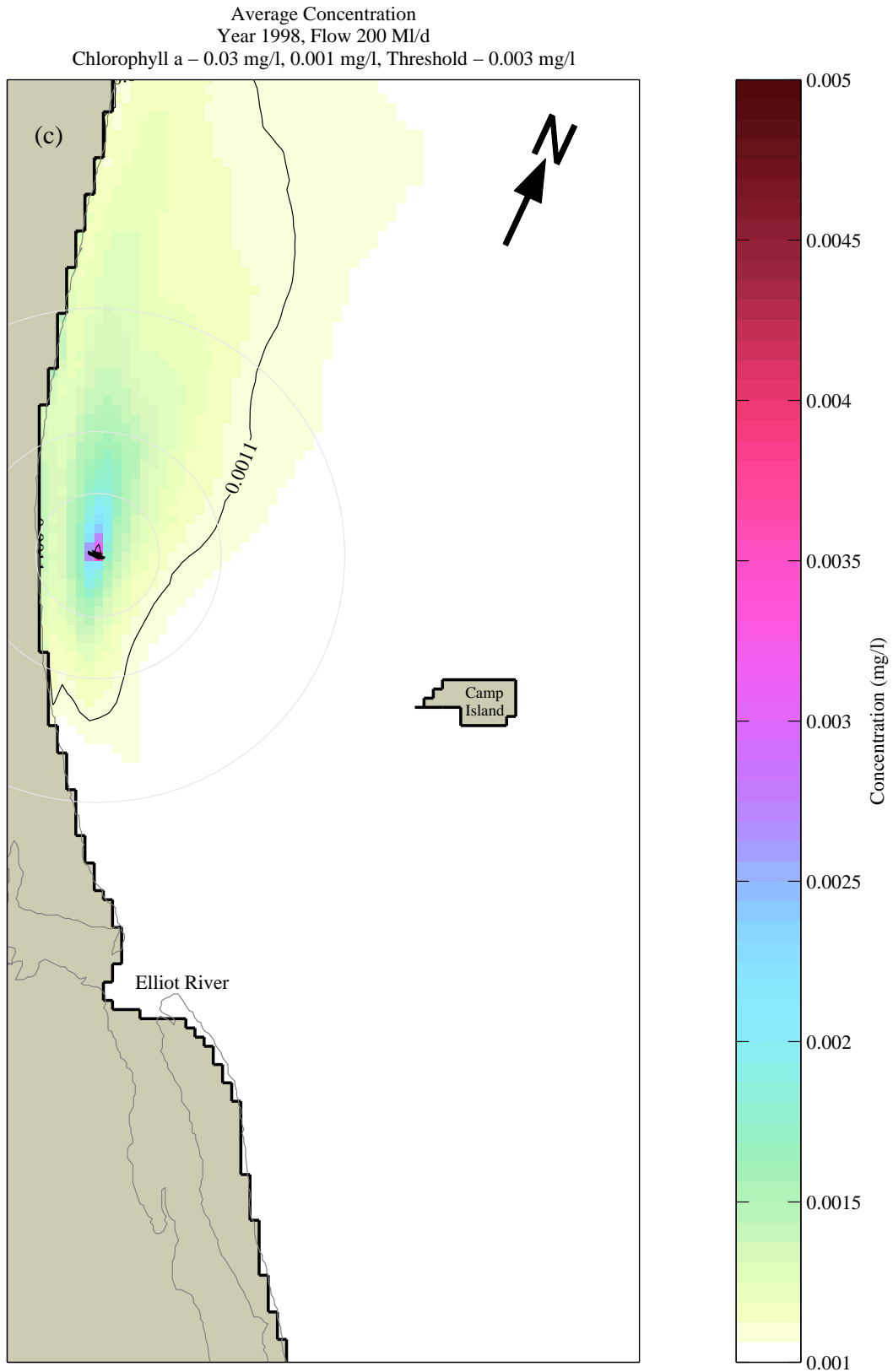


**Figure 21c.** Average Concentration (*Chlorophyll-a*) for the six-month discharge period of 1998 (200ML/d). Contours indicate the background plus 10% (0.0011 mg/l) and the threshold (0.003 mg/l) levels. Concentric circles at 500, 1000 and 2000 m radii.

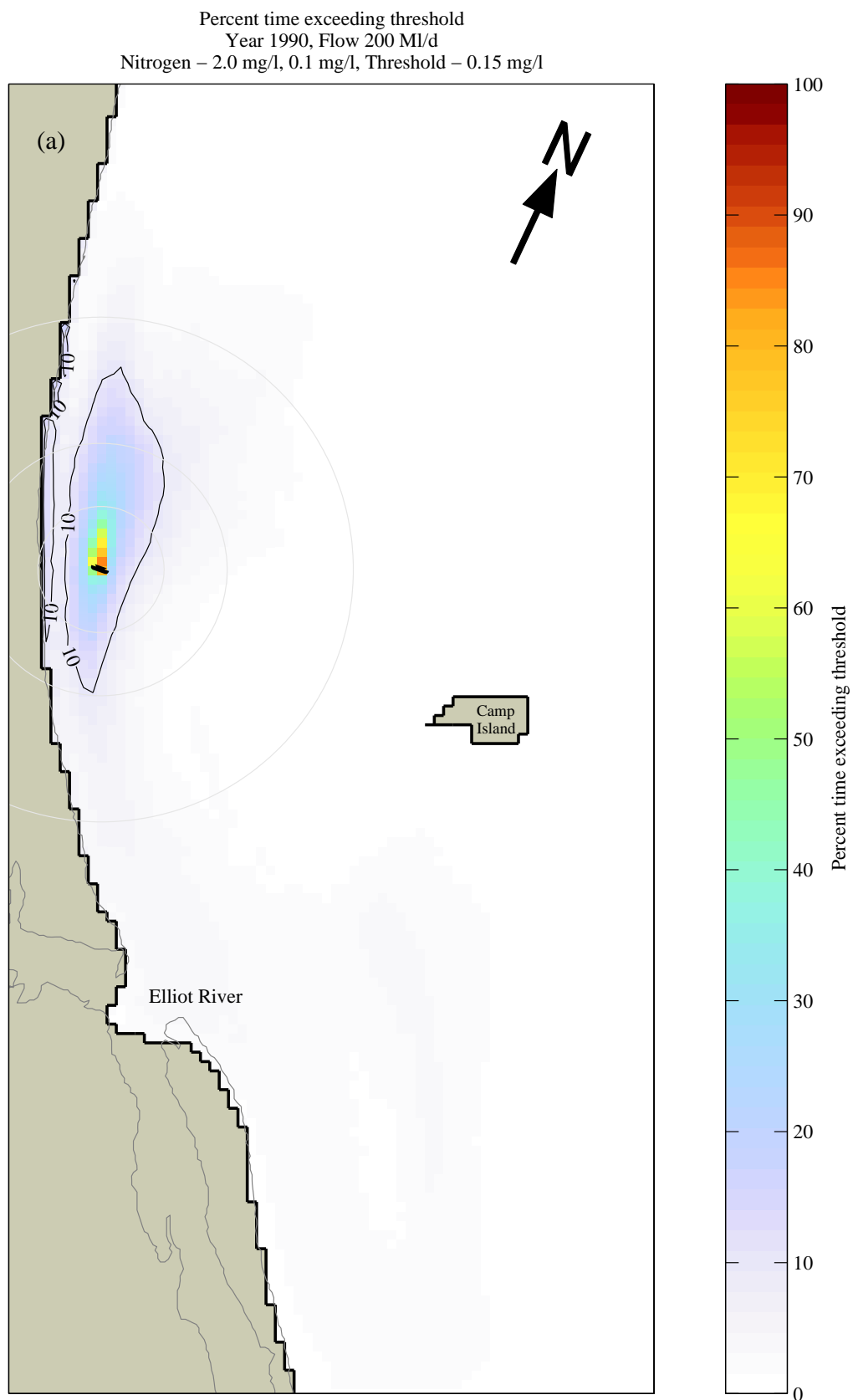


**Figure 22a.** Percent time exceeding threshold (*Nitrogen*) for the six-month discharge period of 1990 (200MI/d). Threshold level is 0.15 mg/l. The contour is at 10% level. Concentric circles at 500, 1000 and 2000 m radii.

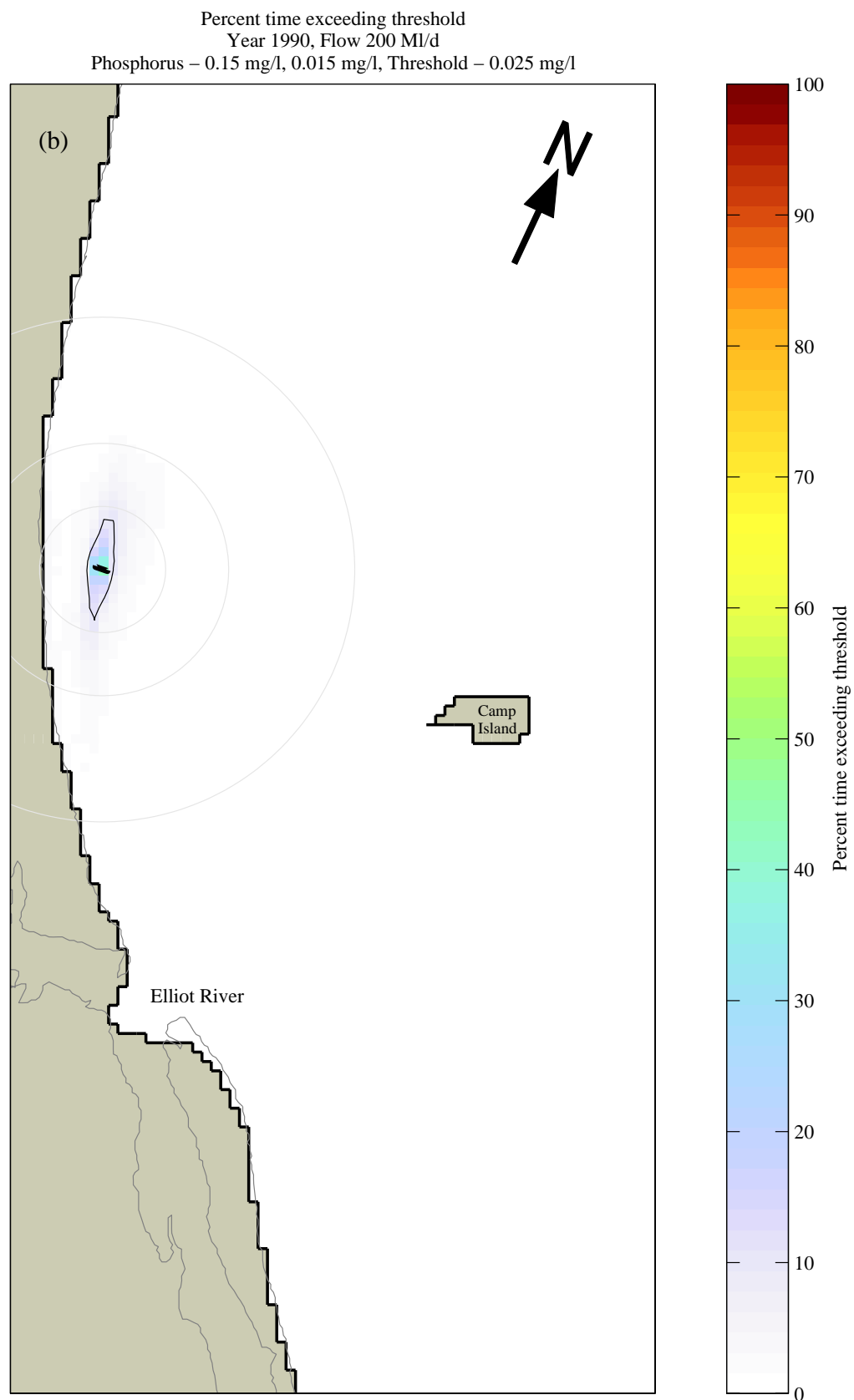


**Figure 22b.** Percent time exceeding threshold (*Phosphorus*) for the six-month discharge period of 1990 (200Ml/d). Threshold level is 0.025 mg/l. The contour is at 10% level. Concentric circles at 500, 1000 and 2000 m radii.

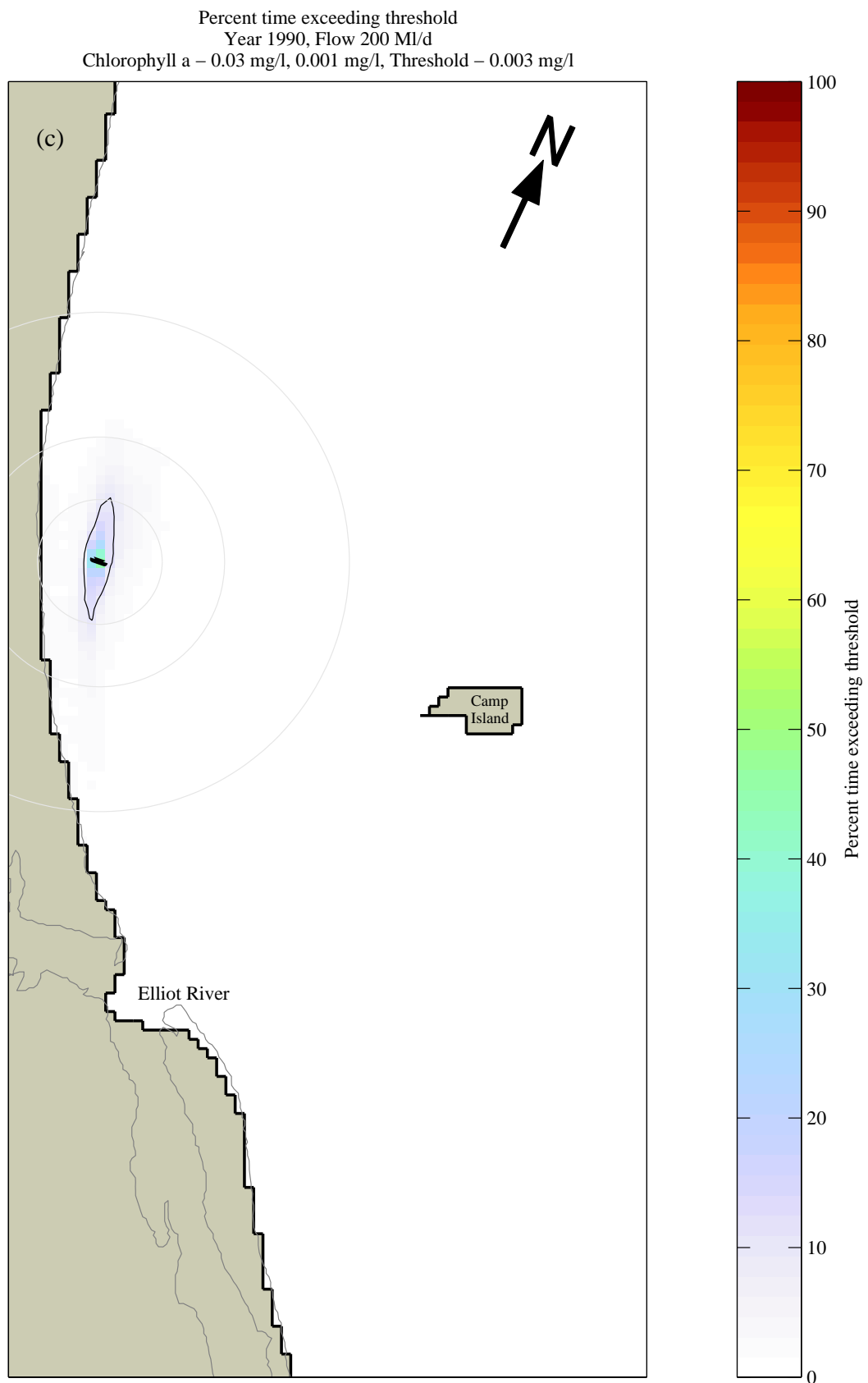


**Figure 22c.** Percent time exceeding threshold (*Chlorophyll-a*) for the six-month discharge period of 1990 (200MI/d). Threshold level is 0.003 mg/l. The contour is at 10% level. Concentric circles at 500, 1000 and 2000 m radii.

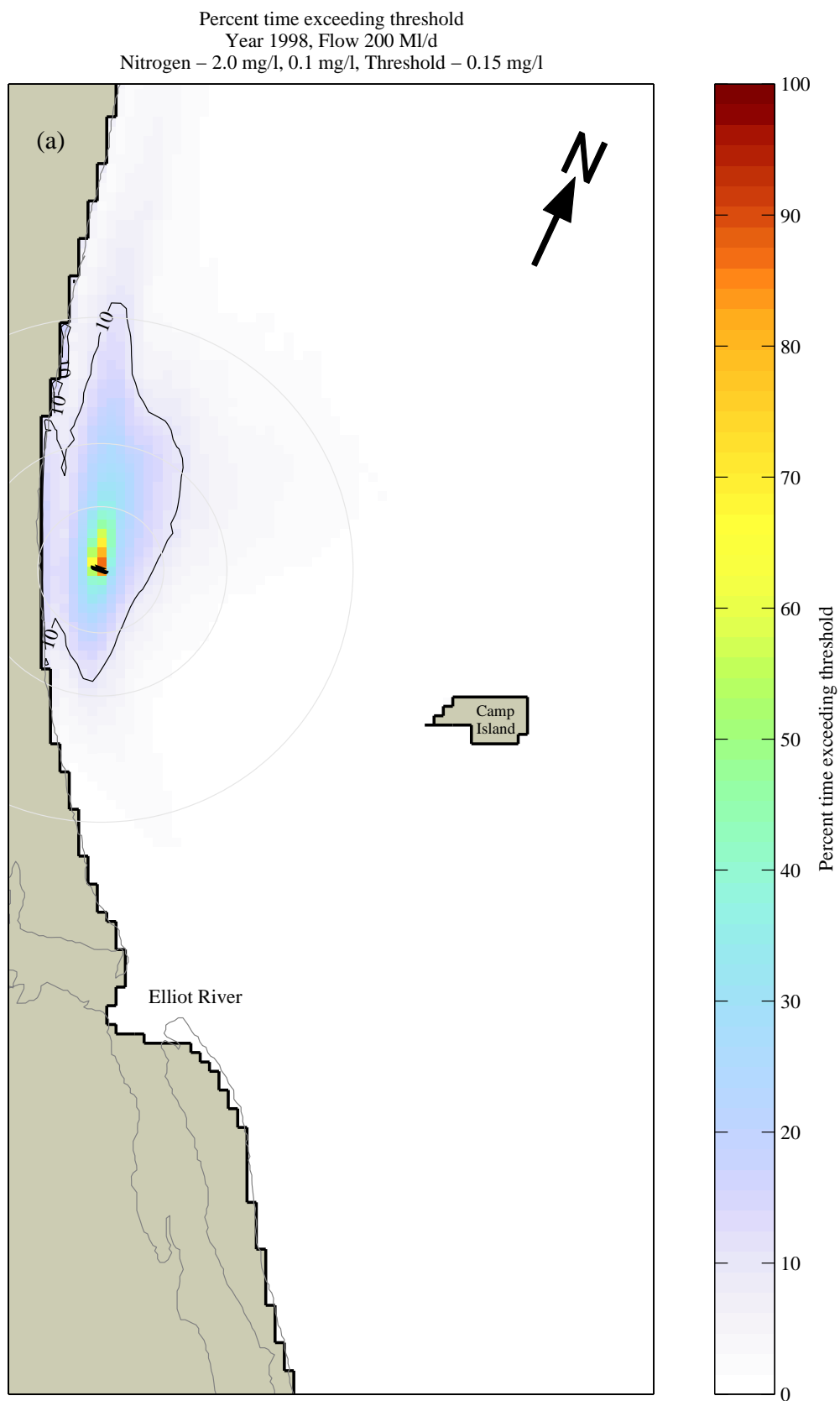


**Figure 23a.** Percent time exceeding threshold (*Nitrogen*) for the six-month discharge period of 1998 (200Ml/d). Threshold level is 0.15 mg/l. The contour is at 10% level. Concentric circles at 500, 1000 and 2000 m radii.



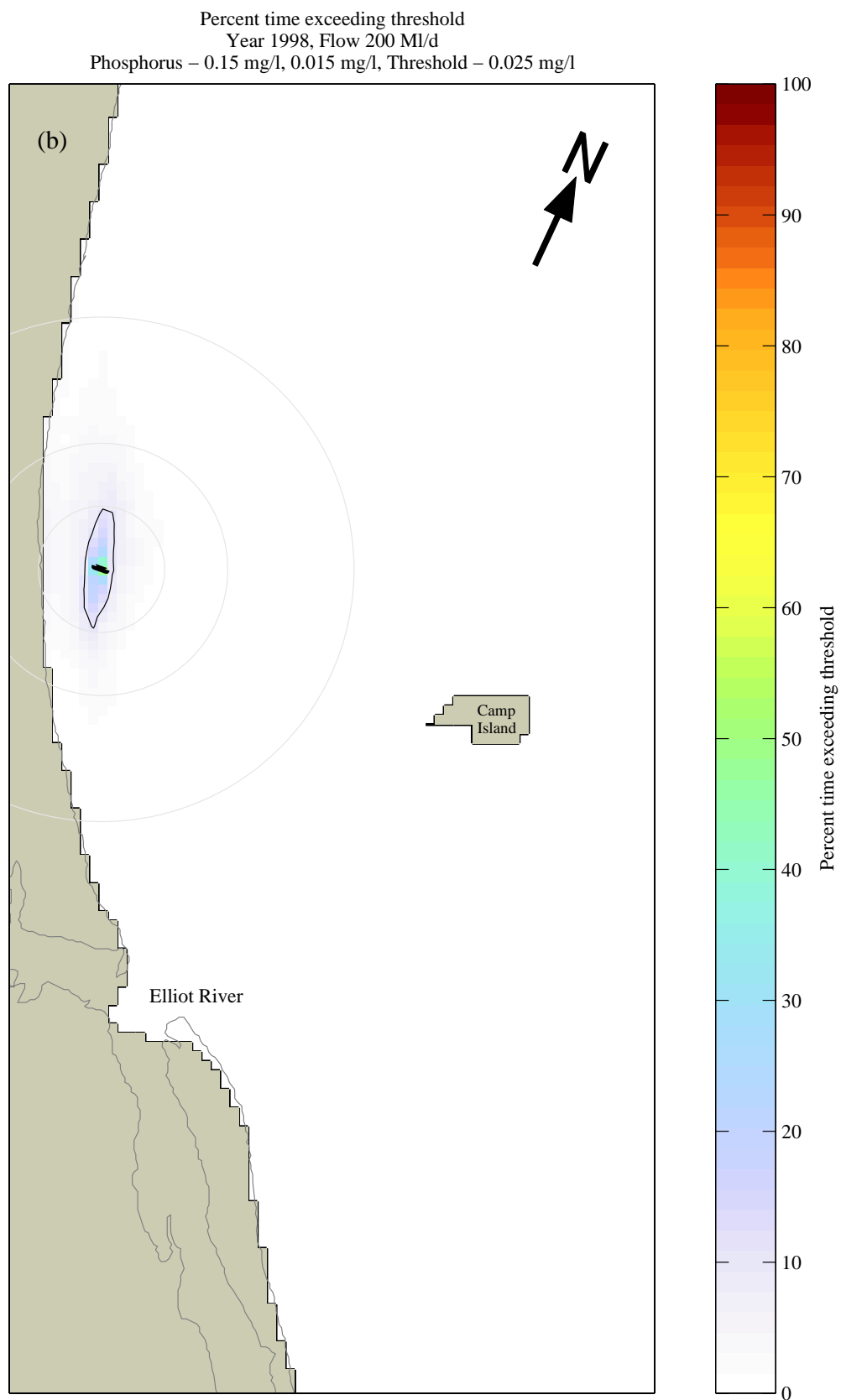


**Figure 23b.** Percent time exceeding threshold (*Phosphorus*) for the six-month discharge period of 1998 (200Ml/d). Threshold level is 0.025 mg/l. The contour is at 10% level. Concentric circles at 500, 1000 and 2000 m radii.

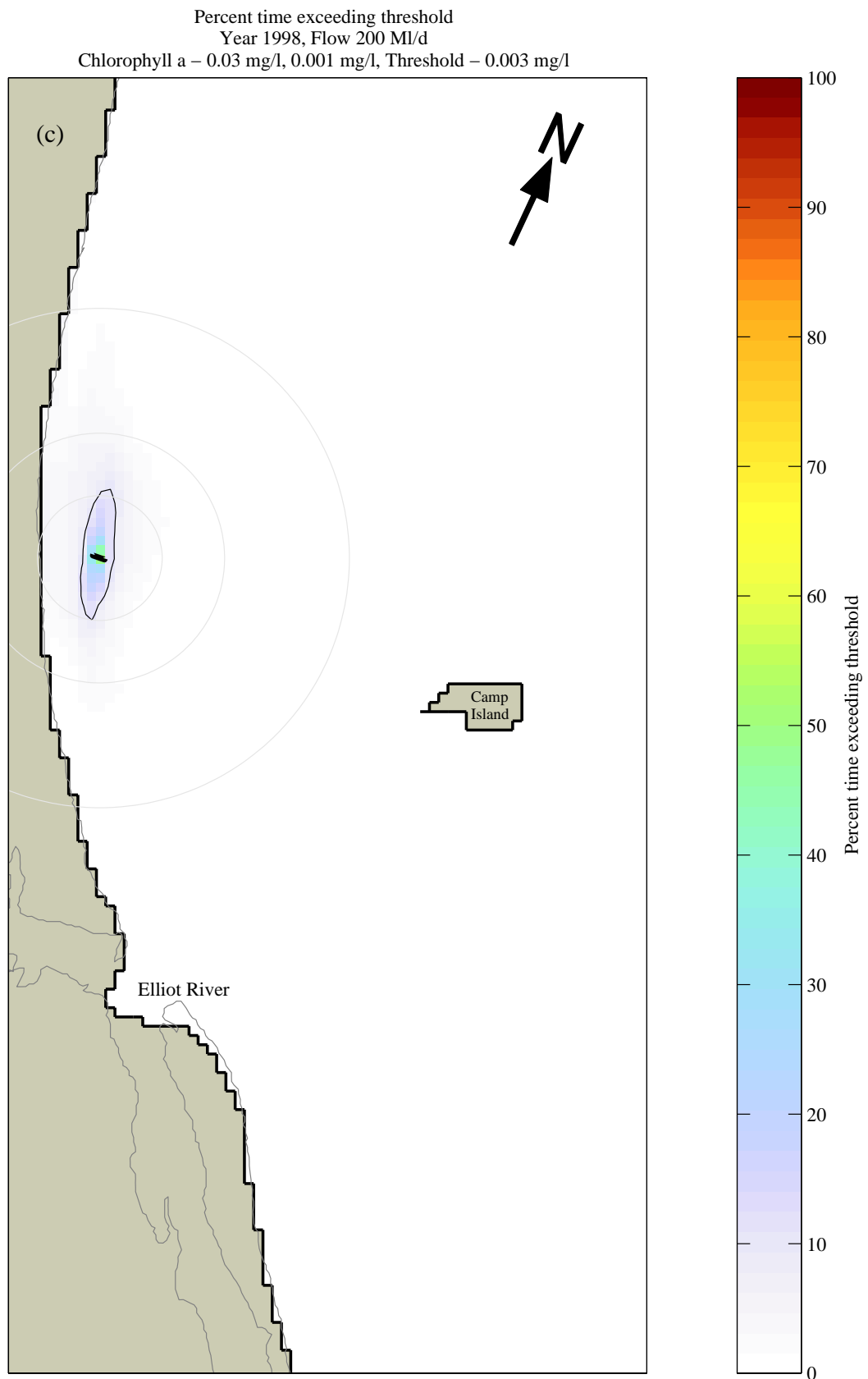


**Figure 23c.** Percent time exceeding threshold (*Chlorophyll-a*) for the six-month discharge period of 1998 (200MI/d). Threshold level is 0.003 mg/l. The contour is at 10% level. Concentric circles at 500, 1000 and 2000 m radii.

(a)

This map displays the spatial distribution of total suspended solids concentration in the Elliot River estuary. The color scale ranges from 0.1 mg/l (light yellow) to 0.25 mg/l (dark red). A prominent plume of high concentration (red/pink) is visible near the river mouth, extending towards the northeast. Concentration contours are labeled at 0.11 and 0.15 mg/l. The map includes a north arrow pointing towards the top right, a label for "Camp Island", and the "Elliot River" name. The coastline is shown as a thick black line.

50

Average Concentration  
 February 1990, Flow 200 MI/d  
 Phosphorus – 0.15 mg/l, 0.015 mg/l, Threshold – 0.025 mg/l

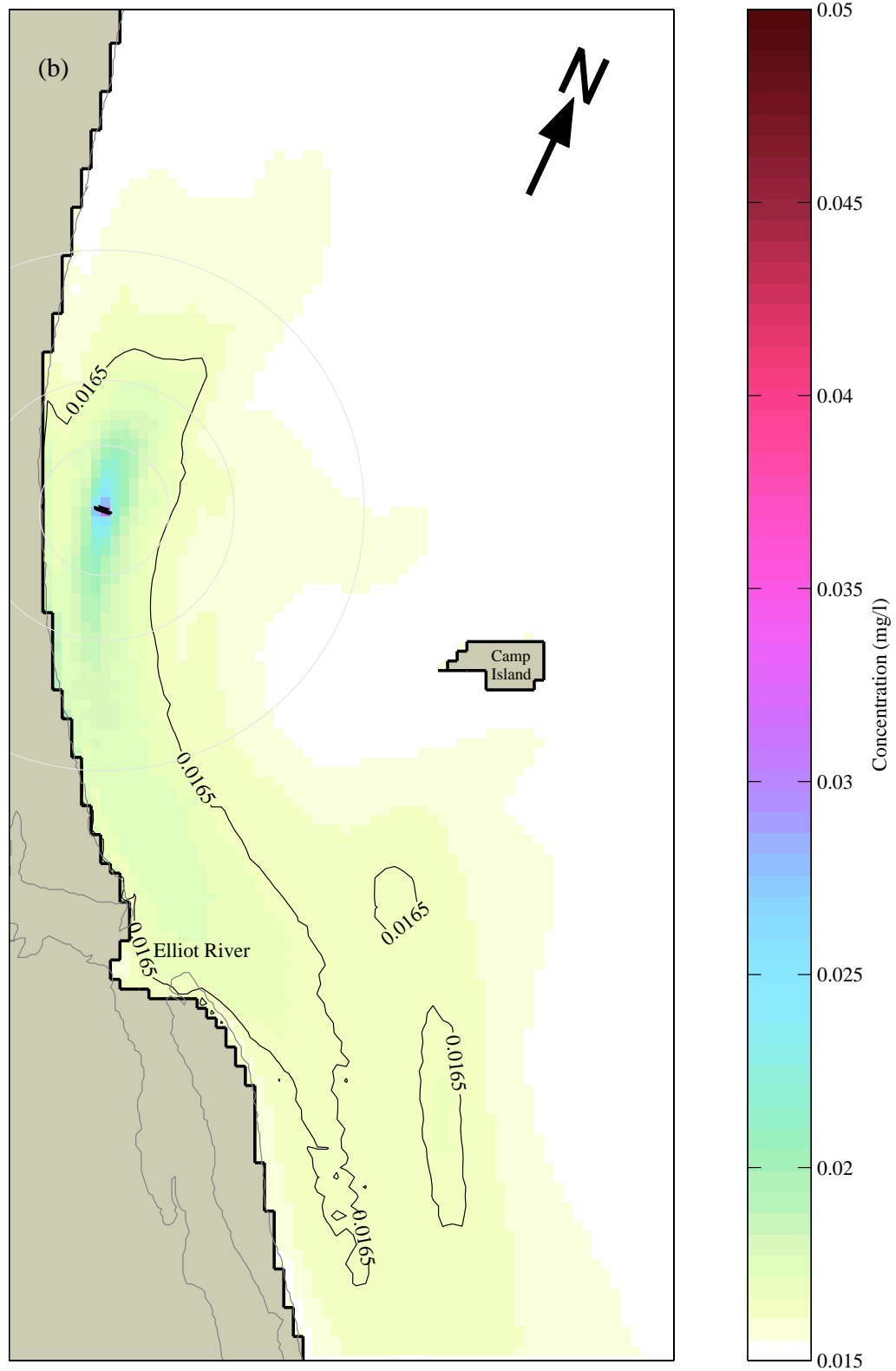


**Figure 24b.** Average Concentration (*Phosphorus*) for the February discharge period of 1990 (200MI/d). Contours indicate the background plus 10% (0.0165 mg/l) and the threshold (0.025 mg/l) levels. Concentric circles at 500, 1000 and 2000 m radii.



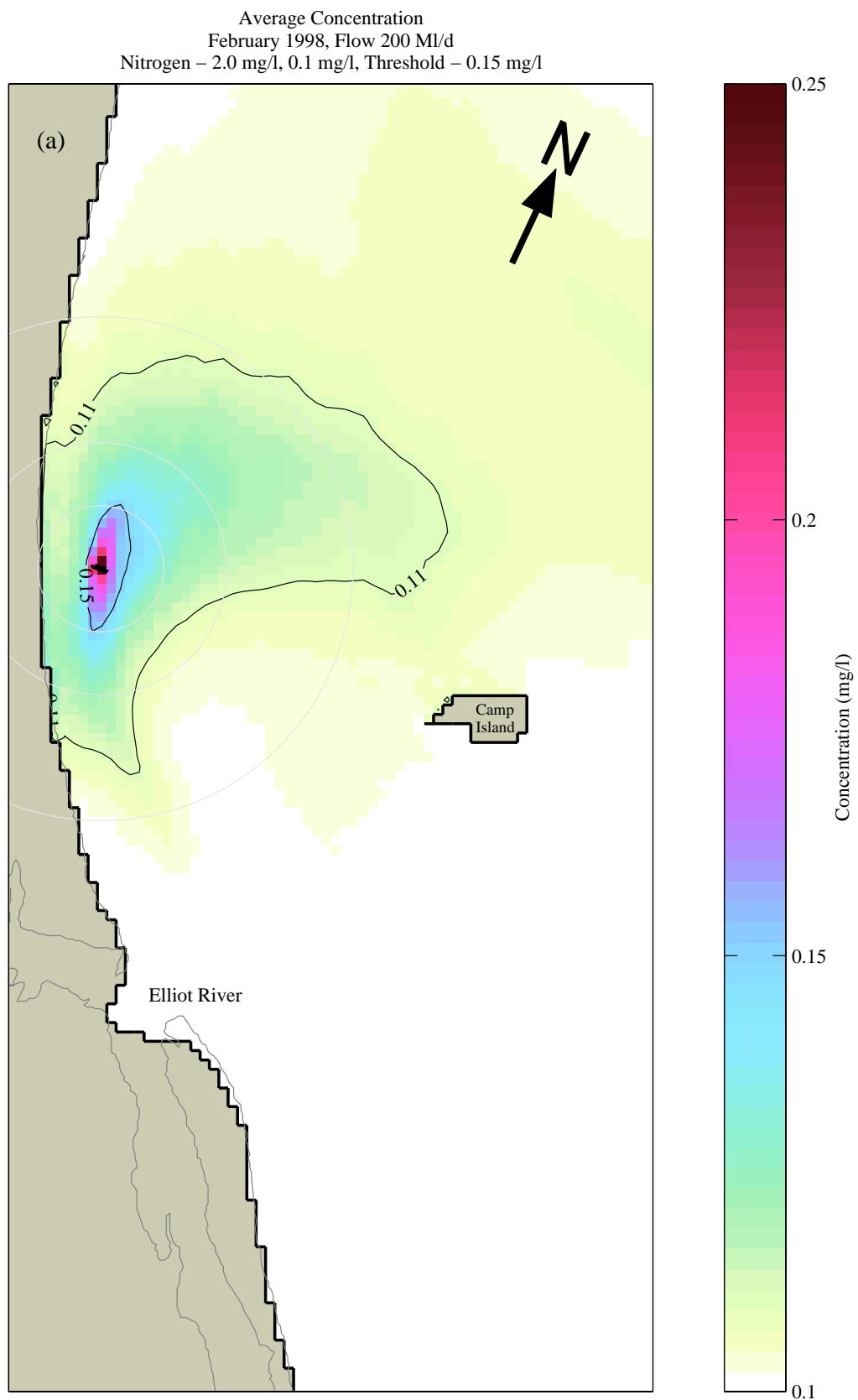


**Figure 25a.** Average Concentration (*Nitrogen*) for the February discharge period of 1998 (200MI/d). Contours indicate the background plus 10% (0.11 mg/l) and the threshold (0.15 mg/l) levels. Concentric circles at 500, 1000 and 2000 m radii.

Average Concentration  
 February 1998, Flow 200 MI/d  
 Phosphorus – 0.15 mg/l, 0.015 mg/l, Threshold – 0.025 mg/l

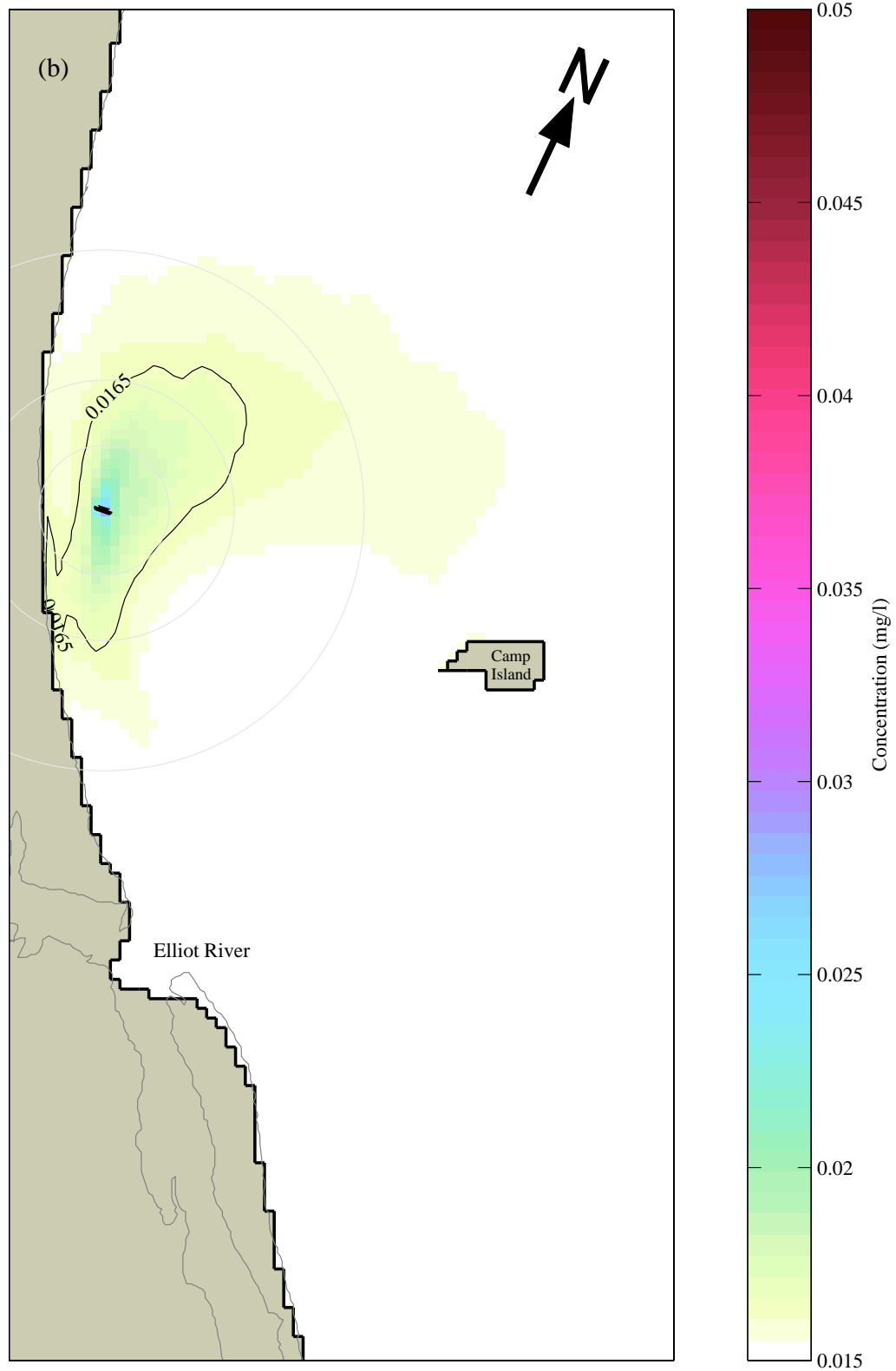


**Figure 25b.** Average Concentration (*Phosphorus*) for the February discharge period of 1998 (200MI/d). Contours indicate the background plus 10% (0.0165 mg/l) and the threshold (0.025 mg/l) levels. Concentric circles at 500, 1000 and 2000 m radii.





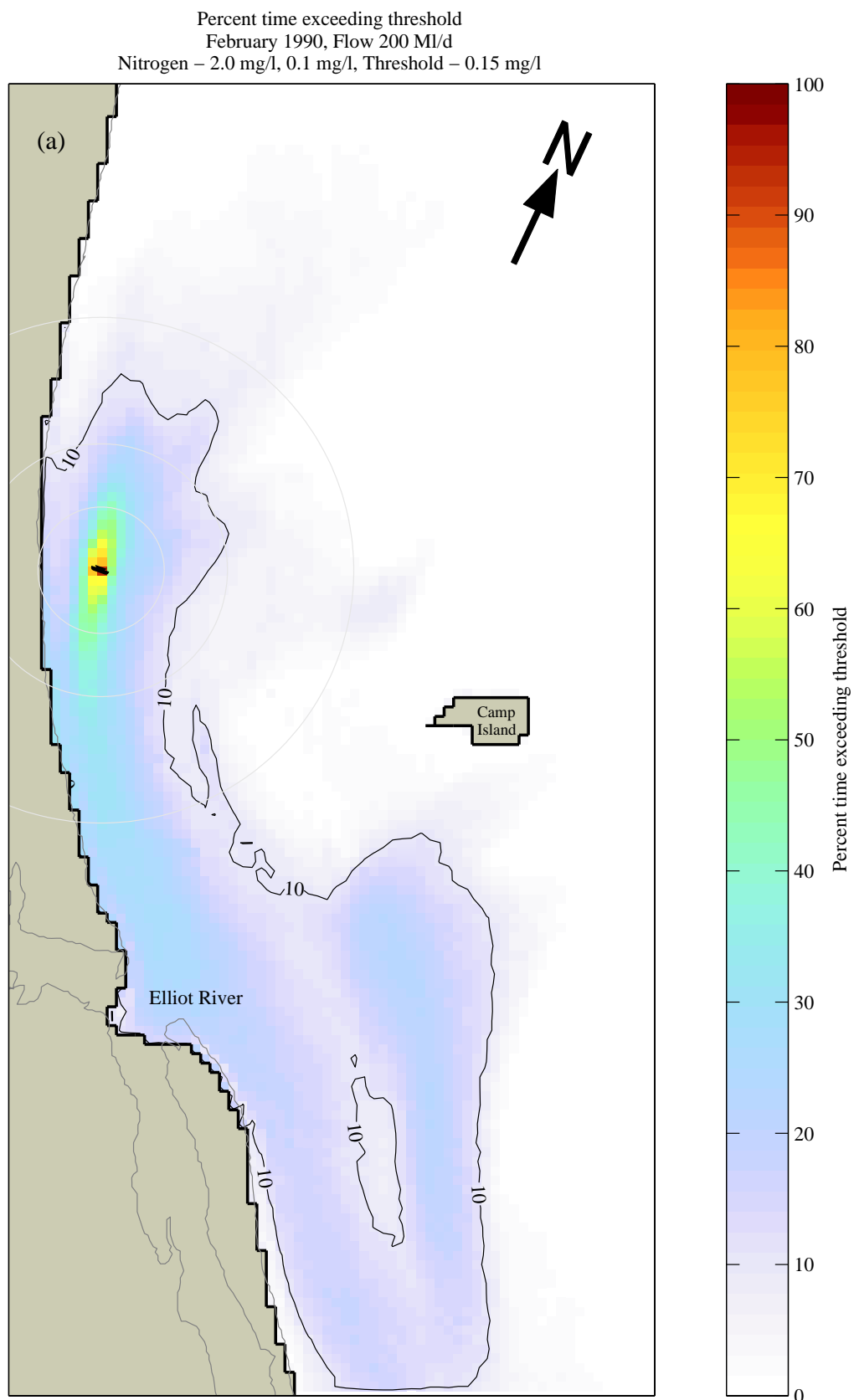


**Figure 26a.** Percent time exceeding threshold (*Nitrogen*) for the February discharge period of 1990 (200MI/d). Threshold level is 0.15 mg/l. The contour is at 10% level. Concentric circles at 500, 1000 and 2000 m radii.

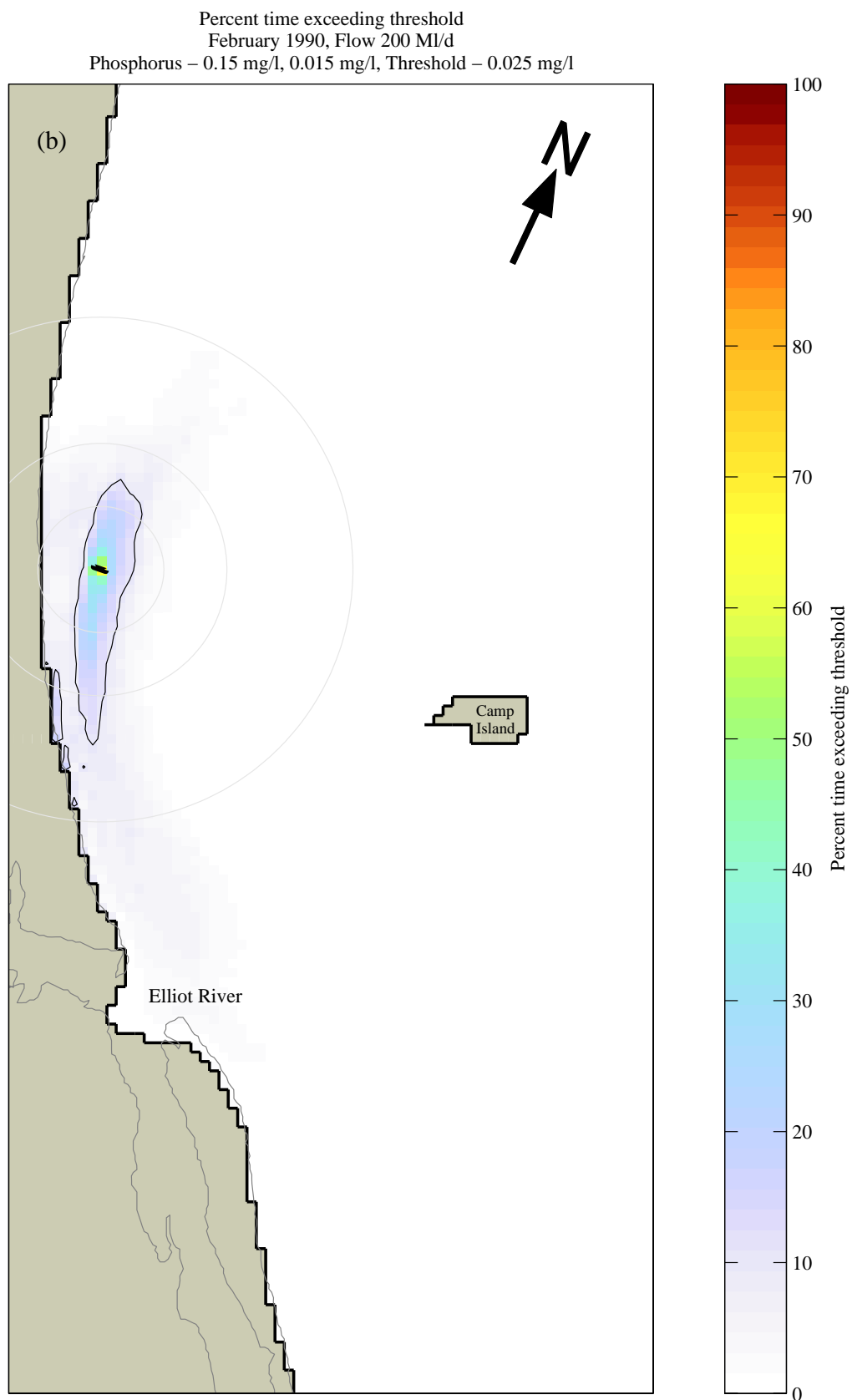


**Figure 26b.** Percent time exceeding threshold (*Phosphorus*) for the February discharge period of 1990 (200Ml/d). Threshold level is 0.025 mg/l. The contour is at 10% level. Concentric circles at 500, 1000 and 2000 m radii.

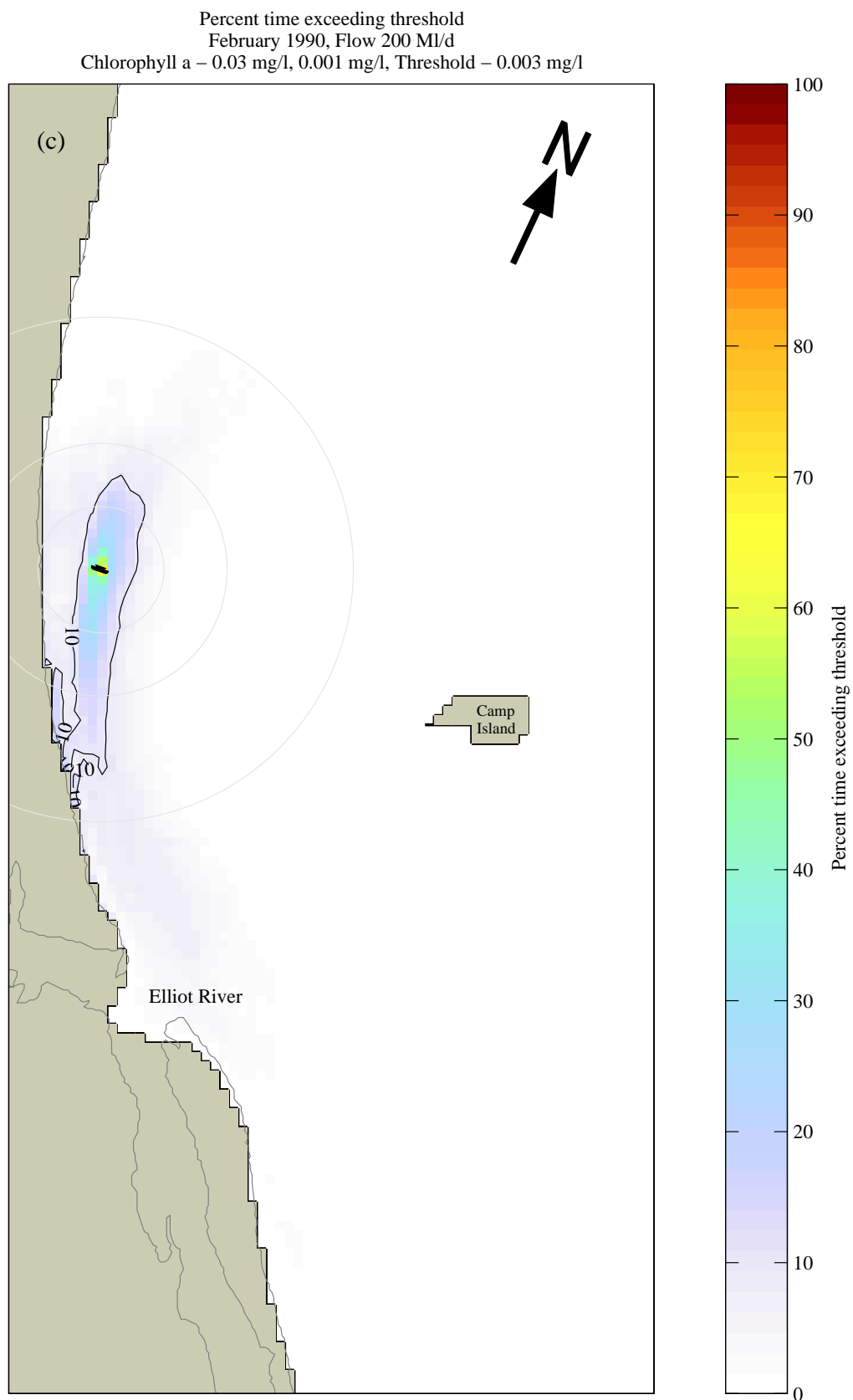


**Figure 26c.** Percent time exceeding threshold (*Chlorophyll-a*) for the February discharge period of 1990 (200Ml/d). Threshold level is 0.003 mg/l. The contour is at 10% level. Concentric circles at 500, 1000 and 2000 m radii.

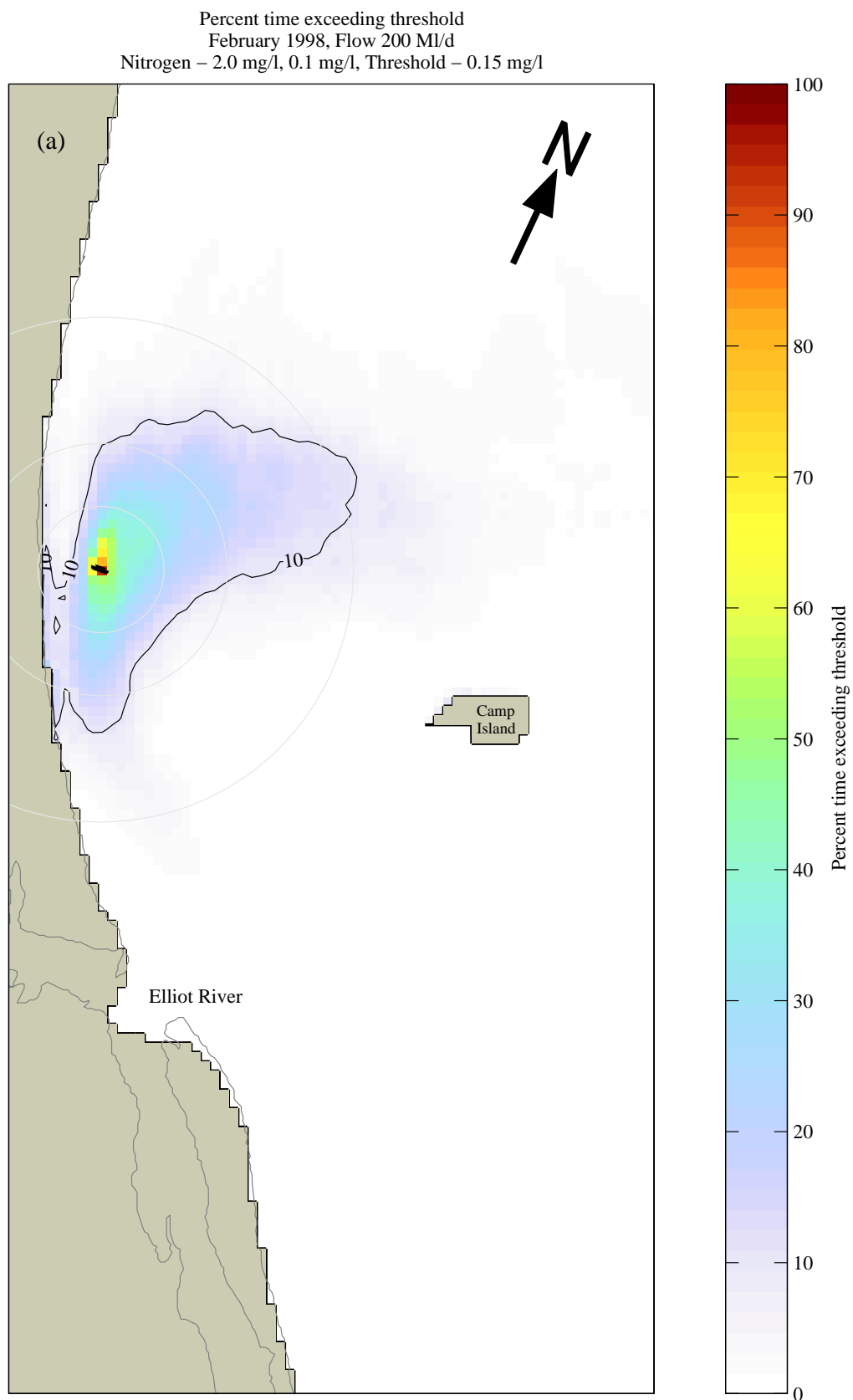


**Figure 27a.** Percent time exceeding threshold (*Nitrogen*) for the February discharge period of 1998 (200Ml/d). Threshold level is 0.15 mg/l. The contour is at 10% level. Concentric circles at 500, 1000 and 2000 m radii.

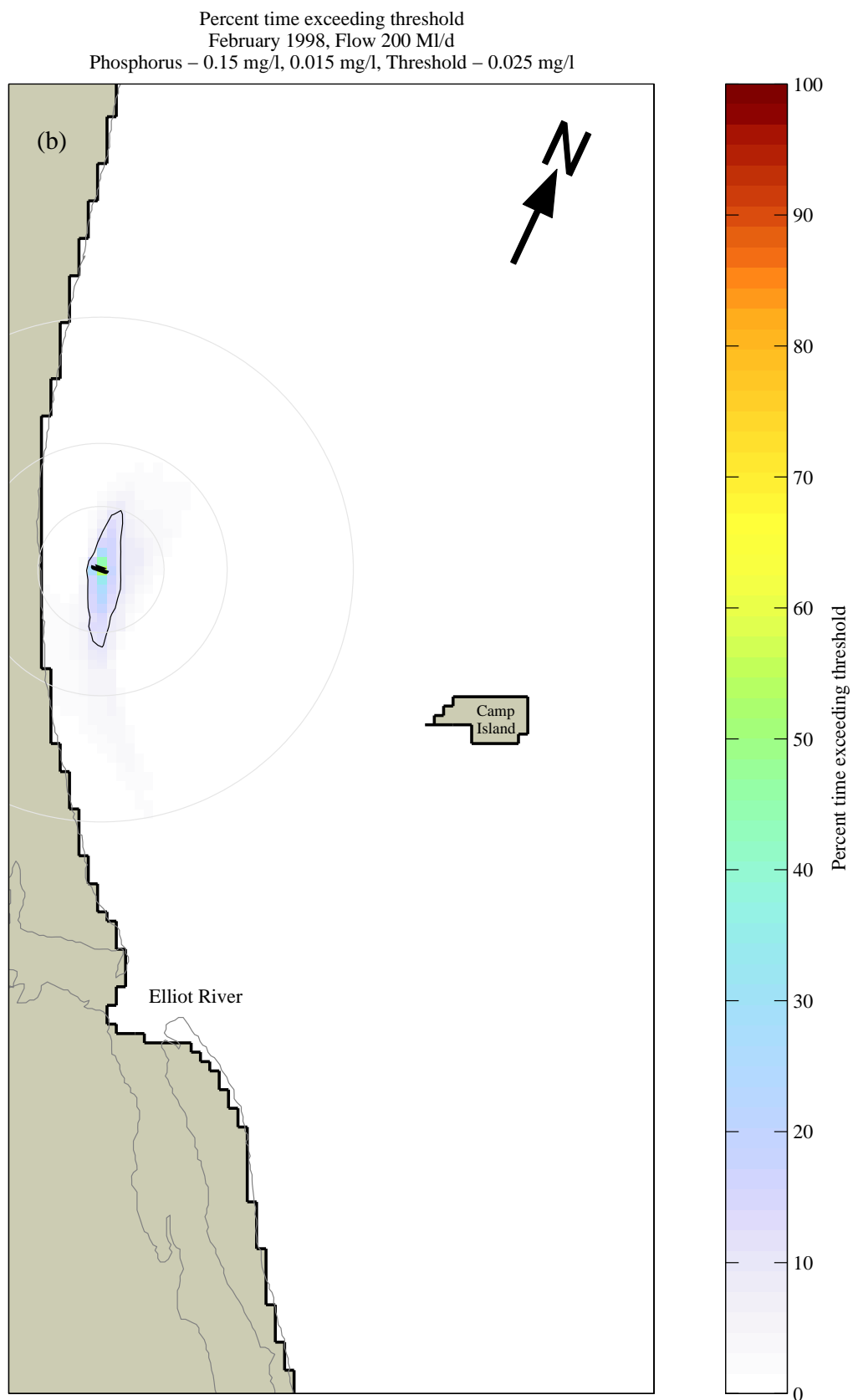


**Figure 27b.** Percent time exceeding threshold (*Phosphorus*) for the February discharge period of 1998 (200Ml/d). Threshold level is 0.025 mg/l. The contour is at 10% level. Concentric circles at 500, 1000 and 2000 m radii.

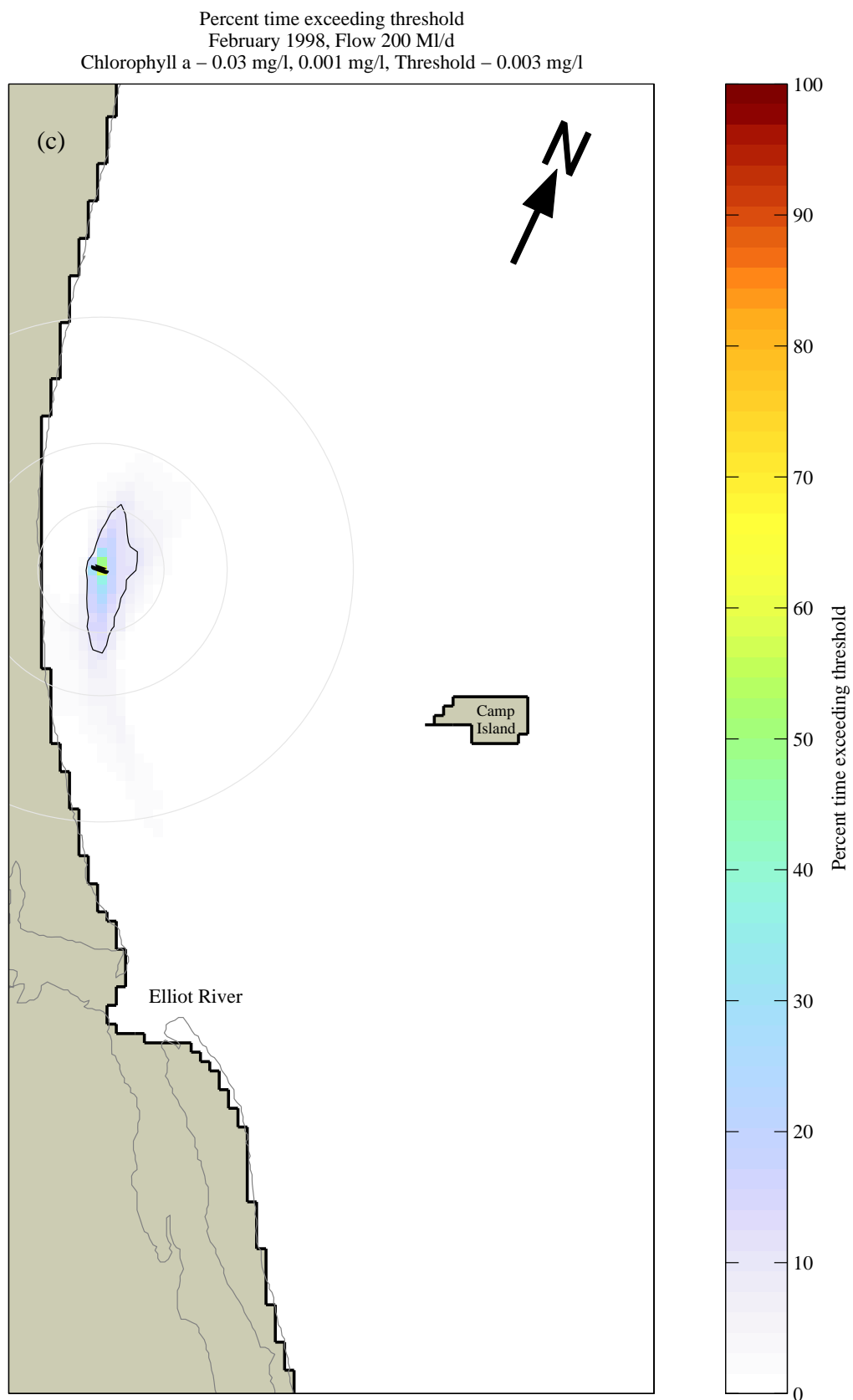


**Figure 27c.** Percent time exceeding threshold (*Chlorophyll-a*) for the February discharge period of 1998 (200Ml/d). Threshold level is 0.003 mg/l. The contour is at 10% level. Concentric circles at 500, 1000 and 2000 m radii.

## Appendix: Additional Discharge Rate (100 MI/d).

Following the completion of the main component of the original scope of work, the client requested additional results for a discharge rate of 100 MI/d. Recall that the original work used a discharge rate of 200 MI/d. In this section we present results corresponding to Figures 16 to 19 (time history of concentration), Figures 20 and 21 (average concentrations for the six-month period) and Figures 24 and 25 (average concentrations for February) in the original work.

For this additional work, the discharge, background and threshold concentrations for total nitrogen, phosphorus, and chlorophyll-a are the same as those used for the original work. This means that the discharge mass flux of these substances will be half that simulated in the original work and should produce significant reductions in discharge concentrations in the receiving waters. Note that instantaneous concentration levels will not be halved. However, the concentration range above background will be halved. This effect can be seen in the time history Figures 28 to 31. When these figures are compared to Figures 16 to 19 the effect becomes obvious. In all cases the time history patterns remain the same but the range of concentrations above background is halved.

The average concentrations for the 100 MI/d discharge rate are shown in Figures 32 and 33 for six-month periods in 1990 and 1998 and in Figures 34 and 35 for February of the same years. As expected, the extent of the *background plus 10%* and the *threshold* contours, for all the average concentration plots, have been significantly reduced compared to the 200 MI/d discharge rate case. For the *background plus 10%* concentration, the area enclosed by the contours in Figures 32 to 35, are in the range of 25 to 50 % of the areas enclosed by the corresponding contours in Figures 20, 21, 24 and 25 for the 200 MI/d results. In the case of the *threshold* contours the reduction in area is much greater. In Figures 32a and 33a, the six-month average concentrations for nitrogen, the area bound by the *threshold* contour is now limited to small area in the vicinity of the outfall. The average concentrations for nitrogen during February, shown in Figures 34a and 35a, again show a significant reduction in the area bounded by the *threshold* contours. The area bounded by this contour is approximately 10 % of the area originally bounded in the 200 MI/d discharge scenario. For phosphorus and chlorophyll-a the area bound by the *threshold* contour was small in the original scenario and cannot be detected for the present flow rate.

All discussions and conclusion made for the 200 MI/d discharge rate hold true for the 100 MI/d scenario. The concentration patterns remain the same but are at a significantly reduced level.

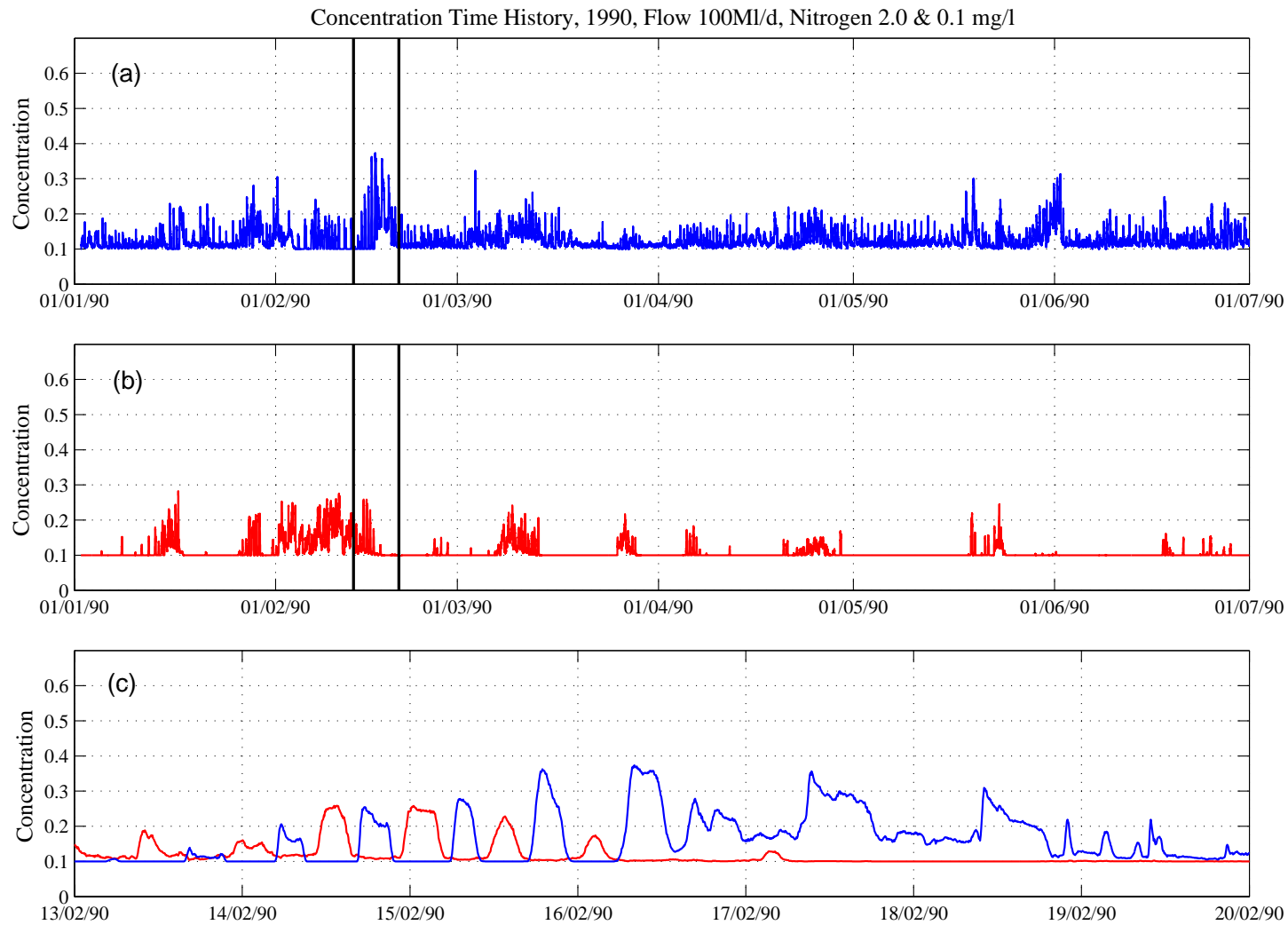


**Figure 28.** Concentration time history for Nitrogen during year 1990; (a) blue, point 500 m north of outfall; (b) red, point 500 m south of outfall; (c) shorter time window indicated by vertical lines in (a) and (b). Assumes a discharge of 100 ML/d, Discharge concentration 2.0 mg/l, Background concentration 0.1 mg/l. Concentric circles at 500, 1000 and 2000 m radii.



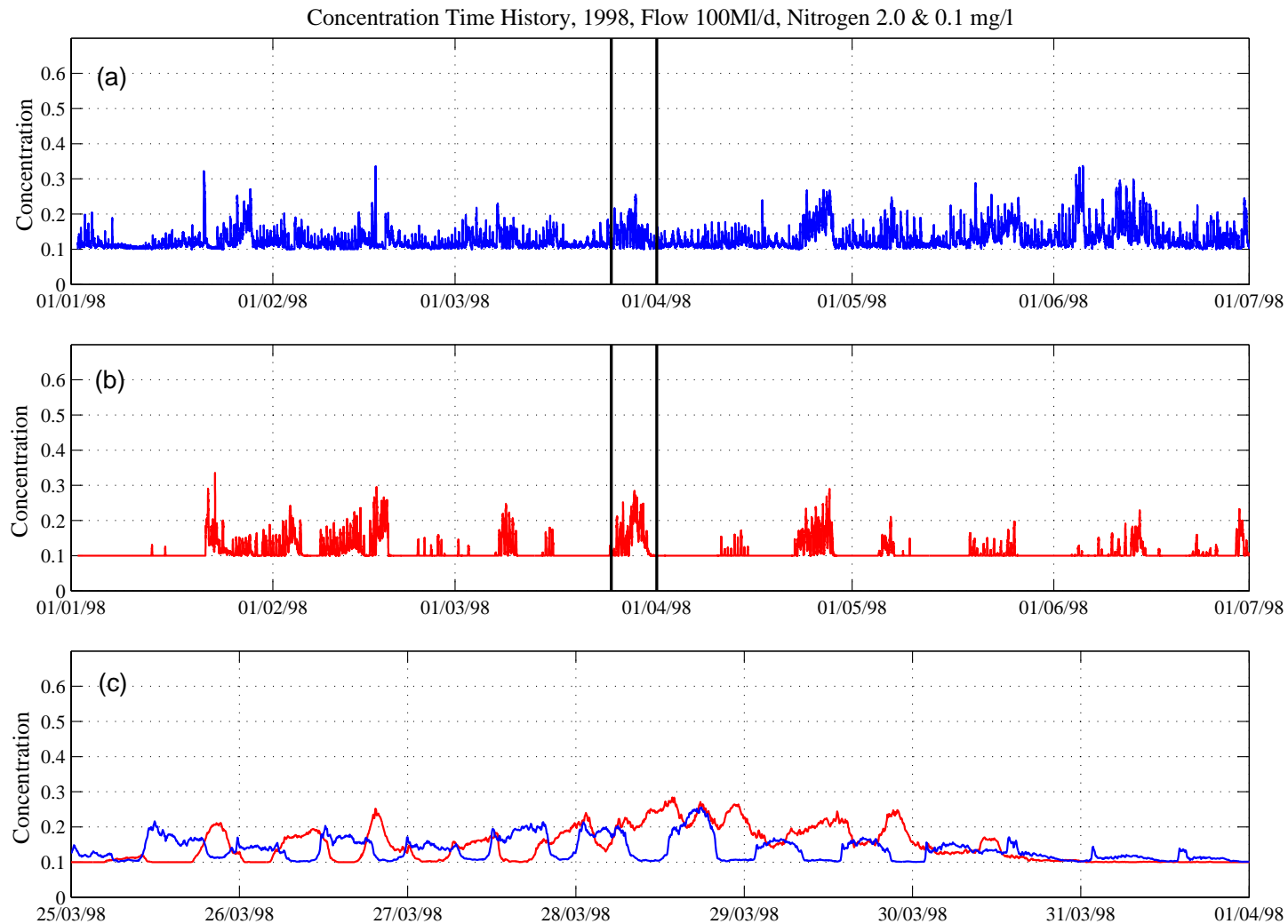


**Figure 29.** Concentration time history for Nitrogen during year 1998; (a) blue, point 500 m north of outfall; (b) red, point 500 m south of outfall; (c) shorter time window indicated by vertical lines in (a) and (b). Assumes a discharge of 100 MI/d, Discharge concentration 2.0 mg/l, Background concentration 0.1 mg/l. Concentric circles at 500, 1000 and 2000 m radii.

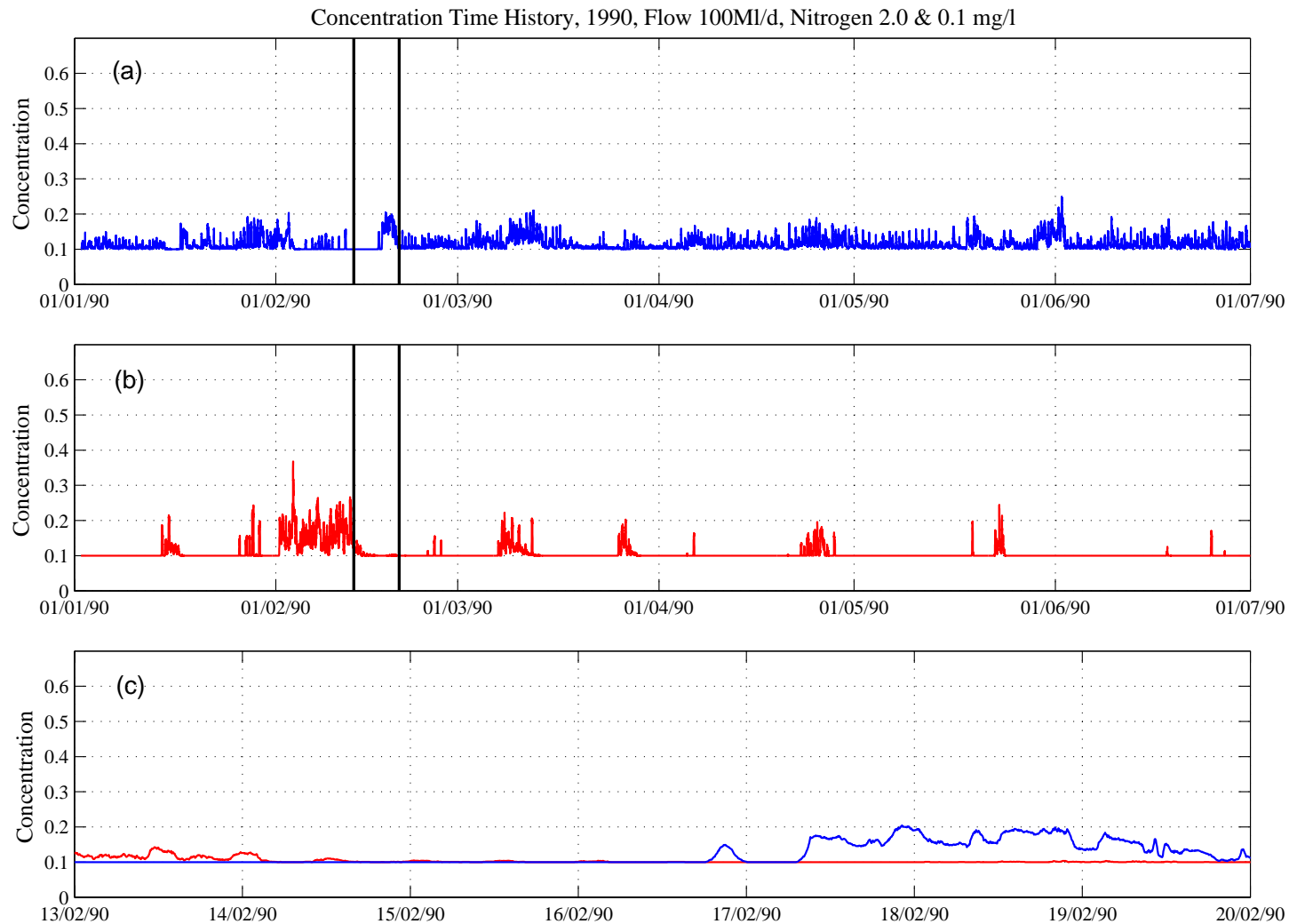


**Figure 30.** Concentration time history for Nitrogen during year 1990; (a) blue, point 1000 m north of outfall; (b) red, point 1000 m south of outfall; (c) shorter time window indicated by vertical lines in (a) and (b). Assumes a discharge of 100 Ml/d, Discharge concentration 2.0 mg/l, Background concentration 0.1 mg/l. Concentric circles at 500, 1000 and 2000 m radii.

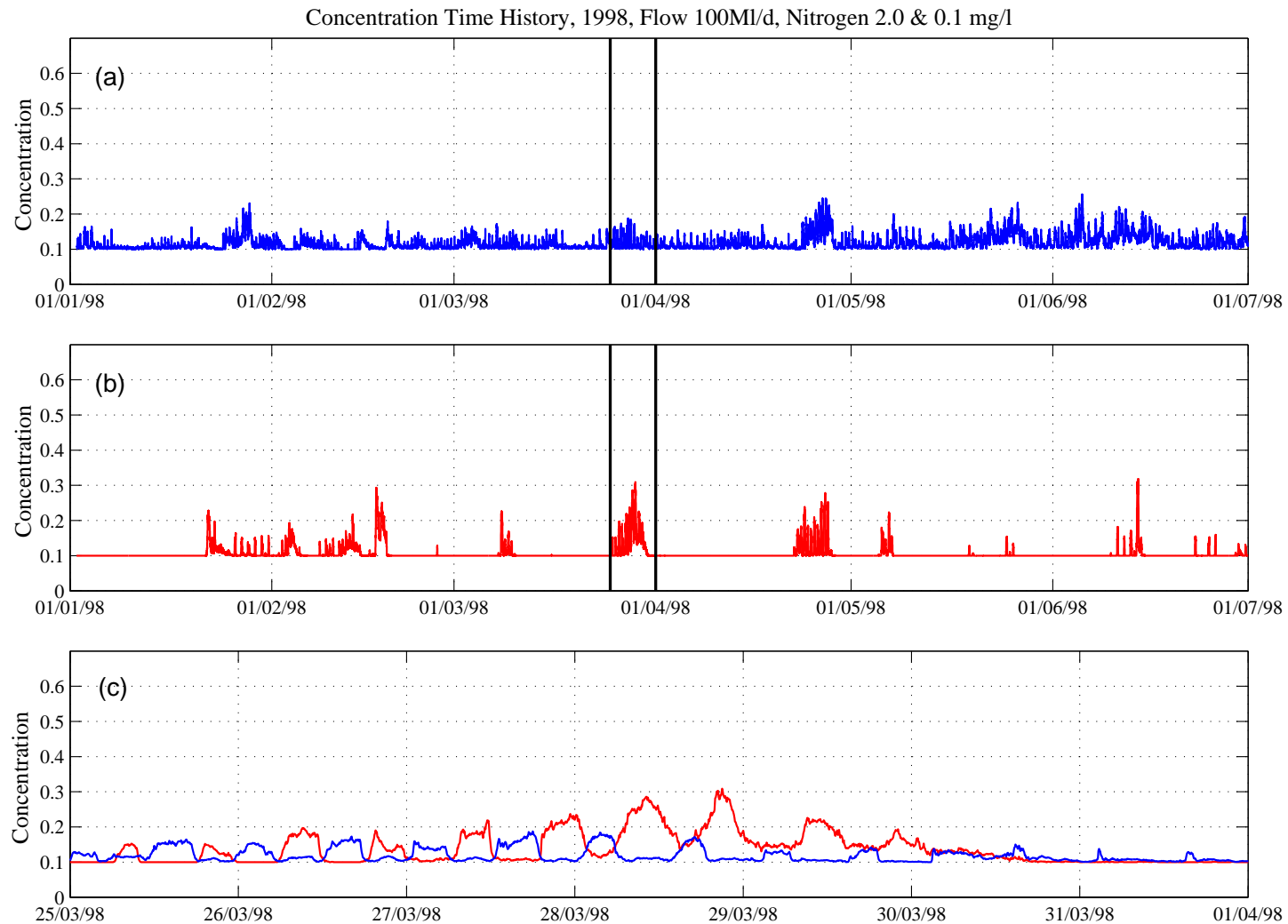


**Figure 31.** Concentration time history for Nitrogen during year 1998; (a) blue, point 1000 m north of outfall; (b) red, point 1000 m south of outfall; (c) shorter time window indicated by vertical lines in (a) and (b). Assumes a discharge of 100 Ml/d, Discharge concentration 2.0 mg/l, Background concentration 0.1 mg/l. Concentric circles at 500, 1000 and 2000 m radii.

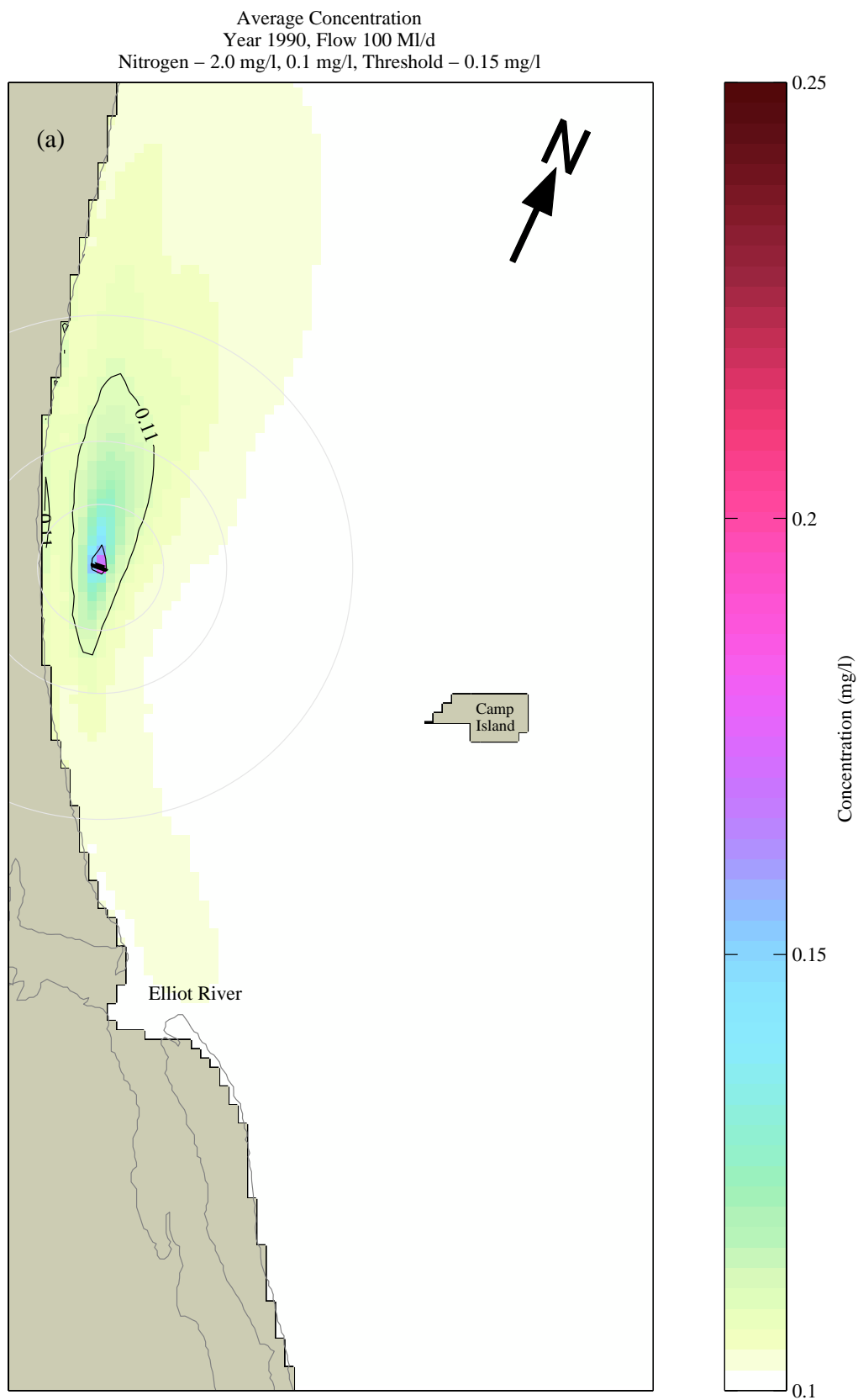


**Figure 32a.** Average Concentration (*Nitrogen*) for the six-month discharge period of 1990 (100Ml/d). Contours indicate the background plus 10% (0.11 mg/l) and the threshold (0.15 mg/l) levels. Concentric circles at 500, 1000 and 2000 m radii.

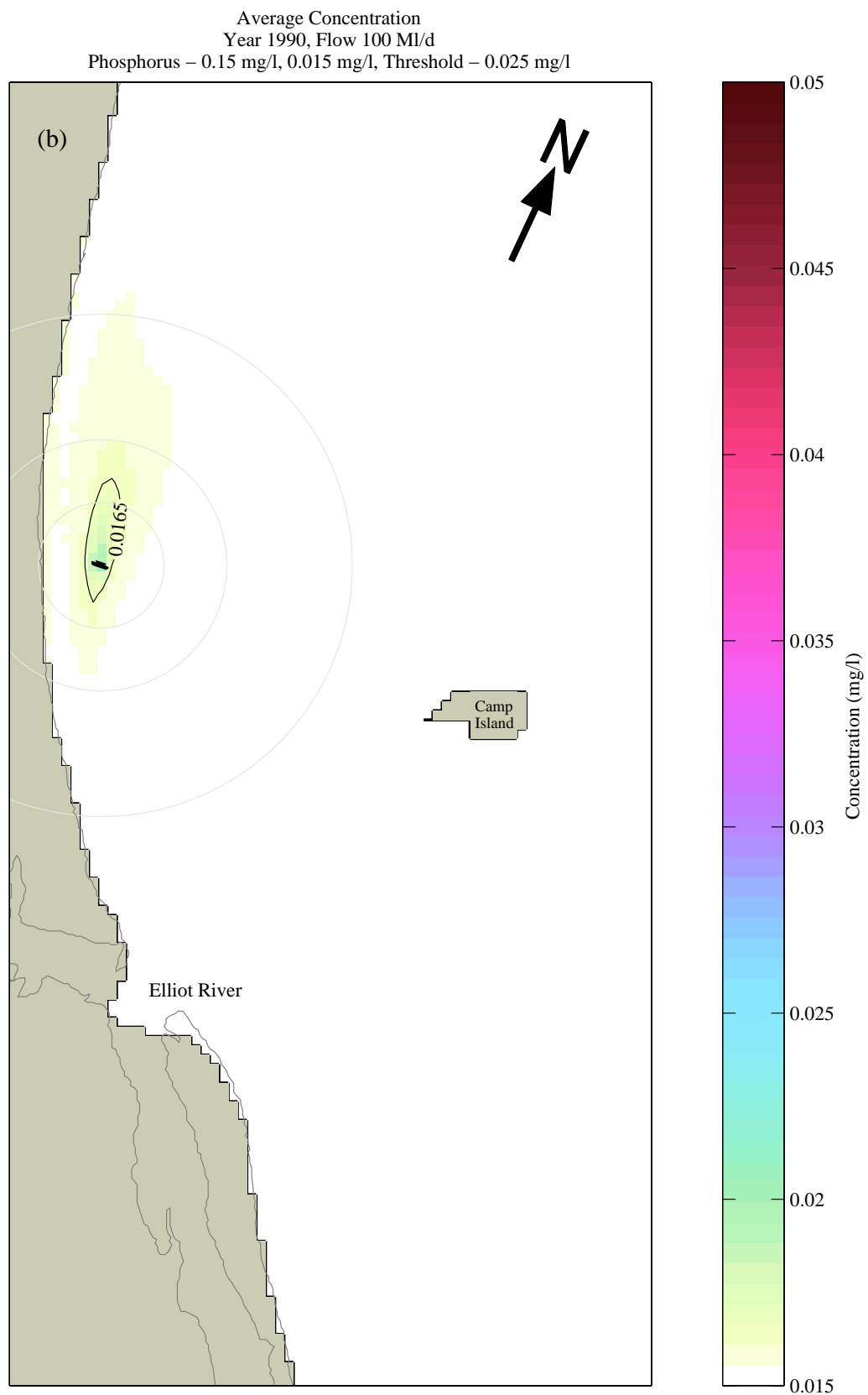


**Figure 32b.** Average Concentration (*Phosphorus*) for the six-month discharge period of 1990 (100MI/d). Contours indicate the background plus 10% (0.0165 mg/l) and the threshold (0.025 mg/l) levels. Concentric circles at 500, 1000 and 2000 m radii.

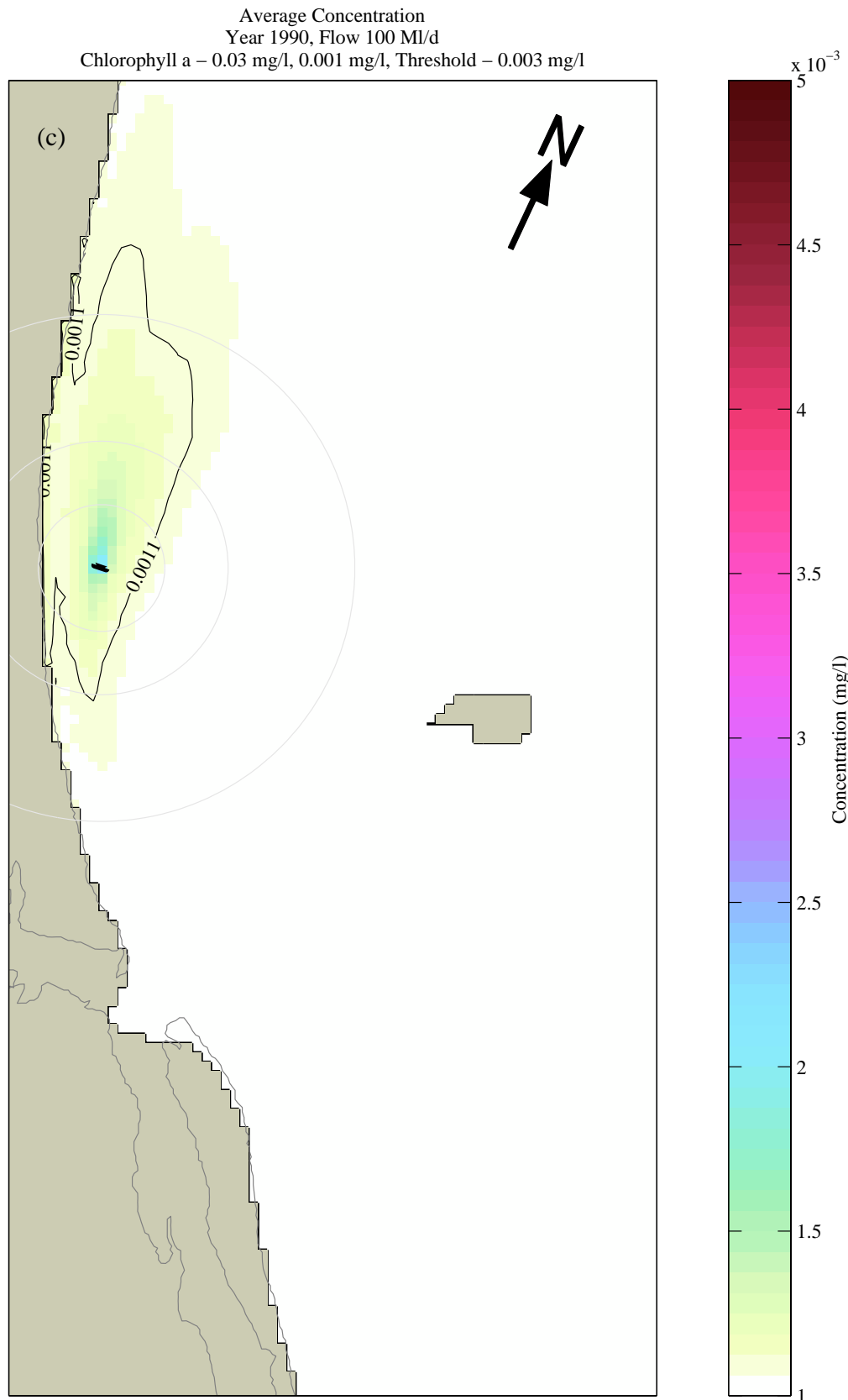


**Figure 32c.** Average Concentration (*Chlorophyll-a*) for the six-month discharge period of 1990 (100ML/d). Contours indicate the background plus 10% (0.0011 mg/l) and the threshold (0.003 mg/l) levels. Concentric circles at 500, 1000 and 2000 m radii.

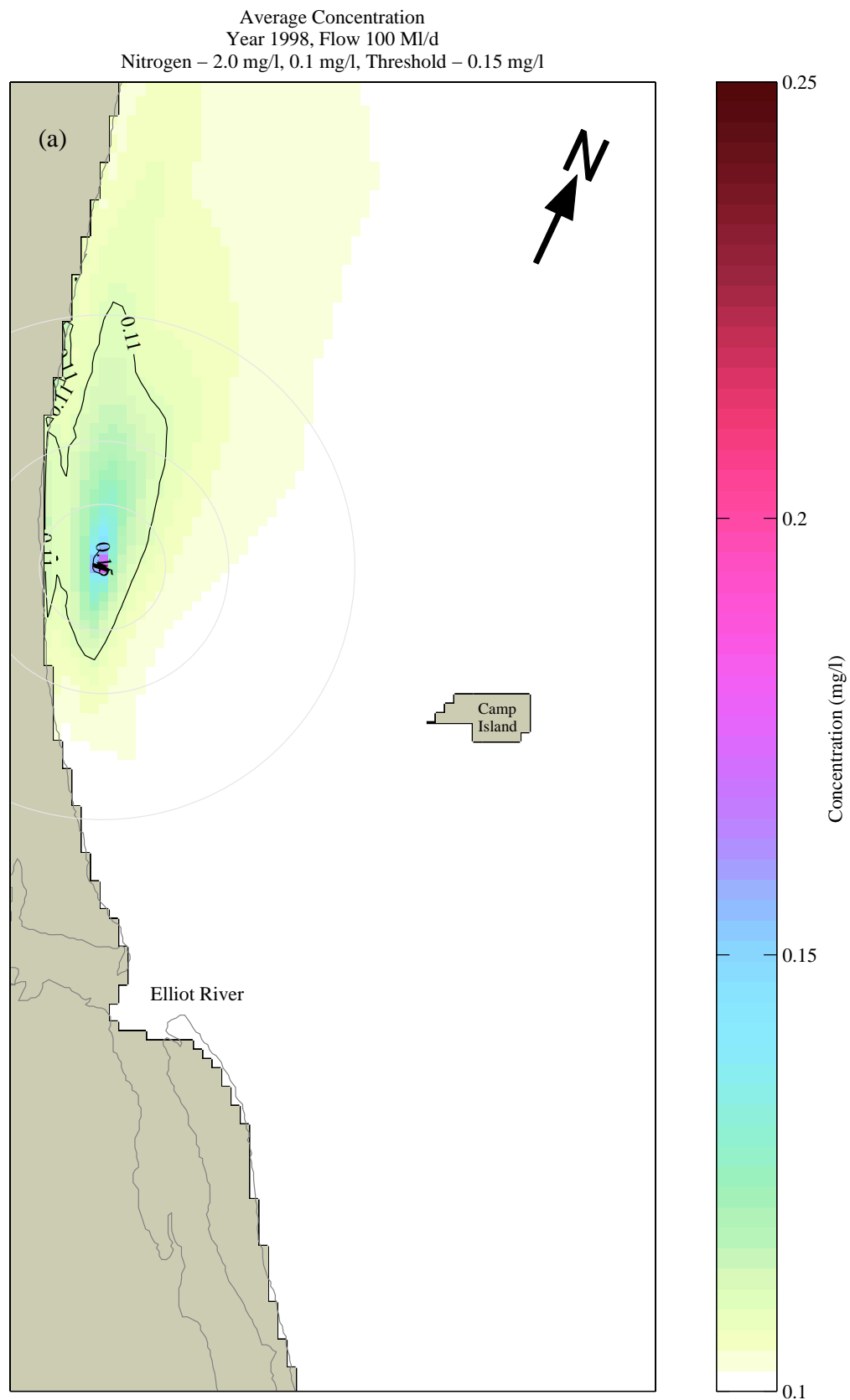


**Figure 33a.** Average Concentration (*Nitrogen*) for the six-month discharge period of 1998 (100ML/d). Contours indicate the background plus 10% (0.11 mg/l) and the threshold (0.15 mg/l) levels. Concentric circles at 500, 1000 and 2000 m radii.

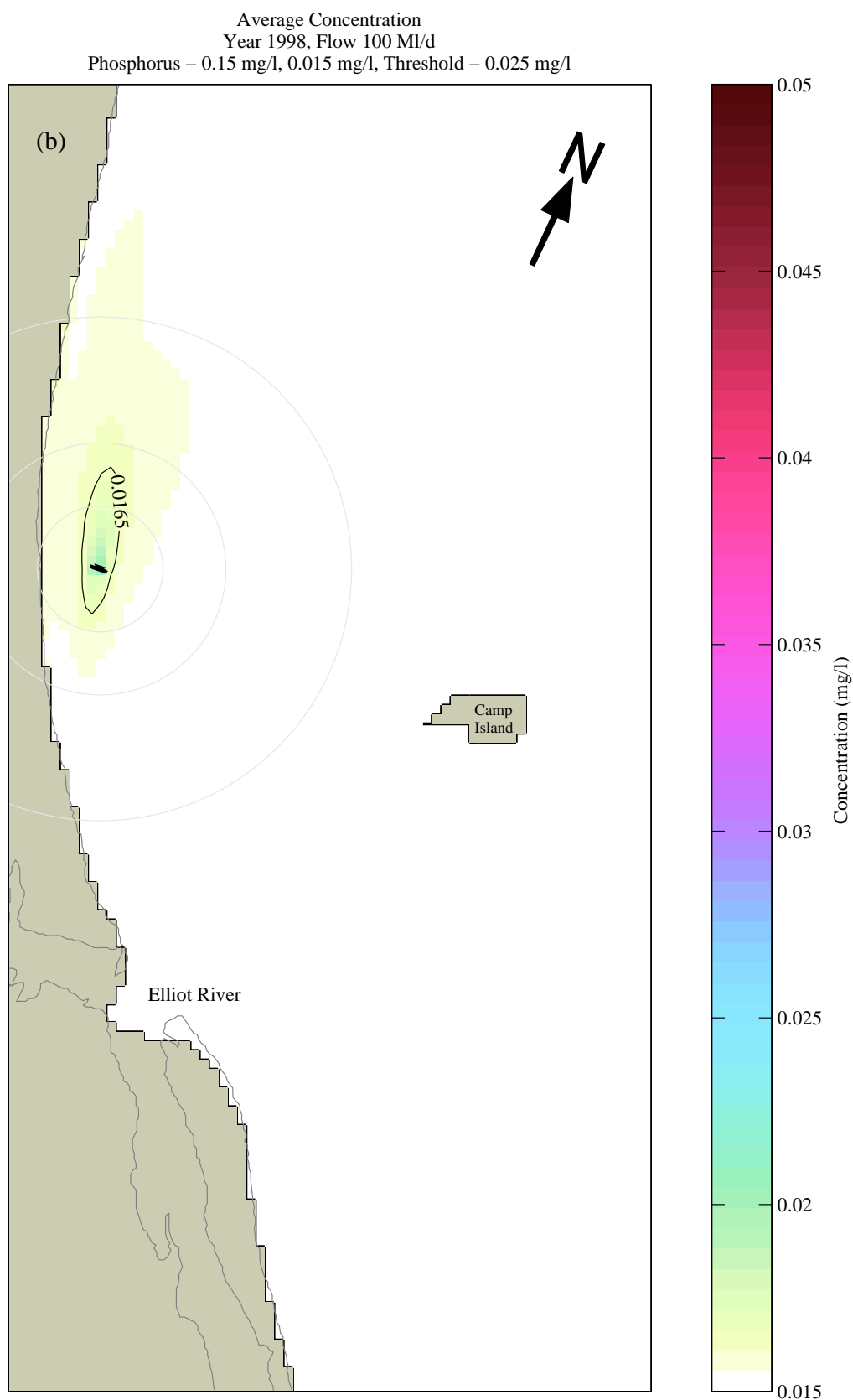


**Figure 33b.** Average Concentration (*Phosphorus*) for the six-month discharge period of 1998 (100Ml/d). Contours indicate the background plus 10% (0.0165 mg/l) and the threshold (0.025 mg/l) levels. Concentric circles at 500, 1000 and 2000 m radii.



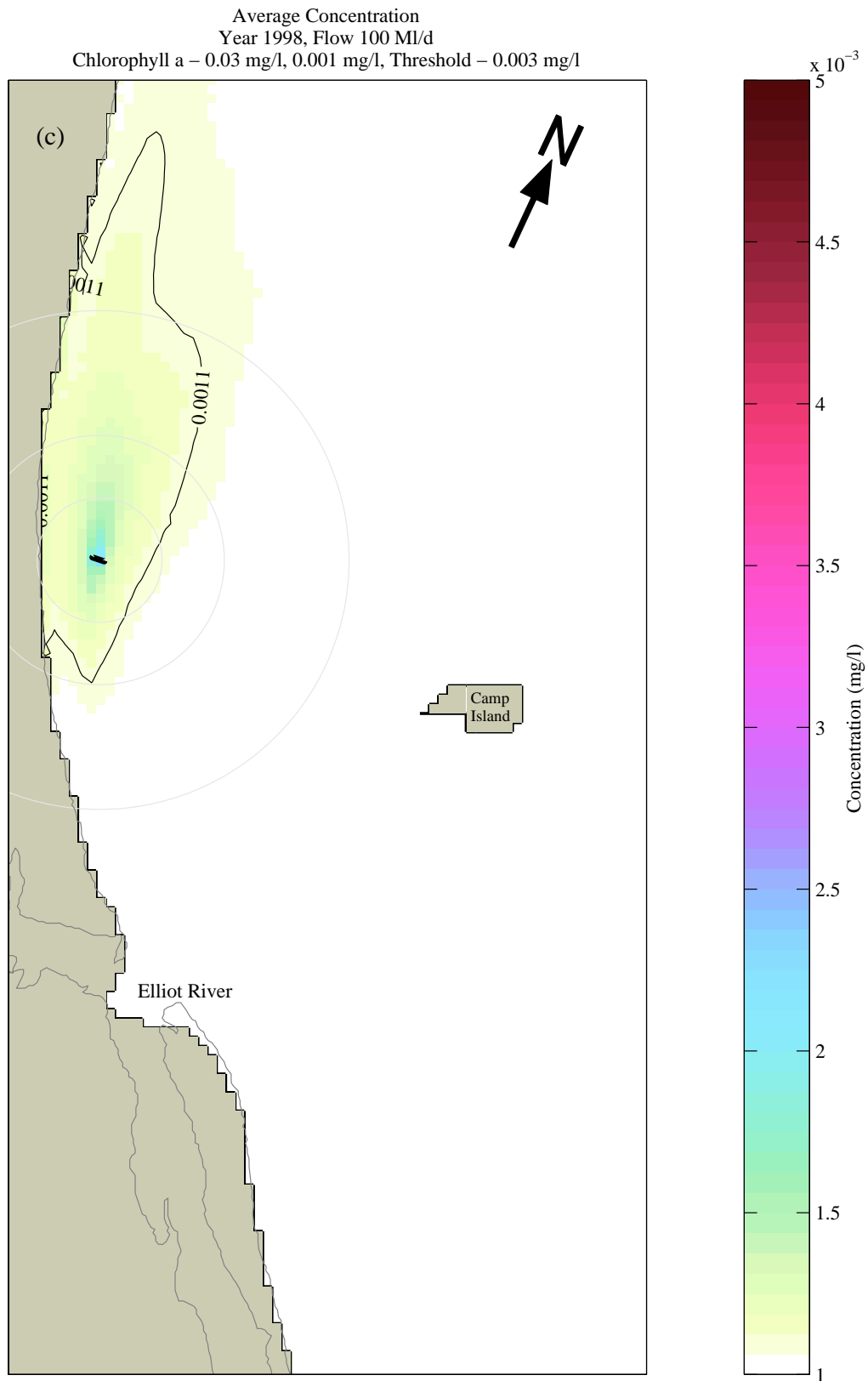


**Figure 33c.** Average Concentration (*Chlorophyll-a*) for the six-month discharge period of 1998 (100Ml/d). Contours indicate the background plus 10% (0.0011 mg/l) and the threshold (0.003 mg/l) levels. Concentric circles at 500, 1000 and 2000 m radii.

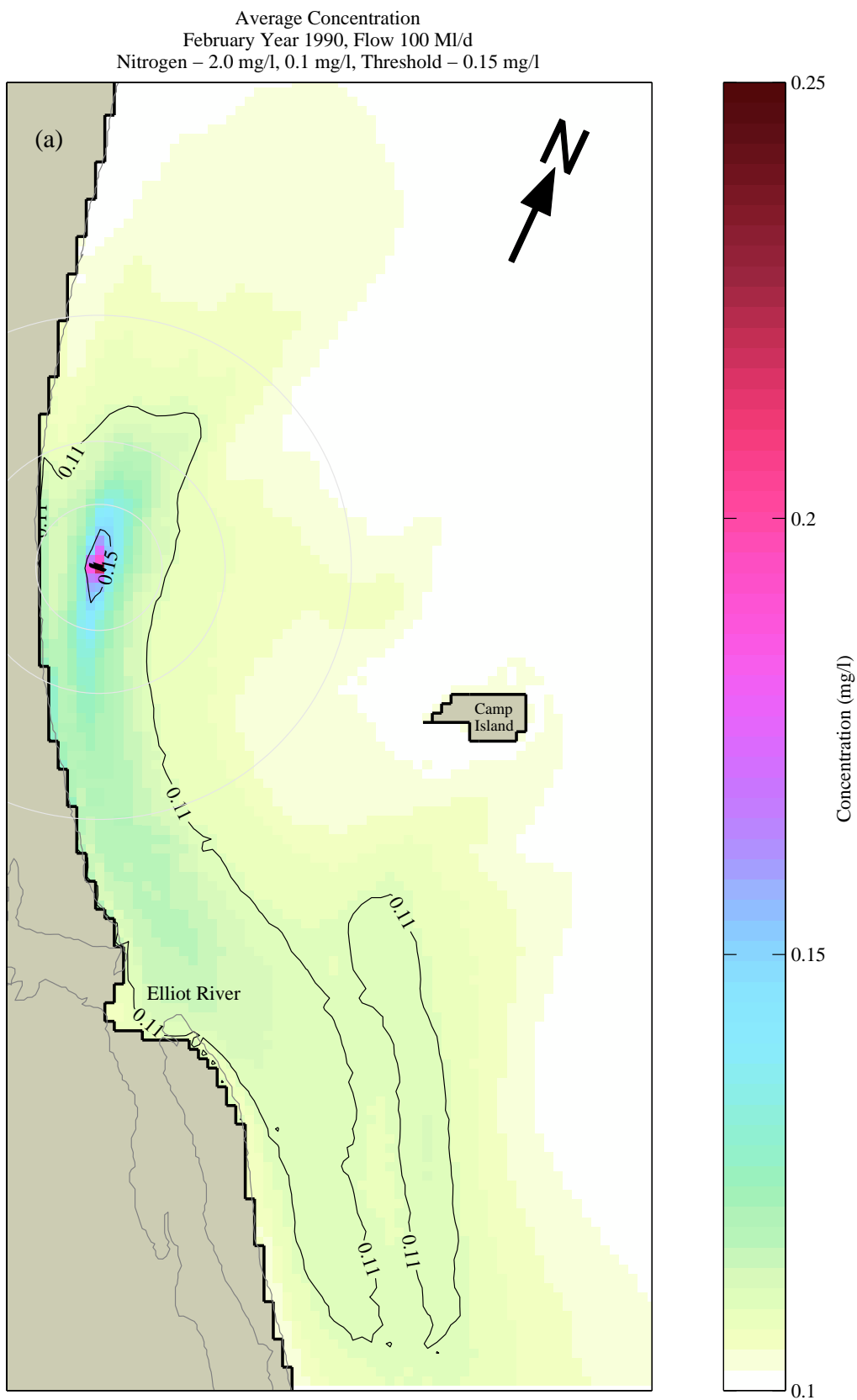


**Figure 34a.** Average Concentration (*Nitrogen*) for the February discharge period of 1990 (100Ml/d). Contours indicate the background plus 10% (0.11 mg/l) and the threshold (0.15 mg/l) levels. Concentric circles at 500, 1000 and 2000 m radii.

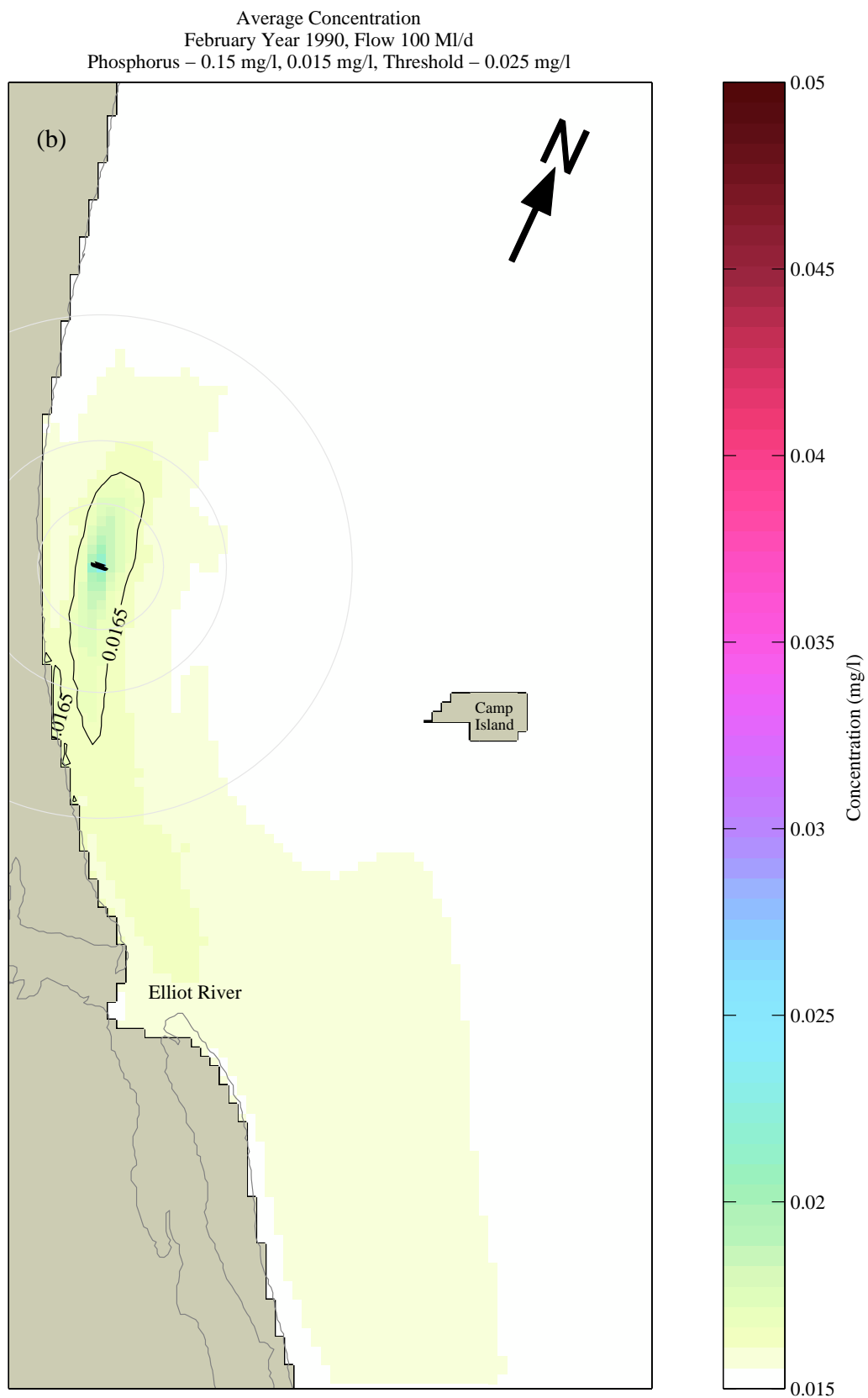


**Figure 34b.** Average Concentration (*Phosphorus*) for the February discharge period of 1990 (100Ml/d). Contours indicate the background plus 10% (0.0165 mg/l) and the threshold (0.025 mg/l) levels. Concentric circles at 500, 1000 and 2000 m radii.

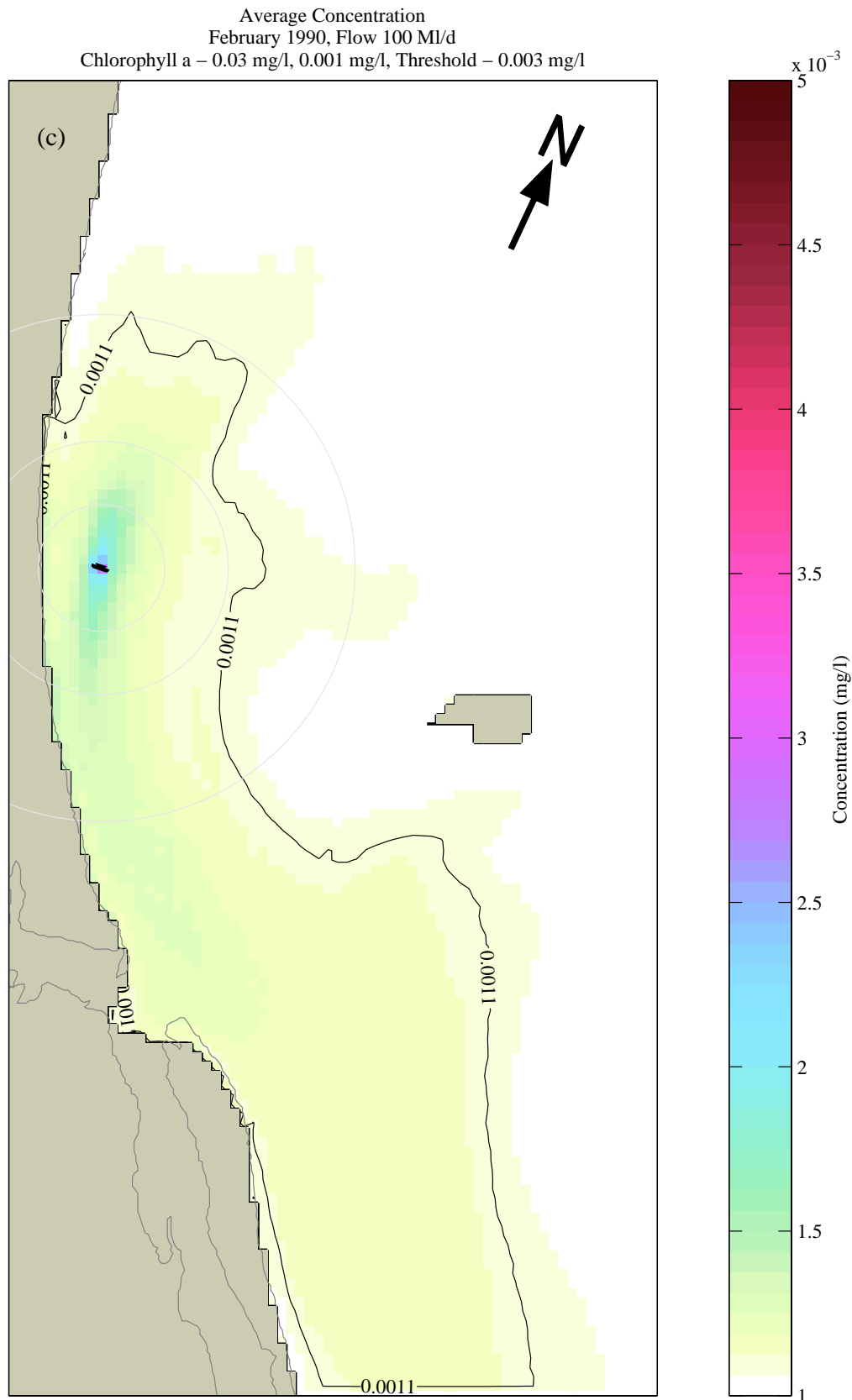


**Figure 34c.** Average Concentration (*Chlorophyll-a*) for the February discharge period of 1990 (100MI/d). Contours indicate the background plus 10% (0.0011 mg/l) and the threshold (0.003 mg/l) levels. Concentric circles at 500, 1000 and 2000 m radii.

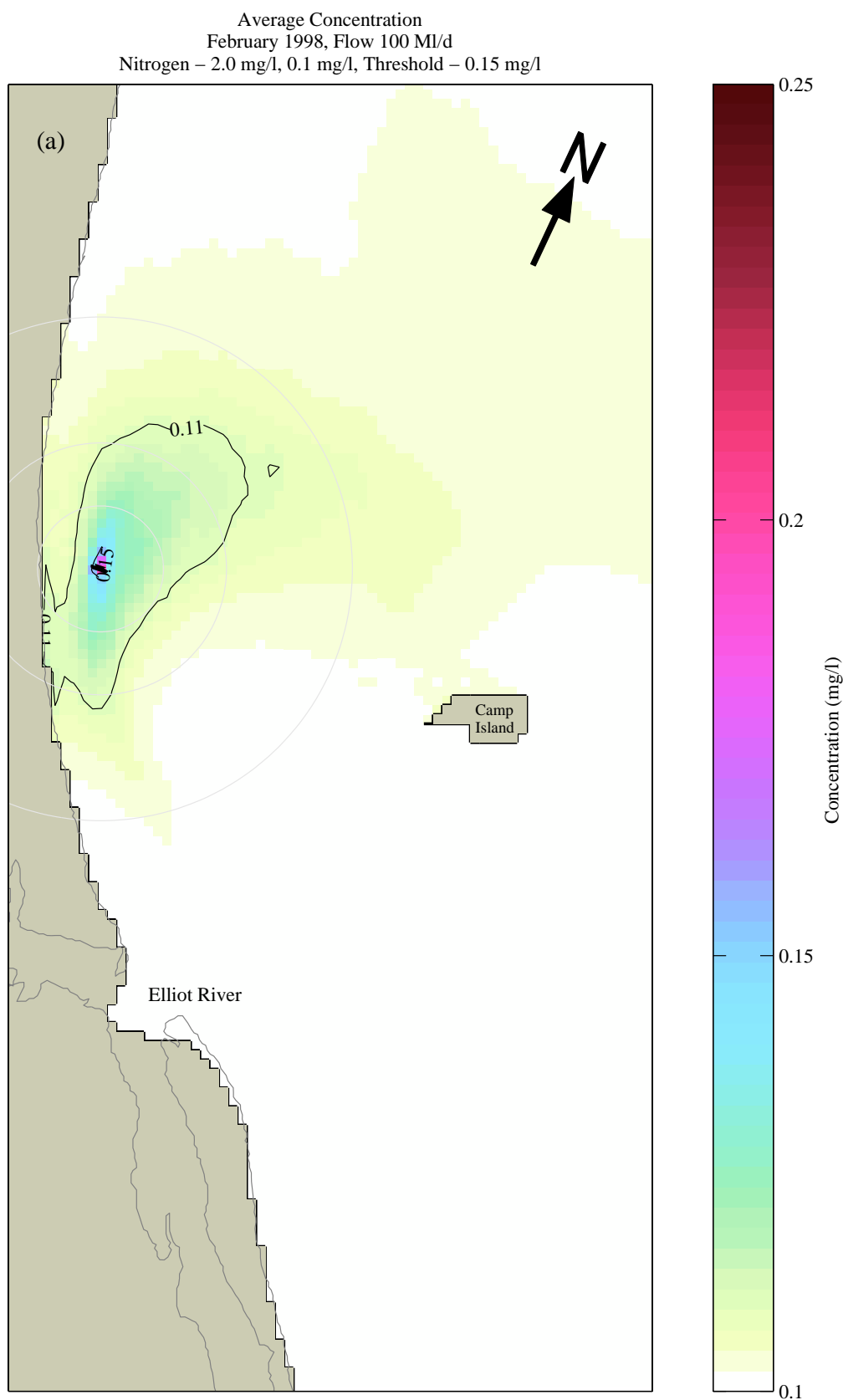


**Figure 35a.** Average Concentration (*Nitrogen*) for the February discharge period of 1998 (100ML/d). Contours indicate the background plus 10% (0.11 mg/l) and the threshold (0.15 mg/l) levels. Concentric circles at 500, 1000 and 2000 m radii.

Average Concentration  
 February 1998, Flow 100 Ml/d  
 Phosphorus – 0.15 mg/l, 0.015 mg/l, Threshold – 0.025 mg/l

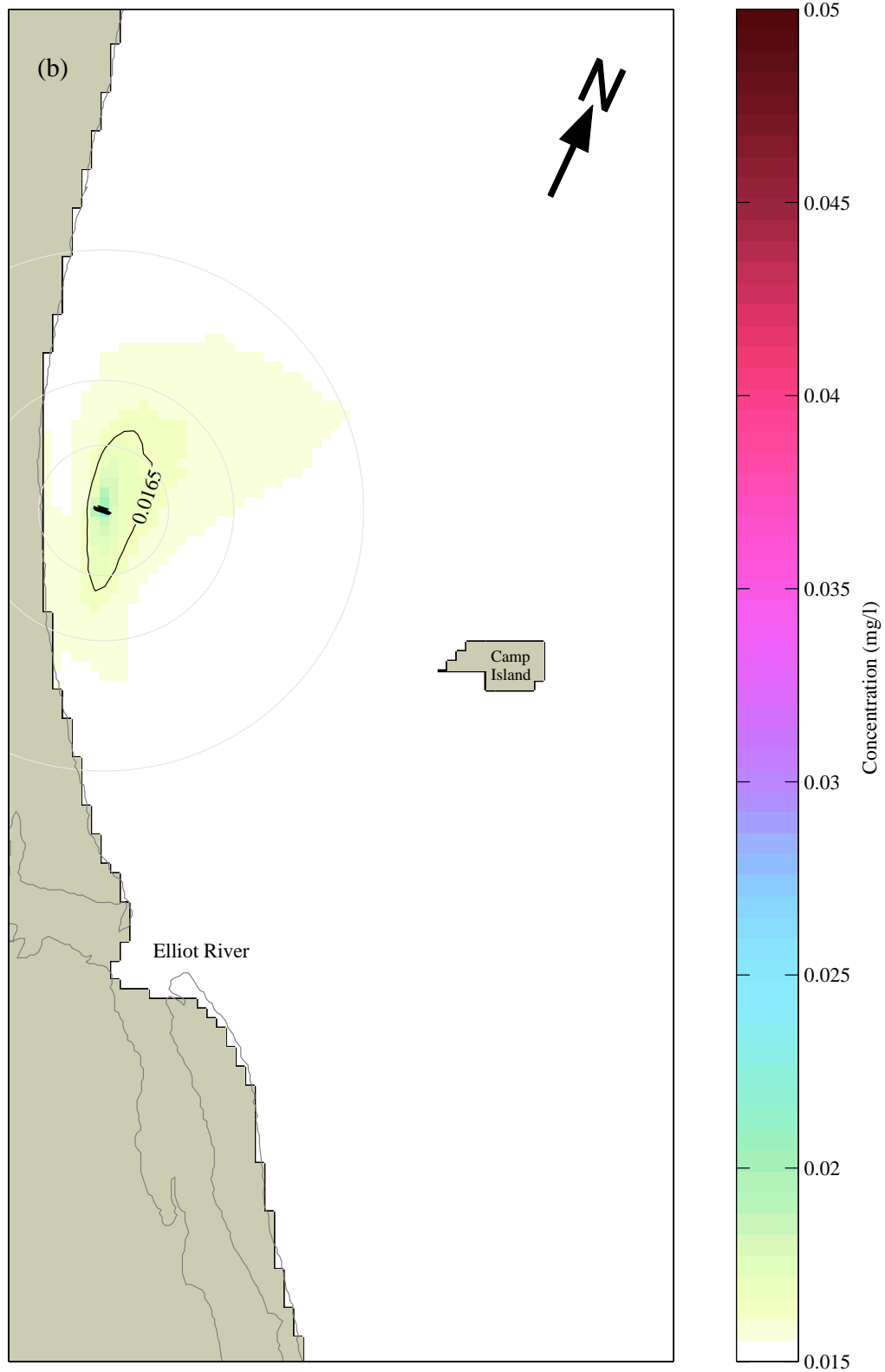


**Figure 35b.** Average Concentration (*Phosphorus*) for the February discharge period of 1998 (100Ml/d). Contours indicate the background plus 10% (0.0165 mg/l) and the threshold (0.025 mg/l) levels. Concentric circles at 500, 1000 and 2000 m radii.

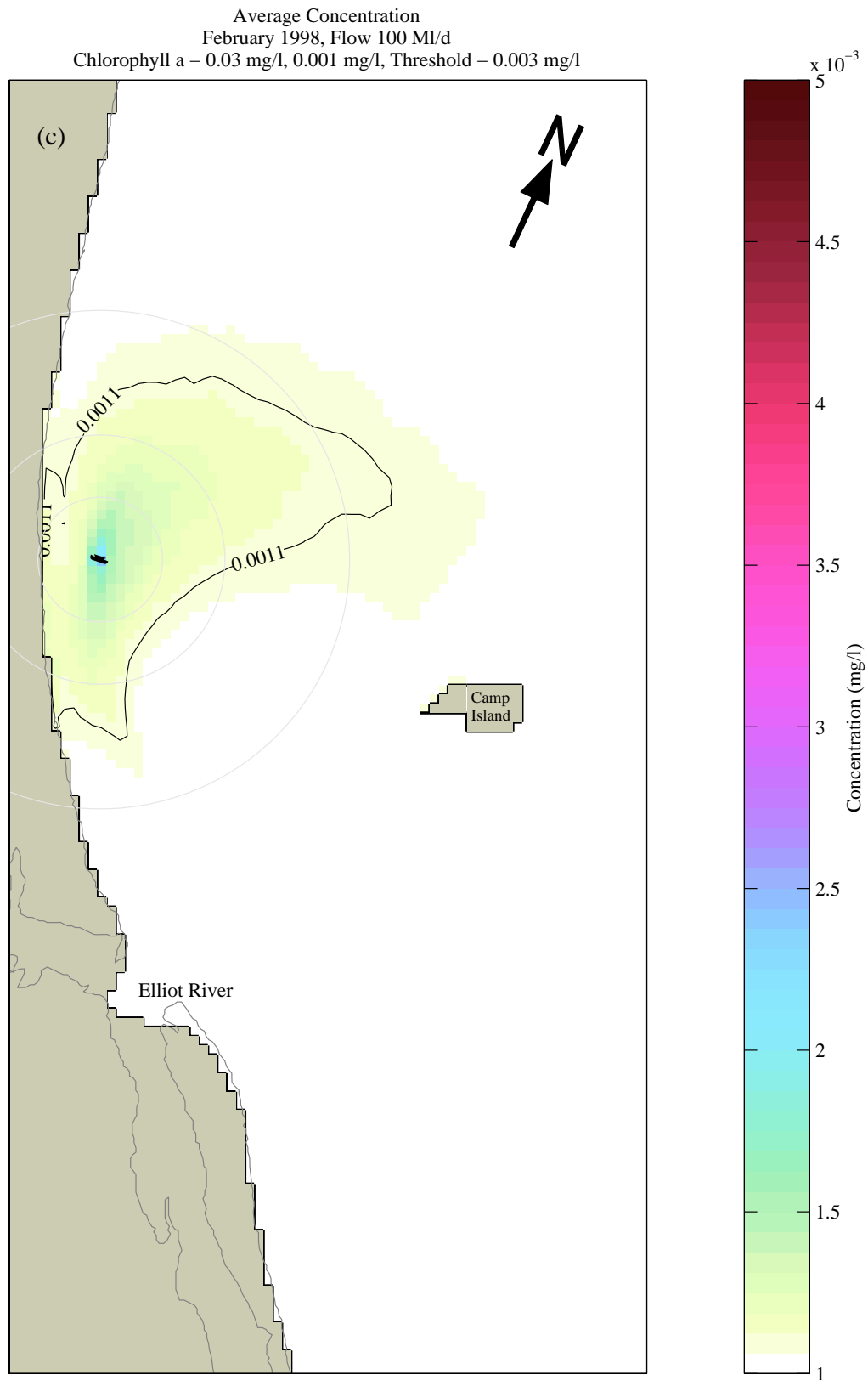


**Figure 35c.** Average Concentration (*Chlorophyll-a*) for the February discharge period of 1998 (100ML/d). Contours indicate the background plus 10% (0.0011 mg/l) and the threshold (0.003 mg/l) levels. Concentric circles at 500, 1000 and 2000 m radii.